FABRICATION AND CHARACTERIZATION OF ‘GREEN’ RESINS AND ‘GREEN’ HYBRID COMPOSITES USING CHICKEN FEATHER FIBERS, SOY PROTEIN ISOLATE, AND JUTE FABRIC

A Thesis

Presented to the Faculty of the Graduate School

of Cornell University

In Partial Fulfillment of the Requirements for the Degree of

Master of Science

by

Adith Narayan Shankar

December 2021

ABSTRACT

Dwindling petroleum sources and rising levels of non-biodegradable plastic pollution have led researchers to develop sustainable and environmentally friendly alternatives to replace the petroleum-based plastics and composites that are so ubiquitously used today. In this work, chicken feather fibers (CFF), soy protein isolate (SPI), and jute fabric (JF) were used to produce fully green CFF/SPI resins and fully green JF/(CFF/SPI) hybrid composites. The necessity of an external crosslinking reagent was explored through the comparison of glutaraldehyde (GA) crosslinked CFF/SPI resins and JF/(CFF/SPI) composites with their GA-free counterparts. The results suggested that for most properties, GA-free CFF/SPI resins and JF/(CFF/SPI) composites were superior. In the few instances that GA improved properties, the difference was not significant and was further minimized with the addition of CFF. In addition, this work resulted in neat (GA- and CFF-free) SPI resins that differed visually (in color), mechanically, thermally, and spectrally than previous iterations of neat SPI resins. The results suggested that this difference could potentially be due to semi-crystallinity and/or internal crosslinks, possibly derived from the alternative resin preparation.

BIOGRAPHICAL SKETCH

Adith Shankar joined Professor Anil Netravali's Green Resins and Composites Lab to earn his Master of Science (M.S.) degree.

This work is dedicated to my parents Maya Gopalan and Udaya Natarajan, who traveled from India to give me a better future. To my baby brother Shrivatsav, who got my back despite all our squabbling. To my grandfather Kannuswamy Gopalan, who taught me the importance of hard work and being a good person, and my grandmother Kalyani Gopalan, whose strength is truly an inspiration and motivation. To my other mother, Yamuna Kamakshi, and the rest of my family and friends whose prayers and kind words helped me every step of the way. And finally, to my rock, Michelle Zundury Gutierrez, without whom graduate school would have been far less interesting and far more difficult.

ACKNOWLEDGMENTS

I want to acknowledge the people who contributed to this work's fruition. Thank you to Professor Anil Netravali for accepting me into his research group, guiding me through my work, and having the patience, understanding, and good-natured temperament that made my time in his group a pleasure. To my peers Sripathi, Anusha, Nina, and KT for their generosity in sharing their time and knowledge with me. To Cornell personnel Marissa Porter, Charles Beach Jr., Vincent Chicone, Robert Page, Mick Thomas, May Boggess, Katherine Spoth, and Emily Cotman for being so accommodating with their scheduling and consequently helping me finish my lab work in time. To Ms. Rhoda Mensah and Professor Oisik Das' group in Luleå University of Technology, Sweden for performing the necessary MCC characterization. Finally, to Professor Justin Barone and Tata Cornell Institute for providing the chicken feather fiber used in this work.

TABLE OF CONTENTS

LIST OF FIGURES

LIST OF TABLES

LIST OF ABBREVIATIONS/SYMBOLS

CF – Chicken Feather

CFB – Chicken Feather Barb

CFF – Chicken Feather Fiber

CFP – Chicken Feather Powder

CFQ – Chicken Feather Quill

DSC – Differential Scanning Calorimetry

DSF – Defatted Soy Flour

ATR-FTIR – Attenuated Total Reflectance Fourier Transform Infrared

GA – Glutaraldehyde

JF – Jute Fabric

MR – Moisture Regain

MCC – Microscale Combustion Calorimetry

PLA – Poly Lactic Acid

PP – Polypropylene

RF – Ramie Fiber

RPP – Recycled Polypropylene

SAM – Stearic Acid Modified

SEM – Scanning Electron Microscopy

SF – Soy Flour

SP – Soy Protein

SPC – Soy Protein Concentrate

SPI – Soy Protein Isolate

TGA – Thermo Gravimetric Analysis

Tm – Melting Temperature

wGA – with Glutaraldehyde

ΔHf – Enthalpy of Fusion

CHAPTER 1

INTRODUCTION

1.1 AGRICULTURAL WASTE AND VALORIZATION

The development of petroleum-based plastics initiated the wide scale adoption of plastics as an engineering material, transforming entire industries, but simultaneously introducing numerous environmental concerns. Industrial use of plastics was initially hampered by its dependence on scarce raw materials such as coal, vegetables, and animal products. However, the rapid growth of the petrochemical industry post World War II allowed for easy access to oil, a far cheaper raw material compared to its contemporary alternatives. Ultimately, this was the catalyst for the widespread use of plastics in the electric, automotive, packaging, and numerous other industries. As petroleum reserves are depleted by the excessive consumption of this finite resource, alternative technologies must be developed to replace the petroleum-based products that dominate many industries today. In the realm of fiber reinforced composites, petroleum-based plastics such as polypropylene and polyethylene are prevalent in many applications and direly need such substitutions. Agricultural waste is a surprisingly fruitful and inexpensive resource from which numerous sustainable, as well as biodegradable, solutions can be derived. The present research provides one way of valorizing chicken feather waste that would otherwise be detrimentally or dangerously discarded.

1.1.1 Chicken Feather Waste

Industrial poultry processing produces over 400 million metric tons of chicken feather waste (feathers, blood, feces) internationally.[1] The United States alone produces 11.3 million metric tons in dry feather waste (only feathers).[2] Currently, most of this waste is either being

buried (landfilled) or incinerated, both of which are harmful to the environment.[2] While improper burial of feather waste can pollute the environment by poisoning the land and water supplies, even monitored burial is an issue as landfill sites are limited and getting more expensive with higher tipping fees and transportation costs. Incineration, on the other hand, releases toxic air emissions into the atmosphere at a rate higher than modern coal plants and should, thus, be avoided whenever possible.[3] At present, the only method of recycling feather waste involves an expensive process known as hydrolysis that cleans the feathers and converts them into a fertilizer or low-grade feedstock for farm animals.[3] This is an extremely energy intensive method for a product that is not in high demand.

However, this vast amount of waste contains high amounts of keratin, the primary protein in feathers, from which durable organic composites can be formed. Thus, chicken feather can help guide the composite industry to a greener and more sustainable future.

Currently, an increasing number of petroleum-based plastics are used to replace wood, metal, and other heavier materials in automobiles. The use of these plastics improves an automobile's energy efficiency by reducing weight while also increasing the toughness, durability, and design flexibility of the parts. Although they promote less fuel consumption from their lower weight, these plastics are still environmentally unfavorable. Automotive commissions in Europe have passed laws requiring that 85% of the plastic used in cars must be recycled in an attempt to curb the harmful nature of producing these plastics and at the same time to recycle them and, thus, reduce the petroleum consumption.[4]

Composites that incorporate chicken feathers offer an excellent opportunity to replace existing plastics for roughly the same cost while improving overall properties and decreasing the environmental impact.[5] Focusing on interior components such as paneling, bumpers, dashboard,

seating, trim, etc., Table 1 clearly shows the dominance in petroleum-based plastics used in automobiles. It should be possible to develop green composites with similar mechanical and other properties to replace the conventional composites currently being used.

Table 1: All plastics used in an average automobile[6]

Component	Main Types of Plastics Used	Weight in Average Car (kg)
Bumpers	PS, ABS, PC/PBT	10.0
Seating	PUR, PP, PVS, ABS, PA	13.0
Dashboard	PP, ABS, SMA, PPE, PC	7.0
Fuel Systems	HDPE, POM, PA, PP, PBT	6.0
Body (Including Panels)	PP, PPE, UP	6.0
Under-Bonnet Components	PA, PP, PBT	9.0
Interior Trim	PP, ABS, PET, POM, PVC	20.0
Electrical Components	PP, PE, PBT, PBT, PA, PVC	7.0
Exterior Trim	ABS, PA, PBT, POM, ASA, PP	4.0
Lighting	PC, PBT, ABS, PMMA, UP	5.0
Upholstery	PVC, PUR, PP, PE	8.0
Liquid Reservoirs	PP, PE, PA	1.0
TOTAL		**105.0**

1.1.2 Soybeans

Soybeans are another inexpensive agricultural source of engineering potential due to the high level of soybean production and the ability to extract a large concentration of protein to synthesize environmentally friendly plastics.[7–14] As noted by the Environmental Protection Agency (EPA), soy protein based engineering materials are fully biodegradable/compostable and decrease the use of harmful disposal techniques.[15]

Soy protein (SP) is commercially available in three major forms: soy flour (SF), soy protein concentrate (SPC), and soy protein isolate (SPI). SF is the most rudimentary product of the three and is produced by dehulling cleaned soybeans and finely grinding them such that 97% of the load passes through a standard 100-mesh screen; this fine nature is what separates SF from its coarser equivalent - soy grits. Both SF and soy grits are further categorized based on their

lipid content. Of the various potential types of soy flour/grits, defatted soy flour (DSF) is the most useful for the creation of green resins and composites as it contains less than 1% oil while having the highest protein concentration (with respect to other forms of SF) of 56%.[16] The production of SF is detailed in the schematic diagram in Figure 1.

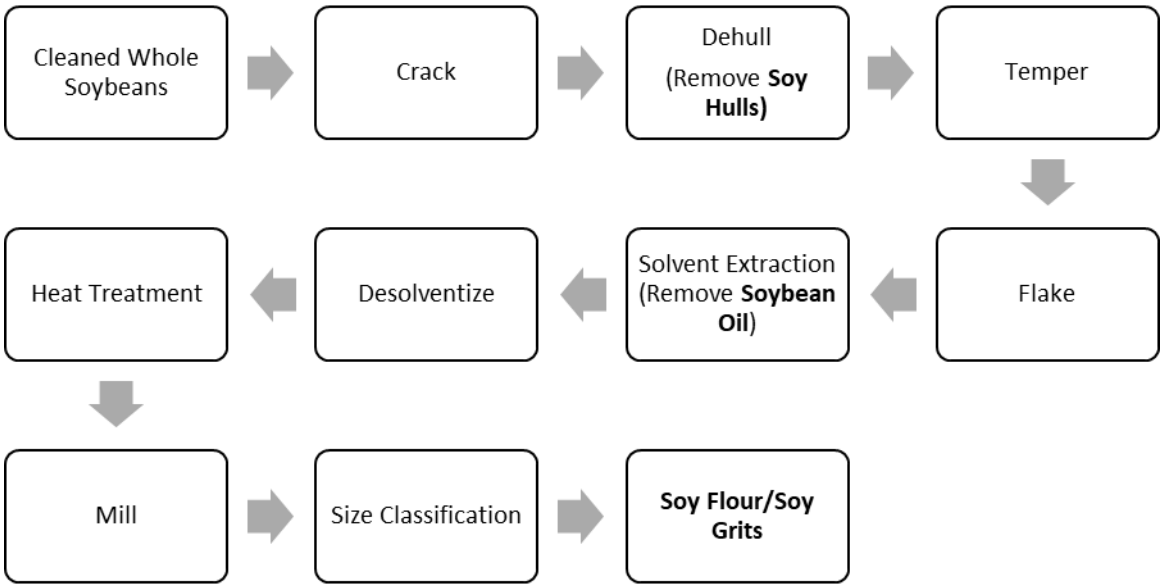

Figure 1: Schematic diagram of soy flour/grits process

DSF can be further refined into SPC by removing much of the soluble carbohydrate content while retaining the protein.[17] Various methods to refine SPC include alcohol extraction using 20-80% ethyl alcohol, acid leaching, and using moist heat to denature the protein before extracting it with water.[17] Regardless of the method, the end result is a product containing between 65-67% protein content as defined by the U.S. Soybean Export Council in 2019.[18]

The protein refinement of DSF culminates with soy protein isolate (SPI), in which the protein content is between 90-92%. The process to obtain SPI involves solubilizing the protein fraction and separating the insoluble fiber and carbohydrate fraction through centrifugation.[17]

1.1.3 Jute

Along with chicken feathers and soy protein, jute fibers also provide an opportunity to use an abundantly available organic resource for engineering applications. Jute is an ancient natural fiber that is still commonly used today; in fact, jute is currently the second most produced plant fiber, behind only cotton.[19] Jute yarn is typically produced by defoliating harvested jute stalks, removing the nonfibrous material such as lignin and hemicellulose by retting, extracting the silky fibers that remain and spinning them into low-twist yarns. Yarns are then chemically finished as necessary and woven or knitted into their final fabric form.

As a woven fabric, jute is very coarse and rough, and lends itself to industrial, rather than apparel, applications. In the past few decades, natural fibers such as jute have been used as a competitive alternative to synthetic fibers in many engineering industries due to their high specific mechanical properties, low cost, and biodegradability.[20]

1.2 OVERVIEW ON POLYMERS AND PLASTICS

1.2.1 Definitions

Polymers are a class of materials comprised of macromolecules (large molecules with molecular weights between thousands to millions g/mole) connected by covalent interatomic bonds.[21] These polymer chains are formed by successive addition of monomer units and determine a polymer's properties based on the chain's length, chemistry, shape, and analogous additional characteristics. From these properties, two fundamental classes of polymers are defined: plastics and rubbers. Rubbers – or elastomers – are amorphous polymers that benefit

from low crosslink densities to allow for large elastic deformation due to the crosslinks acting as anchor points that prevent chain slippage. In order to be classified as a plastic, a linear or branched polymer must be used below its glass transition state (if amorphous), below their melting temperature (if semicrystalline), or crosslinked enough to retain shape. Many authors group rubbers into the category of plastics, given that materials such as flexible polyurethane foams could fall in either definition.[22] This work will follow this logic, and include rubbers under the term “plastic”.

Plastics are an intriguing class of materials to scientists due to their low processing costs, diverse mechanical properties, great thermal and electrical insulation, and resistance to many chemicals and solvents.[22] They can be further divided into thermosets and thermoplastics.

Thermosets undergo an irreversible physical change with heat treatment and/or crosslinking agents (agents that connect, i.e., covalently bond polymer/monomer molecules together) to create a chemically interconnected 3-D network structure.[23] This 3-D interconnectedness prevents intermolecular slippage and chain movement, resulting in a stiffer and stronger polymer. However, this irreversibility of the crosslinking reaction also prevents thermosets from being reused or remolded, limiting their recyclability and, thus, detrimentally impacting the environment.[24]

In contrast, thermoplastics can be heated and recast several times. However, due to their limited interchain crosslinking, thermoplastics can be soluble in solvents and have a low melting temperature depending on the chemistry and crystallinity.[23]

Polymers can take other forms such as fibers or surface coatings, but these forms are not of interest for the scope of this research as they serve distinctly different roles from plastics.

In this work, plastics are referred to as resins when synthesized for the purpose of acting as a binding material. Colloquially, "resin" refers to a naturally derived, highly viscous substance such as amber that through some kind of treatment (UV, heat, etc.) becomes a solid. While materials described by the latter definition could be used as a binder, the former definition inclusively allows for petroleum-based plastics, and other synthetic plastics, to be considered as resins as well.

1.2.2 History

The term "polymer" is credited to Swedish chemist J. J. Berzelius, who in 1833, defined this class of materials as a substance that is composed of many repeat parts.[25] This definition evolved and expanded to become the one defined earlier in Section 1.2.1. H. Staudinger is widely attributed for the acceptance of polymers as a class of materials, as well as its more formal definition, and received a Nobel Prize in 1953 for his efforts.[25] While there are records of ancient civilizations using and interacting with various naturally occurring plastics such as amber or lac, the valorization of plastics as an engineering material is credited to ebonite – a natural rubber processed with sulfur.[22] The first non-rubber type plastics were developed in the 1860s-1890s using cellulose and casein found in agricultural products.[22] However, none of these plastics were able to be mass produced due to the scarcity of the raw materials used to synthesize them.

The genesis of the modern-day plastic industry is owed to the creation of synthetic, petroleum derived polymers. In fact, the popular sentiment is that without oil there would be no mass-scale production, and consequent pervasiveness, of plastics.[22]

This unhealthy reliance on petrochemicals is one of the plastic industry's main drawbacks. Petroleum is a finite resource, meaning that when depleted, there will be no way to

synthesize most plastics used by society today. Furthermore, accidents during oil extractions and transportation have repeatedly caused several environmental disasters leading to catastrophic impacts on ocean, plant, and human life.[26,27] Finally, petroleum-based plastics are non-biodegradable leading to an epidemic of plastic pollution.[28] These issues were only further exacerbated when plastics were found to be useful in the development of a new class of materials: composites.

1.3 OVERVIEW ON COMPOSITES

1.3.1 Definitions

Composites are defined as multiphase materials that benefit from combining the properties of their respective constituents.[29] Phases that compose a composite can be categorized as the matrix (continuous) phase, the dispersed (or discontinuous) phase, and the interphase.

The matrix phase is defined as the continuous material that envelops and binds the other phases. Although the terms “resin” and “matrix” are used interchangeably in industry, there is a marked difference that needs to be emphasized to understand this work. “Resin” is a materials classification, referring to plastics used for the purpose of serving as a binding material. For example, in this work, SPI resin is used as the matrix material. However, the term “matrix” is a component classification, and other types of materials such as metals and ceramics can be used as a matrix. This distinction is necessary when discussing composite properties. For example, the composite property “fiber/matrix adhesion” should not erroneously be referred to as “fiber/resin adhesion”. When discussing resin properties, the term “resin” will naturally be used.

The dispersed phase refers to the material held together by the matrix. The interphase is described as the 3D region immediately surrounding the dispersed and matrix phases from which the properties of the matrix phase transition to those of the dispersed phase. The final region of

interest is the 2D area where the fiber and matrix surfaces meet, known as the fiber/matrix interface. Though not a "phase" as it not a material region but rather a conceptual 2D area, the fiber/matrix interface does influence composite properties along with the three previously mentioned phases.

In the case of structural composites, the purpose of the matrix is to bind the reinforcing dispersed phase, most commonly fibers, together, transfer applied loads from broken fiber to intact fibers through the fiber/matrix interface, and determine the net shape, surface quality, and durability of the composites. Hence, the matrix is generally a more ductile material, compared to the reinforcing fibers, able to withstand cyclic stresses and prevent crack propagation.

In contrast, the dispersed phase is meant to reinforce/stiffen the composite by resisting deformation, thus this phase is generally harder, stiffer, and stronger than the matrix. In most structural composites the dispersed phase employs high strength fibers such as graphite, aramid, glass, etc., which results in composites with high strength and stiffness.

The interphase, existing as the bridge between the matrix and dispersed phases, also is attributed to have a significant role in terms of composite failure and properties. For example, in an interfacial shear strength (IFSS) study, the presence of an interphase with a higher modulus (with respect to the matrix) was theorized to have contributed to the larger calculated shear stress values (compared to the ultimate shear stress of the matrix with no fiber present).[30]

The fiber/matrix interface is crucial in a composite's overall properties. The strength of the interface bond determines how well stress is transmitted between the broken and intact fibers through the matrix. The stronger the interfacial bond, the stronger, stiffer, and less tough the composite.[31] The opposite is true as well. Interfacial bonding can be affected by a number of factors. For example, micro voids formed during resin cooling reduces the interfacial bonding.

Similarly, differences in hydrophilicity/hydrophobicity (surface energetics) between the matrix and fiber can result in an intermediate layer of water collecting between the two, increasing fiber debonding and reducing the fiber-fiber stress transfer, thus decreasing the composite strength.

Composites are generally classified by the geometry of the dispersed phase. Particulate composites contain particulates that can act in two different ways given the size. Large-particulate composites employ particles on the continuum scale, and these particles are generally harder and stiffer than the matrix, restraining the deformation of the matrix within the local area of the particulate and allowing the matrix to share a portion of the applied load with the particle. Small-particulate composites introduce particles that interact with the matrix on an atomic or molecular scale, preventing deformation by impeding dislocation movement (similar to precipitation hardening in metals).[29] Short fiber composites employ short, stiff fibers that act similarly to large-particle composites. A fiber is considered short if its length is too short to carry any significant load. These fibers can be aligned or randomly dispersed. Continuous fiber composites, in which the fibers are typically the length of the composite, can be further split into laminate composites and bundle composites. In laminate composites, layers of fibrous composites are stacked and oriented with respect to the fiber direction in such a way as to maximize mechanical properties in different directions. Bundle composites have the fibers all unidirectionally oriented much like a rope, but without the twist.

Regardless of the type of composite, the sum of these constituent phases creates a material that may not have the full property benefits of any one of the respective phases, but retains enough of each phase to create a material with superior aggregate properties.

1.3.2 History

Through these definitions, many naturally occurring composites can be identified. For example, wood can be classified as a natural composite since its lignin content acts as a matrix and its cellulose fibers/fibrils act as reinforcement. The earliest recorded man-made composite dates back to 5000 B.C. in the Middle East, where pitch was used as a binding matrix to create boats from papyrus reeds.[32] Despite the storied history of composites, this material classification only received a formal definition in 1950s, as this was when they were more actively pursued as a viable alternative to the structural materials of their time.[33]

Composites offer a way to tailor-make an engineering material of desired properties for specific purposes. This flexibility in design is achieved both from a materials perspective as well as a mechanical one. On the materials side, choice of a specific matrix and reinforcing phase can determine the composite's moisture absorbance, its mechanical properties, its thermal and electrical conductivity, among many other properties. Through mechanical analysis, the geometry and shape of the composite can be modified to prioritize isotropic behavior, fatigue prevention, etc. Thus, composites are in many ways the ultimate engineering material.

Materials are given the prefix of "advanced" when they exceed a yield strength above 300 MPa and a tensile strength above 600 MPa.[34] Advanced materials also tend to have high Young's moduli. This definition of 'advanced' also applies to composites. The benefits afforded by advanced composites have led to the replacement of traditional materials in numerous industries. For example, in the aerospace industry, advanced composites were only introduced in 1970, and yet grew to make up 80% of the total weight of business aircraft and rotorcraft by 1990.[32] Many other classifications of aerospace vehicles from military aircraft and large commercial transport have followed similar trends.

1.4 THE RISE OF GREEN RESINS AND COMPOSITES

As mentioned in the previous section, the very first fabricated resins and composites consisted entirely of natural, renewable, and biodegradable materials. These materials fell out of use as newer structural materials, with superior properties, such as steel, aluminum, and fiber reinforced composites were developed. However, due to the aforementioned environmental concerns, there has been a growing movement to return to using "green" materials. The term "green" in this work will refer to materials derived from nature. Typically, green materials are biodegradable and sustainable, but this is not always the case.

"Greener" composites have been developed that incorporate one green phase, generally the reinforcing fiber phase, to create a composite that is somewhat more environmentally friendly than an entirely petroleum-based one. Generally, these composites run into interfacial bonding issues as bio-based phases tend to be hydrophilic while the synthetic phases remain mostly hydrophobic.[35] In addition, these types of greener composites remain a stop gap solution that continue to incorporate some environmentally unfavorable constituents.

Recent efforts to refocus on pure or fully green composites have yielded advanced green composites, i.e. green composites with comparable mechanical properties to traditional advanced composites.[8]

CHAPTER 2

LITERATURE REVIEW

2.1 CHICKEN FEATHERS AND THEIR PROPERTIES

Chicken feathers have a hierarchical structure originating from the main quill (rachis) into secondary branches known as barbs (referred to as the fibers of chicken feathers), into tertiary branches known as barbules, and finally into hooklets.[3] Figure 2 shows the hierarchical structure of the chicken feather.[3] The two main components of chicken feathers most commonly studied are the rachis and the barbs as they are two components large enough to have engineering value.[3] Somewhat confusingly, the literature varies on what exactly a chicken feather "fiber" is. Some authors define "chicken feather fiber" to exclusively refer to the barbs[36,37], while others include the quill as well[3]. In the present work, the term 'chicken feather fibers' (CFF) refers to 'all branches' of this hierarchal structure, i.e., the entire chicken feather. When referring to only the barbs, the term "CFB" will be used, and when referring to only the quills, the term "CFQ" will be used.

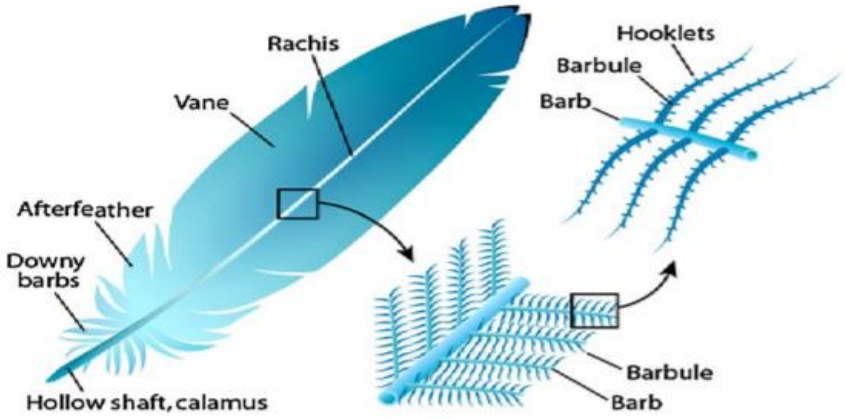

Figure 2: Structure of chicken feathers[3]

Both rachis and barbs are semi-crystalline and hollow, lending themselves well to applications that require low weight but high strength. The hollow structure of the feather fractions means that chicken feathers offer warmth retention as well as acoustic dampening due to the air pockets present inside each fiber.[3] Furthermore, the quills are internally composed in a honeycomb structure that is known to further improve acoustic dampening and provide stiffness. Warmth retention suggests that feather fractions can be used in products like winter jackets or insulating composites while acoustic dampening could work in office cubicle walls or automotive paneling to block engine or outside noise from entering the cubicle or passenger compartment, respectively.

Chicken feathers contain approximately 97% keratin, 8% water, and 1% lipids.[38] Keratin is a macromolecular protein that has great strength and stiffness due to hydrogen bonding from polar groups present in its amino acids, intermolecular and intramolecular S-S crosslinks formed by the cysteine amino acid, as well as from its semi-crystalline structure.[39]

Keratin's molecular weight is 10,500 g/mole which corresponds to roughly 90 amino acids, i.e., the degree of polymerization (DP) of about 90. The breakdown of the amino acids

present in keratin is given in Table 2. The key takeaway from Table 2 is the presence of high cysteine concentration. Cysteine allows for the formation of the previously mentioned S-S intermolecular crosslinks which facilitate the formation of 3-D protein structures that provide structural stability, higher stiffness and flexural modulus.[40]

Table 2:Amino acid breakdown of keratin in chicken feathers[3]

Functional Group	Amino Acid	Percent Content
Positively Charged	Arginine	4.30
Negatively Charged	Aspartic Acid	6.00
	Glutamine	7.62
Hydrophobic	Tyrosine	1.00
	Leucine	2.62
	Isoleucine	3.32
	Valine	1.61
	Cysteine	8.85
	Alanine	3.44
	Phenylalanine	0.86
	Methionine	1.02
Hygroscopic	Threonine	4.00
	Serine	16.00
Special	Proline	12.00
	Asparagine	4.00

The main difference between the rachis and the barbs is that the rachis is composed of beta type keratin sheets, which means that they can be packed together more tightly, creating a harder, more dense material from a molecular geometry point of view.[41] Barbs, on the other hand, are primarily composed of alpha-helical keratin structure (41%) but also have 38% beta-sheet type, resulting in a softer, but more durable material for similar geometric reasons.[41] Beta keratin sheets have a much higher concentration of cysteine compared to the alpha helical keratins, which is an additional reason as to why the rachis are much harder and stiffer than barbs.[41] Tensile tests performed across eight birds have shown that the Young's modulus of

keratin based rachis is similar (except for one) at around 2.5 GPa.[42] This study concluded that flexural stiffness was a product of cross-sectional shape and morphology rather than the keratin chemistry.

The second key difference between the rachis and barbs is that the rachis is almost entirely hydrophobic while the barb fibers are roughly 40% hydrophilic (and 60% hydrophobic). This is due to the different amino acids present in the respective components and consequently limits the uses of the rachis and barbs with certain materials. Tesfaye et al. demonstrated that the average moisture content of CFF maintained a static maximum of 10.5% which indicated that CFF based materials could be safely stored without fear of microbial growths and resulting degradation of their properties.[39] These two differences – protein arrangement and hydrophilicity – affect the difference in thermal stability between the two fractions as well. TGA characterization of the barbs and rachis indicated that the predominantly β-sheet rachis thermally degrades at a lower temperature than the predominantly α-helix barbs.[43] This is attributed to the higher packing efficiency of the α-helix structure requiring more energy to thermally degrade compared to the β-sheet conformation.[43]

The flammability of chicken feathers has been explored to gauge their usefulness in creating a fire-resistant structural material.[39] Burning tests have been conducted on various chicken feather fractions (rachis, barbs, whole feathers) and they have all been found to be self-extinguishing.[39] There are several contributing factors for this behavior. First, proteins absorb 6-8% water under normal conditions. They also contain high nitrogen concentration because of the amino acids. In addition, when heated, reactions between –OH and –COOH groups as well as between –OH and -NH_2 groups can occur. Both these reactions are condensation type reactions

that kick out a H_2O molecule every time these groups react. These reactions provide additional water that can help their self-extinguishing properties.

The rachis is the most resistant of the various CF fractions to burning, emitting no smoke even when burning, not melting, and supporting combustion away from the flame only with great difficulty.[39] The fibers do emit an orange smoke, melt, and support combustion, but do so at a very limited rate.[39] As can be expected, the whole feather has aggregate properties of the two.

This suggests that CF can be used for basic fire-proofing techniques – i.e., flame retardant and protective finishers – in structural materials where avoiding burning is critically important. The flame test has also proved conclusively that chicken feathers are a protein fiber.[39]

2.2 SOY PROTEINS AND THEIR PROPERTIES

Soybeans contain several types of proteins of varying molecular weights and chemical properties due to different amino acid compositions. These proteins are Bowman-Birk Trypsin Inhibitor, Kunitz Trypsin Inhibitor, Hemagglutinin, Lipoxygenase, 7S Globulin, 11S Globulin, and Urease.[44] When the term "soy protein" is used in literature, it refers to the sum of all these fractions and thus it is key to remember that it is not a singular globulin and that these various fractions may respond differently to treatments and processes.

For example, the Kunitz Trypsin Inhibitor is a low molecular weight (21 M) protein with disulfide (S-S) linkages, formed by cysteine amino acid. The S-S links (intermolecular crosslinks) aid in creating a stiffer polymer due to the stronger nature of S-S bonds. However, another fraction of soy protein is Hemagglutinin, a medium molecular weight (100-110 M) protein that does not contain any S-S linkages. Thus, if the procured SP had a greater proportion of Hemagglutinin to the Kunitz Trypsin Inhibitor, the resulting resin would be heavier and weaker.

As mentioned previously, SPC and SPI can both be produced from SF through a variety of methods; however, each method can alter the chemical properties – and thus the proteins' functionality – in distinct and important ways.[45] For example, in 2003, Gianazza et al. demonstrated that certain soy protein fractions tend to accumulate more predominantly in ethanol washed specimens.[46] These fractions have different properties, such as the 7S Globulin aiding in cholesterol lowering effects upon digestion, meaning that ethanol treated soy protein is not comparable to untreated soy protein despite the overall protein percentage being the same at the end of the manufacturing process. Erdman et al. noted that this lack of understanding has caused researchers to draw incorrect correlations, such as isoflavone differences incorrectly attributed for differences between soy products when the differing protein and peptide compositions were potentially the true reasons.[45] This is an important point to make as, for the application of green resins and composites, the type of soy material used should be carefully chosen as its chemical composition will affect both the functionality of the protein, its binding characteristic with the reinforcing agent and, ultimately, the final mechanical properties of the product. Table 3 presents the amino acid profiles of commercially available soy proteins used in two earlier studies.[7,47] The data presented are with respect to 1 g per 100 g of raw material.

Table 3: Amino acid profiles of commercially available soy proteins[7,47]

Amino Acid	Gorissen et al.	Chavan
Alanine	2.8	4.3
Arginine	4.8	8.2
Aspartic Acid	Not Measured	12.0
Cysteine	0.2	1.2
Glutamic Acid	12.4	19.9
Glycine	2.7	4.3
Histidine	1.5	2.7
Isoleucine	1.9	4.7
Leucine	5.0	8.3
Lysine	3.4	6.4
Methionine	0.3	1.4
Phenylalanine	3.2	5.4
Proline	3.3	5.5
Serine	3.4	5.3
Threonine	2.3	3.9
Tryptophan	Not Measured	1.1
Tyrosine	2.2	4.2
Valine	2.2	4.7

Protein reorganization, or denaturation, of soy protein is crucial for their use in developing green resins due to the globular nature of the various soy protein fractions. Caustic soda (NaOH) processing involving high pH of 9 and above, temperature, and time has been used to unfold the globulins and expose the polar (reactive) groups, e.g., amine, hydroxyl and carboxyl, to aqueous contact.[48] By adjusting the pH to above 10.5 and temperature between 40 and 70 °C, it was demonstrated that not only would the globular soy proteins unfold (denature) with minimum backbone chain cleavage, but also that internal crosslinking between the amino acid groups was propagated through this physico-chemical treatment.

The higher pH and temperature levels can cause cysteine and serine groups to create dehydroalanyl through Beta elimination reactions.[44] In turn, the dehydroalanyl residue can react with lysine, potentially crosslinking protein chains to form a stronger polymer. Thus, caustic

treatment of soy protein can be utilized to aid in creating a soy protein-based resin. However, internal crosslinking by itself is not sufficient to obtain desired properties of the soy protein-based resins because it can provide only limited crosslink density.

To further enhance the mechanical properties of soy protein resin, additional crosslinking provided by external crosslinkers is critical. Of the various fractions, the 7s and 11s are the two major globulins of interest as they occupy the greatest portion as well as are capable of forming disulphide, lysinoalanine, and lanthionine crosslinkages.[10] Many researchers have crosslinked soy proteins using a variety of crosslinkers such as glutaraldehyde, glyoxal as well as sugar-based aldehydes which have significantly enhanced the mechanical properties of soy protein based resins depending on the crosslink density.[49] These improvements have been detailed later in Section 2.4.2.

2.3 JUTE FIBER AND ITS PROPERTIES

Jute is a lignocellulosic fiber with a chemical composition of 41.3% cellulose, 46% hemicellulose, 11.8% lignin, 0.2% pectin, 1.1% water soluble content, 0.5% wax, 10% water (10%).[50] Jute fibers been experimentally determined to have a tensile strength (fracture stress) of 331-414 MPa and stiffness or Young's Modulus of 28.43 GPa, all while retaining a density of a range from 1.35 to 1.49 g/cc.[51, 52] Untreated jute undergoing thermal degradation is reported to have three peaks at around 64.7-100, 297.0, and 362.2 °C.[53] These peaks are associated with moisture evaporation, hemicellulose degradation and α-cellulose degradation, respectively.[53] Differential scanning calorimetry (DSC) performed on jute fiber in air revealed an endothermic peak at around 100 °C, and a large exothermic peak with maximums at 381 °C and 546 °C.[54] The initial endothermic peak is associated with volatilization of absorbed water and the following

broad exothermic peaks are attributed to the combined exothermic peaks of hemicellulose and lignin.[54]

Coupled with high fabric breathability attained by loose weave, decent heat retention, and high specific mechanical properties, jute fabrics have been used in recent years in reinforcing biodegradable composites, besides many other applications.[55]

2.4 GREEN RESINS

The following sub-sections summarize studies conducted on the use of CF and SP to fabricate resins.

2.4.1 Resins Based on Chicken Feathers (CF)

Due to the fibrous nature of CF, it has thus far been impossible to create a film without pulverizing the feathers to achieve a powder for resin casting.

Barone et al. developed a method to produce films incorporating CF in water and performed tensile tests to determine mechanical properties as well as DSC and NMR characterization to understand changes in their molecular structure as a function of the hot-pressing time and temperature.[56] They ground the CFF into a fine powder with fiber lengths between 0.0053 cm and 0.0075 cm. The result was that some of the mechanical benefits obtained from the structure of the CFF were lost in lieu of creating a cohesive film. The CFF powder was mixed with glycerol, a plasticizer, at ratios varying from 15 wt% up to 80 wt% in order to lower the melting temperature for better processing. They noted that glycerol content greater than 50% produced films with holes and thus were not fit to test mechanically, and so only films with 15, 20, 30, 40, and 50 wt% glycerol content were tested mechanically.

Through tensile testing, Barone et al. found that the Young's modulus and fracture stress decreased while the fracture strain increased with increased hot pressing time, and that the films

deformed in a nonlinear viscoelastic manner.[56] DSC characterization revealed that the hydrophilic glycerol had replaced water in the keratin structure, potentially through solubilizing at the -OH groups present in keratin. This resulted in a reduction in the crystallinity towards more of an amorphous polymer, allowing for easier resin casting through the prevention of recrystallization post-processing. NMR characterization confirmed the intimate bonding between glycerol and the keratin structure.[56]

Another method Barone and his group used to create a CF based biopolymer was to extrude a blended mix of ground (size ranging from 0.1 to 0.0038 cm) feather/quills and sodium sulfite (redox reagent), DI water, and glycerol.[57] Die temperature was found to affect swelling, as an increase in die temperature at a given shear stress increased the swelling of the extrudate. Lowering the die (and barrel) temperature also increased the viscosity, up to 100 °C, below which the extruded material remained the powdery mixture it was inserted in as. Glycerol and water were added in set ratios. Increasing the glycerol concentration of this glycerol:water ratio resulted in lower viscosity and faster flow, while increasing the water concentration resulted in greater viscosity and slower flow.

Sodium sulfite was added to help extrude the material by breaking S-S bonds present in keratin to decrease apparent viscosity. Raman spectroscopy showed that there was a decrease in apparent viscosity up to 3% (with respect to percentage of feather keratin used) added sodium sulfite. Above 3% the apparent viscosity increased again.[57]

The CFF used in this study were obtained from various sources, each with their own processing and cleaning protocol. Feather “quality” was defined by the authors as the extent to which the respective CFFs had been cleaned and dried during its processing. The CFF specimens were characterized using solid state NMR spectroscopy and it was demonstrated that peak

quality was inversely associated with hydrogen bonding. An increased presence of hydrogen bonding resulted in increased mechanical properties, which the researchers believed were a result of decrease in potential sites for the glycerol to plasticize. Thus, the feathers that had not been cleaned or dried as thoroughly, had superior stiffness and fracture strength than the "higher quality" specimens.

Through these two studies, the authors concluded that chicken feathers were viable materials for creating green resins that could biodegrade and be used for packaging.[56,57]

2.4.2 Resins Based on Soy Protein (SP)

As previously noted, soy protein is completely biodegradable and renewable, inviting many researchers to probe potential engineering applications from it. However, pure soy protein resins are difficult to fabricate and its use has been limited as the resulting resin is brittle and moisture absorbent[58]. These concerns have been addressed by the introduction of high strength particulates/fibers[8,13], plasticizing agents[59], chemical modification[10], crosslinking[11,60–63], and other, less popular methods[58].

Crosslinking is a popular solution in improving the properties of SP-based resins as it addresses a number of these issues. Mechanical properties such as tensile fracture strength and Young's modulus increase as crosslinks restrict molecular movement[64], thermal stability improves as more energy is required to break apart the covalently bonded structure[29], moisture absorbance decreases as crosslinks reduce hydrophilic groups[49,61,65].

Crosslinked soy protein resins, particularly those using Maillard type chemistry between amine groups in protein with aldehydes from external crosslinkers, undergo a color change to indicate the stage of curing that they are in. These stages are illustrated in Figure 3 when oxidized sucrose (aldehyde) was used as the crosslinker.[9]

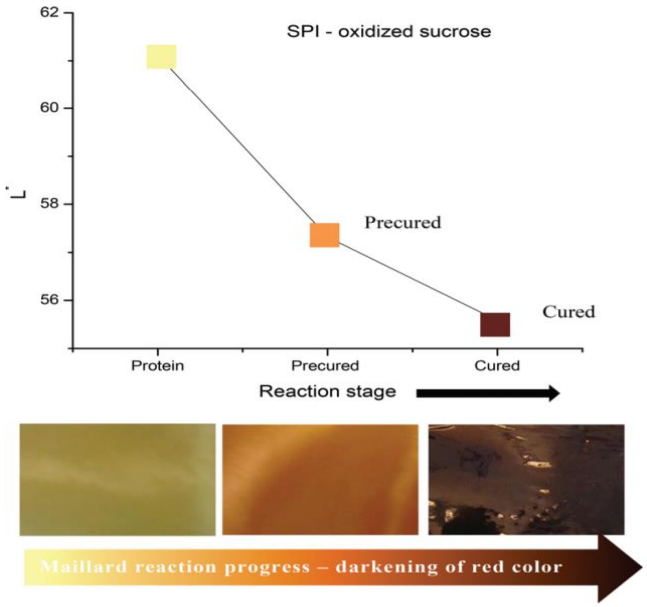

Figure 3: Color changes of a fully crosslinked SP resin[9]

Dastidar and Netravali created a fully green crosslinked SF resin without the use of any external crosslinker by filtering the SF solution into two components: soy proteins and the soluble sugars.[9] This was done by insolubilizing the SF protein in water by decreasing the pH level to the protein isoelectric point of 4.5 to precipitate the proteins while dissolving the sugars and then filtering into two separate parts. The soy flour extract (SFE) filtrate – consisting of the sugars and water – was oxidized using H_2O_2 to create a crosslinking agent containing aldehyde groups. The purified soy proteins (PSF) were denatured in water, after which the oxidized SFE was added to initiate crosslinking, and then fully crosslinked at 120 °C for 20 min in a hot press.

For comparison, a precured SF resin was fabricated that differed only in that the SFE extract added was not oxidized, preventing further crosslinking. Microfibrillated cellulose (MFC) fibers, 5% by SF weight percentage, were added to both resins for tensile testing.

They found that that the crosslinking increased the Young's modulus, fracture stress, and fracture strain from 1106 to 6375 MPa, 9.2 to 58 MPa, and 1.8 to 2.7%, respectively. In addition, the initial degradation temperature increased from 219 to 233 °C making it more stable.

While crosslinking addresses many issues, it tends to decrease ductility. Thus, plasticizing agents are added to prevent brittle behavior. Polyol plasticizers are commonly used for SP resins but with caution as they can leach out over time and the additional polar groups increase the moisture absorbance, which reduces their tensile properties significantly.[10,59] Lodha and Netravali explored a way to obtain SPI resins without adding external plasticizing agents by using stearic acid to chemically modify the SPI resin.[10] Stearic acid can plasticize SPI through the formation of ester bonds and amide linkages by reacting with the hydroxyl and amino side/end groups respectively.[66] The SPI resins were prepared by adding SPI powder to varying ratios of a plasticizer (glycerol), mixing with water, adjusting the pH to 10 and stir heating in a water bath set at 80 °C. Stearic acid was added after 30 min, at varying ratios, after which the resin was precured in an oven and finally pressed and cured through hot pressing and further drying. With 30% glycerol, stearic acid was shown to reduce moisture content of the resin from 15.2 to 12.5%, decrease fracture stress from 9 to 6.2 MPa, increase Young's modulus from 120.2 to 193.2 MPa, and decrease fracture strain from 168.4 to 25.6% as stearic acid content was increased from 0 to 30%. With 0% glycerol and 23% stearic acid, the fracture strain was 3.6%, which the authors deemed sufficiently ductile for composite application.

From the above examples, it is clearly illustrated that soy protein-based resins have been extensively developed and studied and can thus be used as green matrices in green composites. Typical tensile values found in literature for SPI resins synthesized with only a plasticizing agent are as follows: tensile fracture stress: 2.26-9 MPa, tensile fracture strain: 11.85-206.4%, and

Young's modulus of 98.7-127.4 MPa depending on the preparation and conditioning.[11,63,66,67] Typical thermal values of SPI resins are as follows: thermal degradation peaks at temperature ranges of 100-150 °C, 300-400 °C, and 500-800 °C, enthalpy of fusion of 5.4 J/g, and melting temperature of around 66.6 °C.[67,68]

2.5 GREEN/GREENER COMPOSITES

The following sections summarize studies about composites that have used CF and SPI resins as matrices. The CF based composites explore the use of the various fractions – CFQ, CFB and a powdered form of the whole feather – and the reasoning behind the specific fraction selections. The SPI based composite references the previously mentioned stearic acid modified SPI resins to give an example of successful implementation of a modified SPI resin. All composites were evaluated for potential industrial uses as well.

2.5.1 Jute/Chicken Feather Powder (CFP) Composites

In order to create a fully green and biodegradable composite, Reddy et al. ground chicken quills and barbs into a fine powder (CFP).[69] The CFP powder was sprayed into mats made of carded jute fibers at varying proportions (40%, 50%, 60%, 70%) and compression molded into composites. These jute/CFP composites had their tensile, flexural, and acoustic properties measured and compared to a 40/60 composite made from jute fibers and PP matrix from a previous study in which highest tensile and flexural properties were obtained.[70] Overall sound absorption of jute/CFP composites was shown to be lower compared to using whole feather quills or barbs. This is most likely because the hollow structure of the two were destroyed when the feather fractions were powdered. Despite this, jute/CFP showed better sound absorption compared to jute/PP from 3 kHz to 5 kHz indicating that the use of CFP was a net benefit despite the loss of the honeycomb structure of the quill.

Maximum tensile strength of 28.2 MPa, Young's modulus of 13 GPa, and flexural strength of 68 MPa were found at a jute/CFP ratio of 50/50. This was a significant improvement from the maximum tensile strength (12.2 MPa), Young's modulus (7 GPa), and flexural strength (48.7 MPa) obtained for 40/60 jute/PP composites. Increasing CFP proportions beyond 50%, however, resulted in decreasing tensile properties due to the softness of CFP compared to the reinforcing jute fibers. It is important to note that the jute/CFP composites were shown to have better properties than jute/PP composites despite PP having better mechanical properties (modulus/stiffness) than CFP. It was theorized that CFP matrix had better compatibility with the jute fibers compared to PP, most likely, because the organic/hydrophilic nature of both the CFP and the jute allowed for better cohesion.[69] On the other hand, hydrophobicity of PP did not allow it to bond well to jute fibers.

A major drawback in jute/CFP composites, however, was in its water absorption characteristics. Absorbed water plasticized the matrix, making it softer and at the same time weakened the fiber/matrix interfacial adhesion. Both of which decreased the mechanical properties. Due to this hydrophilicity of both the CFP matrix and jute fibers, conditioning the jute/CFP composites in 90% relative humidity (RH) for 48 h reduced the tensile strength from roughly 27 to 17 MPa and the flexural strength from roughly 68 to 25 MPa. In comparison, jute/PP composites did not experience significant change in mechanical properties after conditioning.[69]

Applications of jute/CFP composites can only be limited to environments that avoid high humidity or moisture/water due to the hydrophilicity of the composites. However, the net increase in tensile and flexural properties means that for arid conditions or indoor applications jute/CFP composites would be excellent "green" replacement for jute/PP composites. Office

spaces with controlled temperatures and humidity levels would be ideal, and these composites could serve as office cubicle walls with their superior sound absorbing capabilities.

2.5.2 Poly Lactic Acid (PLA)/CF Barb (CFB) Composites

PLA is a biodegradable polymer made from raw agricultural goods, particularly starches, fermented into lactic acid and then polymerized to higher molecular weight polymer.[71] PLA is known for its relatively high strength (compared to most biopolymers) but brittle behavior with low fracture strain. In a recent study CF barbs (CFB) were introduced in weight percentages from 2 to 10% to create a more ductile material.[71] Like the jute/CFP composites discussed earlier, PLA/CFB composites are also green and fully biodegradable.

PLA and CFB were blended using a twin-screw extruder and composites were prepared using injection molding process. The process involved heat treatment of PLA and CFB to remove excess moisture and feeding them into the extruder at 180 °C to become a molten mixture after which the mixture was fed into the injection molding machine at 200 °C to prepare dog bone shaped composite samples.

Tensile tests on CFB/PLA composites showed that the tensile fracture stress fell while Young's modulus and fracture strain increased until the CFB% reached 8 wt%. While the decrease in fracture stress was minimal (10 MPa max at 10 wt% CFB) it still limited CFB/PLA composites to non-load bearing applications. Young's modulus, however, increased from 3.6 to 4.2 GPa as CFB was added from 0 to 6 wt%. Fracture strain behavior was a bit more complicated with a 56% increase at 2 wt% of CFB but decreased past 2% CFB, perhaps due to particle agglomeration.[71]

Thermomechanical properties of CFB/PLA composites were also studied since poor dimensional stability can cause warping and can be a cause of early/premature failure.[71]

Thermal stability was observed using thermogravimetric analysis (TGA) which plots weight loss of the material as a function of temperature.[71] Addition of CFB was clearly shown to increase the temperature at which degradation starts (Td). This is due to CFB acting as heat insulators, which hindered the permeation of volatile degradation products in the composite. Higher Td also signifies that these composites can be used at higher temperatures, expanding their applications.

The SEM images of fracture surfaces of CFB/PLA composites indicated no significant protruding CFB, indicating good adhesion between CFB and PLA matrix which is beneficial in creating stronger and stiffer composites.[71] The SEM images also indicated uniform dispersion with no aggregation of CFB and a network it has created in the PLA matrix. This leads to a bridging effect when loaded in tension, meaning that the tensile properties are increased through better load transfer as well as limiting the crack propagation.[71]

The limitations of CFB/PLA composites are primarily because of their low tensile strength. Nevertheless, existing PLA applications can be enhanced with CFB for very little cost (just add CFB during the extrusion process). For example, PLA fibers are now used to make woven textiles for clothing. Addition of CFB can introduce additional insulation with minimal loss of strength. PLA plastics are also used for 3D printing and can have their ductility enhanced with CFB content.[71]

2.5.3 CF Quills (CFQ)/Recycled Polypropylene (RPP) Composites

Natural fibers have been used to reinforce recycled thermoplastics such as RPP to create greener composites. However, the inherent hydrophilicity of cellulosic fibers does not allow them to bond well with hydrophobic matrices such as PP and results in a weaker composite. To address this issue, Amieva et al. added CFQ in weight percentages of 5, 10, and 15% to RPP, and compared their properties to the properties of pure RPP in terms of density, dynamic modulus,

and thermal stability.[35] To prepare the specimens CFQ and RPP were premixed and then blended using a single screw extruder, after which the extruded material was pelletized. For dynamic mechanical testing the pellets were compression molded into CFQ/RPP composite specimens.

Density of the CFQ/RPP composites, at 0.75 g/cm^3, was lowest at 5 wt% of CFQ. This is a decrease from 0.946 g/cm^3 obtained for pure RPP. SEM images of CFQ/RPP fracture surfaces revealed that increasing quill content above 5 wt% increased composite density because voids in the matrix were replaced by CFQ.[35]

The dynamic modulus of the CFQ/RPP composites showed a maximum gain of over 50% from 965 MPa for pure RPP to 1451 MPa for the composites at just 5 wt% of CFQ. TGA measurements also showed an increase in thermal stability (higher Td) with increasing CFQ content.

The increased viscoelastic behavior, low density, and increased thermal stability of CFQ/RPP composites would lend them for use in many automotive and aerospace applications where lower weights are beneficial. By selectively using the quill, this composite can avoid the water retentive tendencies of other CF based composites. Thus, even in situations where moisture is prevalent, the hydrophobicity of this composite would allow it to retain its mechanical functionality.

CFQ/RPP composites can be easily made using existing manufacturing technologies. This can limit manufacturing costs. As mentioned earlier, the only additional step needed in the process would be to blend CFQ to the RPP during the extrusion process.

2.5.4 Stearic Acid Modified (SAM) SPI/Ramie Fiber (RF) Composites

RF is a cellulosic, natural fiber that has a wide range of engineering applications due to its hollow morphology. Low density, thermal insulation, and acoustic dampening are among the

many useful properties reported.[72] Lodha and Netravali used SPI, modified by stearic acid in the manner described by Section 2.4.2, as a matrix and reinforced it with unidirectionally aligned RF to fabricate a green composite.[73] These composites were characterized for their tensile and flexural properties.

To prepare the composite specimens, Lodha and Netravali first characterized various SPI and SAM-SPI resin compositions to optimize the respective resins' mechanical properties for use as matrices.[73] It was determined that for SAM-SPI resins, the optimal composition for mechanical properties was with 20% stearic acid and 0% glycerol. For SPI resins, the optimal composition was with 30% glycerol. With the optimal composition for SPI and SAM-SPI resins determined, RF/SPI and RF/SAM-SPI composites were assembled.

First, RF were spread parallel into thin sheets and impregnated with the precured resin solution. Three resin impregnated sheets were aligned unidirectionally, stacked, and had further resin introduced between each layer for better impregnation and inter-laminate adhesion. These sheets were oven dried at 35 °C for around 24 h, after which they were placed in aluminum molds and hot pressed to fully form the composite.

The tensile results showed that modifying the SPI with stearic acid increased the Young's modulus from 3.42 to 5.82 GPa, the tensile fracture stress from 180.2 to 267.5 GPa, and decreased the tensile fracture strain slightly from 9.02 to 8.42% in the axial direction. The RF's Young's modulus, tensile fracture stress, and tensile fracture strain values were found to be 15.5 GPa, 525.9 MPa, and 3.5% respectively, in the axial direction. This difference was attributed to the SAM-SPI resins absorbing less moisture than their SPI counterparts. They reported that during curing, a higher moisture content leads to void formation through vaporization and

induces longitudinal fiber compression through shrinkage, both of which decrease tensile properties.[73]

The flexural results showed the addition of stearic acid to SPI increased the chord modulus from 7290 to 13,970 MPa, the flexural stress from 106.8 to 184.6 MPa, and slightly decreased the flexural strain from 2.84 to 2.26% in the lengthwise direction. In the crosswise direction the chord modulus increased from 719.6 to 2670.5 MPa, the flexural stress increased from 14.33 to 22.67 MPa, and the flexural strain decreased from 2.75 to 0.96%.[73]

With the reduction in moisture absorbance and increase in mechanical properties compared to RF/SPI composites, RF/SAM-SPI composites could be used to replace moderate-strength petroleum-based plastics. The thermally and acoustically insulating nature of RF could lend this type of composite to be used in sound-proof paneling.

2.6 GREEN RESINS AND COMPOSITES PRODUCED IN THIS WORK

The present research describes the synthesis of green SPI based resins modified by varying fractions of CFF. These resins were then used as the binding matrix to fabricate green composites reinforced by JF. GA-crosslinked CFF/SPI resins and JF/(CFF/SPI) composites were also fabricated for comparison. Mechanical, thermal, and flammability characterization of the various CFF/SPI resin and JF/(CFF/SPI) composites were thoroughly conducted to assess their suitability as replacements for conventional, petroleum-based composites. Additionally, CFF/SPI resins underwent ATR-FTIR and moisture regain characterization to investigate chemical changes and moisture regain under conditioning.

CHAPTER 3

EXPERIMENTAL MEDTHODOLOGY

3.1 MATERIALS

Chopped chicken feather fibers (CFF) were acquired from Prof. Justin Barone of Virginia Polytechnic Institute and State University (Virginia Tech). Soy protein isolate (SPI) powder (PRO FAM® 974) was obtained from Archer Daniels Midland Company (St. Louis, MO). High purity D-Sorbitol was procured from VWR Life Science (Radnor, Pennsylvania), and glutaraldehyde (GA) solution (Grade II, 25% in H_2O) and sodium hydroxide (NaOH) pellets were purchased from Sigma-Aldrich (St. Louis, MO). Teflon® molds for resin casting were produced using 0.508 mm natural virgin polytetrafluoroethylene (PTFE) from ePlastics.com (San Diego, CA). Jute fabric (JF) was purchased from JOANN Fabrics (Ithaca, NY). A photographic image of the fabric swatch is shown in Figure 4.

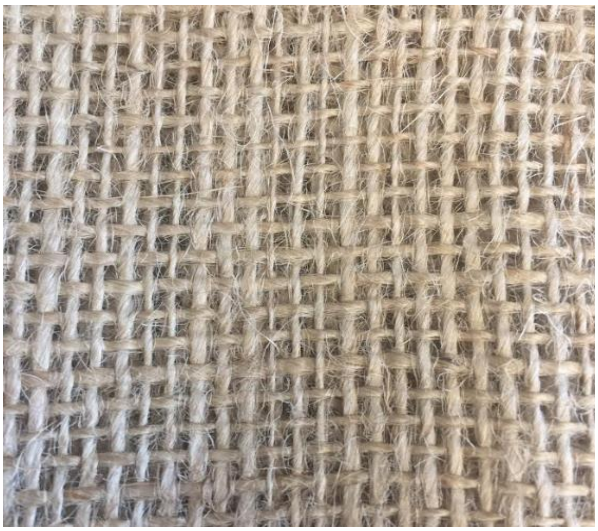

Figure 4: Jute fabric purchased from JOANN fabrics

3.2 FABRICATION

3.2.1 Preparation of CFF/SPI Resins for Flammability Characterization

Pure SPI and CFF/SPI resins were prepared using the following procedure and denoted by their weight fractions, i.e., a X/Y resin contains X percentage of CFF by weight and Y percentage of SPI by weight. The weight fraction of CFF was varied from 0% (pure SPI) to 30% by increments of 10%. The same process was repeated with the application of GA to create externally crosslinked resins. If a resin used GA, the term "wGA' was added after the X/Y ratio, i.e., a 30% CFF GA crosslinked resin will be denoted as 30/70 wGA. GA crosslinked resins are hereafter referred to as GA resins, while resins synthesized without the application of GA are referred to as GA-free resins.

This resulted in eight (four GA free, four with GA) unique compositions of CFF/SPI resins. Each unique composition was prepared at three different times to create a total of 24 resins for testing purposes and confirming the reproducibility of the results.

First, the Thermo Fisher Scientific Precision (Waltham, MA) convection oven was set to a temperature of 49 °C. A water bath was prepared and placed on top of a stirring hot plate set at 80 °C. This was done at the beginning so both can warm up while the rest of the procedure can proceed. In a 600 mL beaker, 15 g of total protein (SPI + CFF) were weighed out in the desired proportions. For example, for the 30/70 resin, 4.5 g of CFF and 10.5 g of SPI were weighed. To this, 165 g of DI water (1:11 SPI+CFF:DI water by mass) was added and hand mixed using a spatula. 4.6 mL of 4 M NaOH was added to this mixture until a pH of 11 was reached. After homogenizing the solution for 15 min, the beaker was transferred to a hot plate and a magnetic stirrer was placed into the beaker and stirred at 280 RPM at 80 °C for an additional 15 min. During this second 15 min period, 1.5 g of D-Sorbitol (10:1 SPI+CFF:D-sorbitol by mass), to be

used as plasticizer, was measured out. If the resin was intended to be crosslinked, 1.5 g of GA (10:1 SPI+CFF:GA by mass) was weighed out during this time and added along with D-sorbitol after the end of this second 15 min period. If the resin was not crosslinked, only the D-sorbitol was added.

The amine-aldehyde Maillard reaction was allowed to proceed for 30 min, after which the contents of the beaker were transferred into a 12.7 cm x 12.7 cm Teflon® mold and placed into the convection oven set at 49 °C for until the resin weighed roughly 21 g. This took approximately 22 and ½ h.

Once removed from the oven, the resin sheets were sandwiched between Teflon® sheets and left to condition for 10 min at 120 °C on a Carver hydraulic hot press (Carver, 3891-4PROA00, Wabash, IN). After conditioning, they were hot pressed using 1.59 mm spacers at 120 °C, 9072 kgs, for 13 min to obtain 1.59 mm thick resin sheets for flammability characterization.

The resin sheets were then laser cut into 100 mm x 100 mm squares for cone calorimetry characterization and the leftover material was broken into 30-50 mg pieces for MCC characterization.

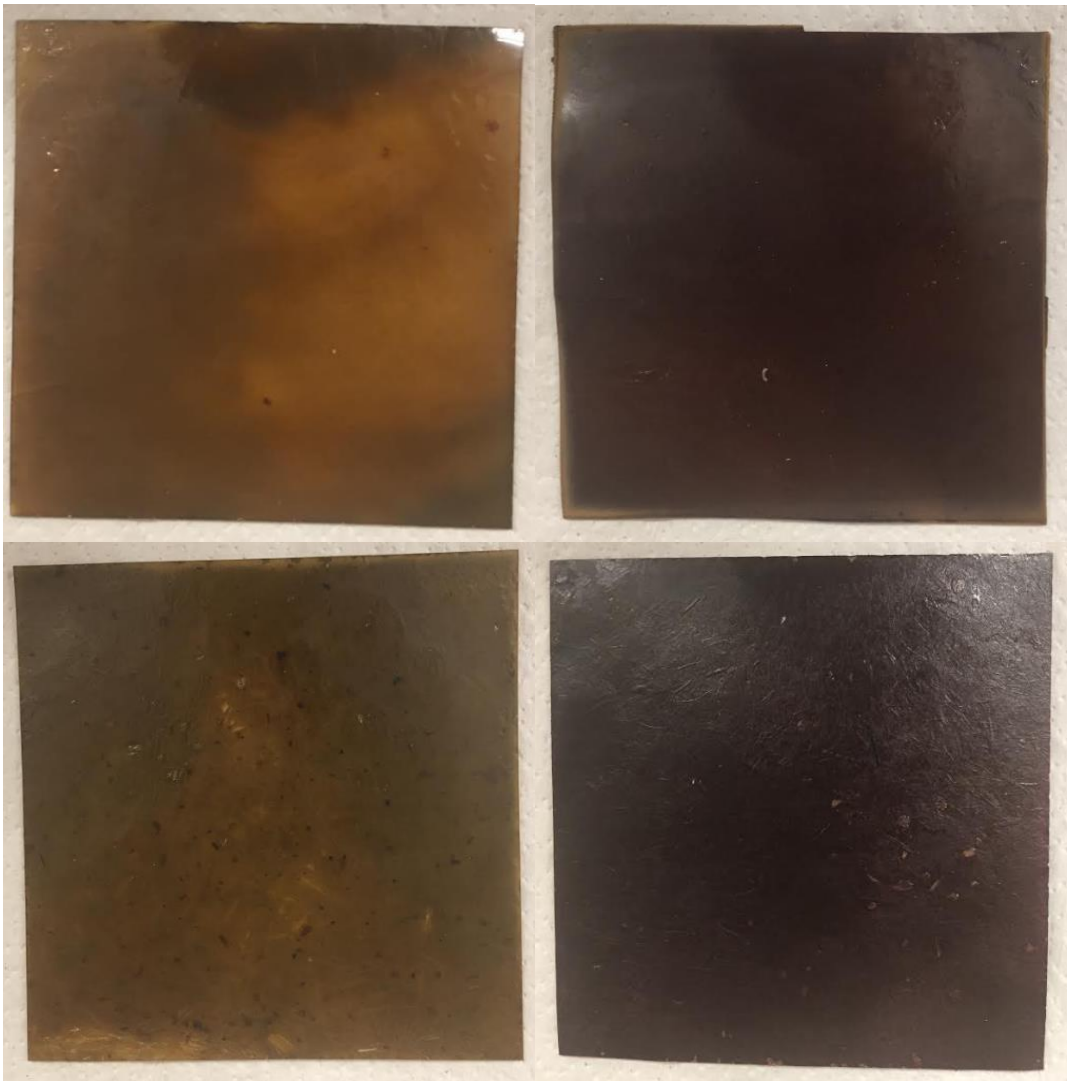

Figure 5: Clockwise from top left: 0/100, 0/100 wGA, 30/70 wGA, 30/70 resin sheets

3.2.2 Fabrication of JF/(CFF/SPI) Hybrid Composites for Flammability Characterization

Jute fabric was cut using a paper cutter into three 12.7 cm x 12.7 cm mats. The aggregate weight of these three mats was 10 g. Using the resin technique described in section 3.2.1, 15 g of resin was prepared in an identical manner up until the point in which they would be transferred into the molds to dry in the oven.

At this step, the resins were evenly applied to both sides of every jute mat. After the resin application, the three mats were stacked on top of one another, placed in a 12.7 cm x 12.7 cm Teflon® mold, and allowed to dry for an identical amount of time with respect to the resin process detailed in section 3.2.1 for parity (22 ½ h).

After the drying period, the stacked resin impregnated mats were hot pressed using the procedure detailed in section 3.2.1, i.e., 10 min of conditioning at 120 °C on the hot press prior to being pressed at 120 °C, 9072 kgs, for 13 min using 1.59 mm spacers.

Using this process, eight (four GA free, four with GA) unique compositions of JF/(CFF/SPI) composites were fabricated. Each unique composite composition was prepared at three separate times to create a total of 24 composite specimens to confirm the reproducibility of the results. All composites contained 60% resin and 40% fabric (jute), by weight. Note that the CFF component of the composite was counted towards the resin and not the fiber weight fraction.

The JF/(CFF/SPI) composites were then laser cut into 100 mm x 100 mm squares for cone calorimetry characterization and the leftover material was broken into 30-50 mg pieces for MCC characterization.

3.2.3 Preparation of CFF/SPI Resins for Moisture Regain, Mechanical, Thermal, Chemical, and Fracture Surface Characterization

Due to the COVID-19 pandemic related restrictions, lab time was minimized and reorganized, which led to the development of a new procedure, unique from the established SPI resin making procedure detailed in Section 3.2.1. Consequently, the following procedure led to resins that demonstrate different physical properties than the resins sent for flammability testing.

This note has been included for acknowledging the necessitation of this change. The chosen CFF/SPI resin compositions remained unchanged.

This procedure resulted in eight (four GA free, four with GA) unique compositions of resins. Each unique resin composition was prepared twice to create a total of 16 resin samples for testing purposes and confirming the reproducibility of the results.

First, the Thermo Electron LED GmbH Robert-Bosch-Straße, Isotemp 100 L Oven FA (Germany) oven was brought to an internal temperature of 61 °C. A water bath was prepared and placed on top of a stirring hot plate set at 80 °C. This was done at the beginning so both could warm up while the rest of the procedure could proceed. In a 600 mL beaker, 30 g of total protein (SPI + CFF) were weighed out in the desired proportion. For example, for a 30/70 resin, 4.5 g of CFF and 10.5 g of SPI were measured. To this, 330 g of DI water (1:11 SPI+CFF:DI water by mass) was added and hand mixed using a spatula. 4 M NaOH solution was added to this mixture, until a pH of 11 was reached. It was observed that the CFF did not contribute to the overall basicity and scaled linearly to the amount of SPI used to achieve a pH of 11, i.e., 9.2 mL of NaOH solution was used for a 0/100 resin, 8.2 mL for 10/90, 7.2 mL for 20/80, and 6.2 mL for 30/70.

After homogenizing the solution for 15 min, a magnetic stirrer was added into the beaker. The beaker containing the resin mixture was transferred to the hot plate and the temperature was raised to 80 °C while stirring at 280 RPM and left to warm up for an additional 15 min. During this second 15 min period, 3 g of D-sorbitol (10:1 SPI+CFF:D-sorbitol by mass), to be used as plasticizer, was measured out. For the resins intended to be crosslinked, 3 g of GA (10:1 SPI+CFF:GA by mass) was added along with D-sorbitol after the end of the 15 min period. For resins that were not crosslinked, only the D-sorbitol was added.

The amine-aldehyde Maillard reaction was allowed to proceed for 30 min, after which the contents of the beaker were transferred into a 12.7 cm x 12.7 cm Teflon® mold and placed into the convection oven set at 80 °C for approximately 46 h to form sheets for property characterization.

Once taken out of the oven, the resin sheets were sandwiched between Teflon® sheets and immediately placed on the Carver hydraulic hot press set at 120 °C and hot pressed using 1.5 mm spacers at 120 °C, 9072 kgs, for 13 min. Post hot pressing, the resin sheets were taken to be laser cut into 10 mm x 80 mm rectangular specimens. The rectangular specimens as well as leftover material were then left to condition in the conditioning room for 72 h maintained at ASTM conditions of 21 °C and 65% RH for moisture regain, mechanical, chemical, thermal, and fracture surface characterizations.

3.2.4 Fabrication of JF/(CFF/SPI) Hybrid Composites for Mechanical, Thermal, and Fracture Surface Characterization

Like the resin procedure described in section 3.2.3, the composites fabricated for mechanical, thermal, and SEM characterization were developed using a new procedure as because of COVID-19 related lab guidelines. The new procedure led to composites that demonstrate different physical properties than the composites sent for flammability testing. This note has been included for acknowledging the necessitation of this change.

Jute fabric was cut using a paper cutter into four 12.7 cm x 12.7 cm mats. The aggregate weight of these mats was roughly 16 g. Using the resin technique discussed in section 3.2.3, 30 g of resin was prepared in an identical manner up until the point in which they would be transferred into the molds to dry in the oven.

At this step, the resins were evenly applied to both sides of each jute mat. After application, the mats were stacked in a 12.7 cm x 12.7 cm Teflon® mold and left to dry for an identical amount of time with respect to the resin process detailed in section 3.2.3 for parity (46 h).

Upon removal from the oven, the composites were placed in between Teflon® sheets on the Carver Hydraulic hot press set at 120 °C and hot pressed using 2 mm spacers at 120 °C, 9072 kgs, for 20 min. Using this method, eight (four GA free, four with GA) unique compositions of JF/(CFF/SPI) composites were fabricated twice at two different times, to confirm the reproducibility, resulting in a total of 16 composites with 65% resin weight and 35% fiber weight. Note that the CFF component of the composite was counted towards the resin and not the fiber weight fraction.

Post hot pressing, the composites were taken to be laser cut into 10 mm x 100 mm rectangular specimens. These rectangular specimens as well as leftover material were then left to condition in the conditioning room maintained at the ASTM conditions of 21 °C and 65% RH for 72 h before characterizing their mechanical, thermal, and fracture surface properties.

3.3 TESTING

3.3.1 Optical and Geometric Characterization of CF Fractions

In order to determine which chicken feather parts were present in the procured CFF material, as well as to determine their geometries, small amounts of CFF were suspended in water on glass slides and observed under an optical microscope (Olympus BX51, Hamburg, Germany). Images were taken of different parts present in the CFF.

3.3.2 Geometric Characterization of the Jute Fabric

The woven jute fabric was characterized for its thickness as well as the warp (ends) and weft (picks) thread counts per cm, EPcm and PPcm, respectively. As per ASTM 1777-96, the thickness of the fabric was measured after conditioning it for 72 h at 65% RH and 21 °C. Thickness was measured using a Sherman W. Frazier compressometer, using a presser foot with a diameter of 25.4 mm (closest to the ASTM suggested diameter of 28.7 mm) and a pressure of 4.14 kPa. To obtain a representative thickness for the jute fabric, five separate fabric specimens were used, and for each specimen, thicknesses were measured at five separate locations and averaged.

3.3.3 Tensile Characterization of the Jute Fabric

Following ASTM D5035-11, the jute fabric was cut into 30 mm x 90 mm rectangular strips in both warp and weft directions. This was done to determine which of the two directions was stronger for preparation of the composites. After being cut to 30 mm, yarns were removed (unraveled) from both sides until the strip was reduced to 20 mm in width – which is the smallest width to be used for testing as designated by the ASTM protocol. This is wider than the final width of JF/(CFF/SPI) composite tensile specimens, which had widths of 10 mm.

The gauge length for testing the jute fabric was chosen to be 40 mm and parallel to the chosen direction, warp or weft, when tensile testing the composite specimens. Nine separate samples for both warp and weft directions were produced and characterized for their tensile yield strength, tensile fracture strain, as well as Young’s modulus.

3.3.4 Microscale Combustion Calorimetry (MCC) Characterization of CFF/SPI Resins and JF/(CFF/SPI) Hybrid Composites

Using the resins and composites produced, as described in section 3.3.1 and 3.3.2, four pieces, weighing between 30 and 50 mg, were obtained for each specific resin/composite composition and shipped to Professor Oisik Das in Luleå Tekniska Universitet in Sweden, for MCC characterization.

Following ASTM D7309, the eight unique resin compositions and eight unique composite compositions were tested to find their specific peak heat release rate, temperature at peak heat release rate, total heat released, and char yield.

For MCC characterization, specimens were placed in the sample chamber of a Deatak™ MCC-3 Microscale Combustion Calorimeter (St. McHenry, IL), and heated at a rate of 1 °C/s to a temperature of 703 °C. A combustor temperature of 900 °C was chosen for complete oxidation. Flow rates of 80 cc/min and 20 cc/min for N_2 and O_2 respectively were used for the pyrolysis and combustion process. Ultimately, each unique composition had three sets of data to obtain average values and standard deviations.

3.3.5 Moisture Regain of CFF/SPI Resins

After a CFF/SPI resin or JF/(CFF/SPI) composite was laser cut into rectangular specimens, they were taken to the conditioning room and weighed. For each CFF/SPI ratio, two samples were prepared, and from each sample, 10 specimens were produced. From this methodology, 20 specimens for each CFF/SPI ratio were produced. All 20 specimens were weighed individually and averaged to obtain the reported “average specimen mass pre-conditioning” reported in Table 6. After 72 h of conditioning at 65% RH and 21 °C, this

weighing process was repeated to obtain the reported "average specimen mass post-conditioning". Moisture Regain (% MR) was calculated with the following equation 1:

$$\%\, MR = \frac{m_1 - m_0}{m_0} * 100\%\,\% \qquad (1)$$

where m_1 is the average specimen mass post-conditioning and m_0 is the average specimen mass pre-conditioning.

3.3.6 Tensile Characterization of CFF/SPI Resins

All eight unique CFF/SPI resin compositions were characterized for their tensile yield strengths, Young's moduli, and tensile fracture strains using Instron universal tester (Instron) (Model 5566) as per ASTM D638. Prior to testing, the resin specimens were attached to tabs made from wooden tongue depressors using a high strength cyanoacrylate glue (Crazy® glue). This was done so that the specimens would not slip in the grips during testing and to obtain the true fracture characteristics. An untested resin specimen attached with wooden tabs and two tested (fractured) specimens are shown in Figure 6.

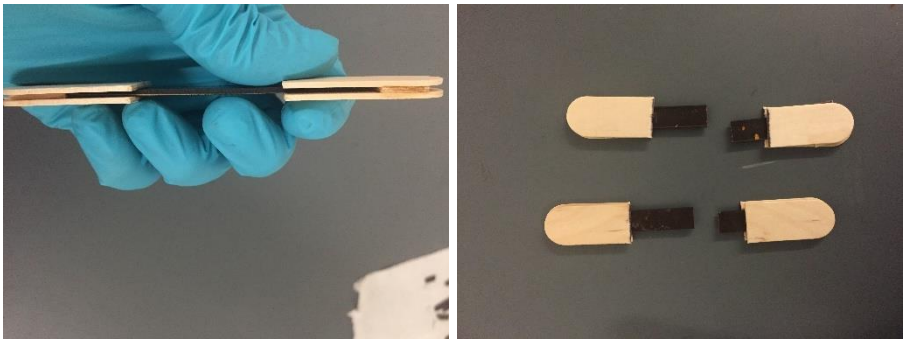

Figure 6: Resin specimen with wooden tabs (left) and two tested resin specimens (right)

The resin specimens were tested at 40 mm gauge length, 1 mm/min crosshead speed (strain rate of 0.025 min^{-1}), and gripped with a pressure of 0.45 MPa during testing. Eight resin specimens were tested for each sample. Over two samples, this meant there were sixteen data

entries for each unique composition to obtain average values and standard deviations. Data for specimens which showed fractures at or very near the grips were not used.

3.3.7 Tensile Characterization of JF/(CFF/SPI) Hybrid Composites

All eight unique JF/(CFF/SPI) composite compositions were characterized for their tensile yield strengths, Young's moduli, and tensile fracture strains. The tests were carried out on using Instron as per ASTM D3039. The composite specimens were tested at 40 mm gauge length, 2.5 mm/min crosshead speed (strain rate of 0.0625 min^{-1}), and were gripped with a pressure of 0.34 MPa during testing. Five composite specimens were tested for each sample. Over two samples, this meant there were ten data entries for each unique composition to obtain average values and standard deviations.

3.3.8 Flexural Characterization of JF/(CFF/SPI) Hybrid Composites

All eight unique JF/(CFF/SPI) composite compositions were characterized to obtain their flexural strength, flexural modulus, and flexural fracture strain using the 3-point bend tests. The tests were carried out using Instron 5566 as per ASTM D7264. The ASTM recommended span length to thickness ratio of 1:32 was maintained, thus the span length for testing was 64 mm. The crosshead speed used was 2 mm/min. Five composite specimens were tested for each unique ratio to obtain the average values and the standard deviations.

3.3.9 Attenuated Total Reflectance-Fourier Transform Infrared (ATR-FTIR) Characterization of CFF/SPI Resins

A flat section of each CFF/SPI resin specimen, post conditioning, was characterized at three different locations using a Perkin-Elmer FTIR Spectrometer (Waltham, MA) with a Perkin-Elmer Universal ATR sampling accessory (Waltham, MA) over a wavenumber range of 4000-600 cm^{-1}, with a resolution of 4 wavenumbers, and an accumulation of 16 scans. Each unique

composition had a sample size of two. With three tests conducted for each sample, there were a total of six spectra obtained for each unique resin or composite composition.

3.3.10 Thermogravimetric Analysis (TGA) of CFF/SPI Resins and JF/(CFF/SPI) Hybrid Composites

CFF/SPI resin and JF/(CFF/SPI) composite specimens, weighing 5-10 mg post conditioning, were characterized using thermogravimetric analyzer TGA-2050 (TA Instruments, New Castle, DE). The test was performed from 30 to 600 °C at a ramp rate of 20 °C/min under nitrogen flow of 40 mL/min (balance) and 60 mL/min (sample) to obtain TGA thermograms. Thermal degradation temperatures and derivative percent weight changes were obtained from these thermograms.

3.3.11 Differential Scanning Calorimeter (DSC) Characterization of CFF/SPI Resins and JF/(CFF/SPI) Hybrid Composites

CFF/SPI resin and JF/(CFF/SPI) composite specimens, weighing 5-10 mg post conditioning, were characterized in Tzero hermetically sealed aluminum pans, using DSC Q2000 (TA Instruments, New Castle, DE). The specimens were scanned from 30 to 330 °C at a ramp rate of 20 °C/min under nitrogen flow of 50.0 mL/min and the DSC thermograms were recorded. Thermal transition (Tm) temperatures and melting enthalpy changes (ΔHf) were obtained from these thermograms.

3.3.12 Scanning Electron Microscopy (SEM) of CFF/SPI Resin and JF/(CFF/SPI) Hybrid Composite Tensile Fracture Surfaces

Post tensile testing, CFF/SPI resin and JF/(CFF/SPI) composite specimens were mounted individually onto aluminum stubs with their fracture surfaces exposed, using double sided sticky tabs from Electron Microscopy Sciences (Hatfield, PA). They were then coated with

gold/palladium (Electron Microscopy Sciences, Hatfield, PA) prior to being placed in a Denton Vacuum V vacuum chamber (Moorestown, NJ). Fracture surface images were recorded using Zeiss SEM (Germany). Figure 7 shows what the composite specimens looked like after being coated, prior to SEM characterization.

Figure 7: Au/Pd coated JF/(CFF/SPI) composite specimens loaded for SEM analysis

3.4 STATISTICAL METHODS

Descriptive statistics employed were means, standard deviation (SD), and coefficient of variation (CV). To compare the effects of the additives between two groups, t-test with unequal variance was used. No adjustments due to multiple comparisons were made because of small sample sizes. Significance was determined at the 5% level. All statistical analyses were performed in Stata 17 (StataCorp LC, College Station, TX). P-values are presented in Appendix A.

CHAPTER 4

RESULTS AND DISCUSSION

4.1 OPTICAL AND GEOMETRIC RESULTS

4.1.1 Optical Images and Geometric Results of CF Fractions

Through optical imaging, the CFF provided was found to contain all parts of CF; quills, barbs, barbules, and hooklets. The CF was observed to have been "chopped". Essentially, during the processing phase, the CF was chopped to small pieces, which is an important observation as such an action directly affects the mechanical properties of the CFF. The geometry of these feather fractions was measured using scale bar measurements and pixel scaling and averages were found to be as follows: barbule length (seen at the top of barb): 510 μm, barbule length (seen in the middle of barb): 223 μm, barbule length (bottom): 111 μm, barb length: 645 μm, quill diameter: 7.08 μm, quill length varied too significantly due to chopping, to have an accurate estimate. These parts of the CF are shown in Figure 8.

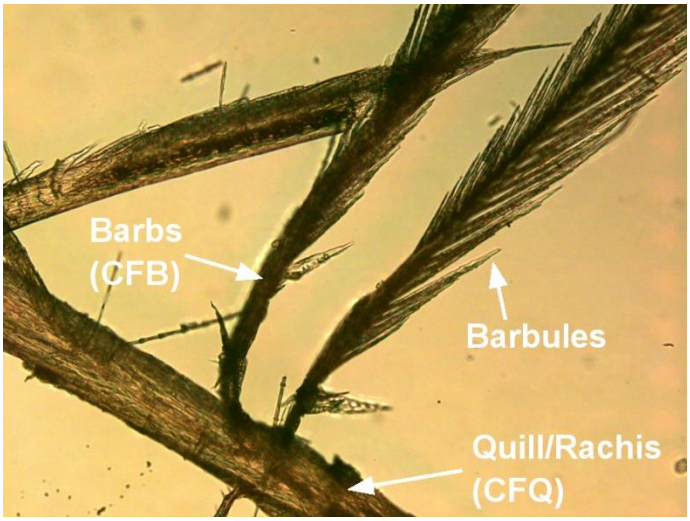

Figure 8: Optical microscopy image of CFF taken at 20X magnification

4.1.2 Geometric Results of JF

Thickness of the JF was determined to be 0.889 mm.

In the warp direction there were 60 yarns every 12.7 cm, or roughly 4.73 yarns/cm. In the weft direction there were 40 yarns every 12.7 cm, or roughly 3.15 yarns/cm.

4.2 FLAMMABILITY RESULTS

4.2.1 MCC Results of CFF/SPI Resins

Table 4 reports the summary of specific peak heat release rate (pHRR), the temperature at pHRR (TpHRR), and the total heat released (THR) results obtained for the CFF/SPI resins.

Specific HRR refers to the rate at which combustion heat is released per unit of initial mass of specimen during controlled thermal decomposition. HRR is considered the most crucial parameter to assess a material's fire hazard.[74] Heat generates more heat as a material burns, and a high HRR aids in spreading fire by more readily aiding in the release of additional heat energy in a positive-feedback loop. Specific pHRR is defined as the maximum specific HRR measured during testing. Thus, the pHRR reveals material's peak potential to contribute to fire hazard. Typically, the parameter heat release capacity (HRC), defined as $HRC = \frac{pHRR}{heating\ rate}$ J/g-K, is also included in flammability report. However, since the heating rate was maintained at a constant 1 °C/s during this testing, HRC and pHRR share the same value and is consequently trivial to include both. TpHRR is the temperature at which the pHRR occurs. Specific total heat rate (THR) is the integral of the specific HRR vs temperature plot, and thus gives the total heat released through combustion of a specimen per unit initial mass. Char yield is the percent mass left post characterization (test) and acts as a supplemental parameter to understanding THR. During pyrolysis a polymer specimen will often develop a char layer which generally acts as heat

insulation and decreases the mass flux of the specimen. Flame retardant additives can reduce flammability in a number of ways, most notably by improving thermal properties, altering pyrolysis pathways, diluting volatile gases, inhibiting chain reactions, and promoting high quality char formation.[75]

Char is essentially a carbonaceous layer that is formed on the outer part of the specimen as it is combusted. It is a critical parameter for flame retarding behavior as a high-quality char layer acts as insulation, preventing further combustion. Additives can help improve the char insulation quality. However, there is always an optimal ratio for additives, and incorporating an additive past this optimal ratio can result in a decrease in char quality and consequently an increase in flammability. Cracks and pores in the char layer can facilitate smoldering by providing a constant supply of oxygen. Smoldering is a type of combustion that can be facilitated by poor char quality propagating pyrolysis deeper within the specimen by focusing the heat flow through radiation or convection through cracks or pores. Post optimal ratios of additives can even result in delamination of the char layer which would result in the unpyrolyzed region to be exposed, further increasing flammability.

Table 4: Average MCC results of CFF/SPI resins

	0/100	**10/90**	**20/80**	**30/70**	**0/100 wGA**	**10/90 wGA**	**20/80 wGA**	**30/70 wGA**
N	3	3	3	3	3	3	3	3
pHRR (W/g)								
Mean	100.9	111.8	117.5	119.9	94.5	107.1	114.4	114.2
SD	(13.6)	(7.2)	(18.9)	(13.8)	(4.7)	(13.3)	(7.2)	(13.9)
CV	13.5%	6.5%	16.1%	11.5%	5.0%	12.4%	6.3%	12.2%
TpHRR (C°)								
Mean	330.7	331.3	330.1	330.8	335.6	332.8	334.0	326.9
SD	(6.3)	(5.9)	(8.7)	(2.5)	(8.7)	(4.5)	(4.7)	(4.9)
CV	1.9%	1.8%	2.6%	0.8%	2.6%	1.3%	1.4%	1.5%
THR (kJ/g)								
Mean	13.9	9.4	9.9	14.7	11.9	10.8	13.6	11.2
SD	(8.2)	(0.7)	(0.4)	(8.2)	(0.6)	(0.4)	(4.8)	(0.7)
CV	59.5%	7.6%	4.1%	56.1%	5.4%	4.1%	34.9%	6.1%

For GA-free CFF/SPI resins, the mean pHRR increased from 100.9 to 119.9 W/g as CFF% was increased from 0 to 30%. Average TpHRR stayed close to 330.7 °C as CFF% increased from 0 to 30%. Average THR initially decreased from 13.9 to 9.4 kJ/g as CFF% increased from 0 to 10%, and then increased to 14.7 kJ/g at 30% CFF. None of the differences between the mean parameters were statistically significant, other than pHRR for 0/100 wGA vs 20/80 wGA ($p = 0.021$).

For CFF/SPI resins with GA, the mean pHRR increased from 94.5 to 114.2 W/g as CFF% increased from 0 to 30%. Average TpHRR decreased from 335.6 to 326.9 °C as CFF% increased from 0 to 30%. Average THR initially decreased from 11.9 kJ/g to its minimum of 10.8 kJ/g as CFF% increased from 0 to 10%, and then increased to its maximum of 13.6 kJ/g with 20% CFF, before decreasing once more to 11.2 kJ/g at 30% CFF. None of the differences between the mean parameters reached significance. P-values can be found in Appendix A.1.

pHRR, TpHRR, and THR box plots are included in Figure 9 help visualize trends with the addition of CFF and GA.

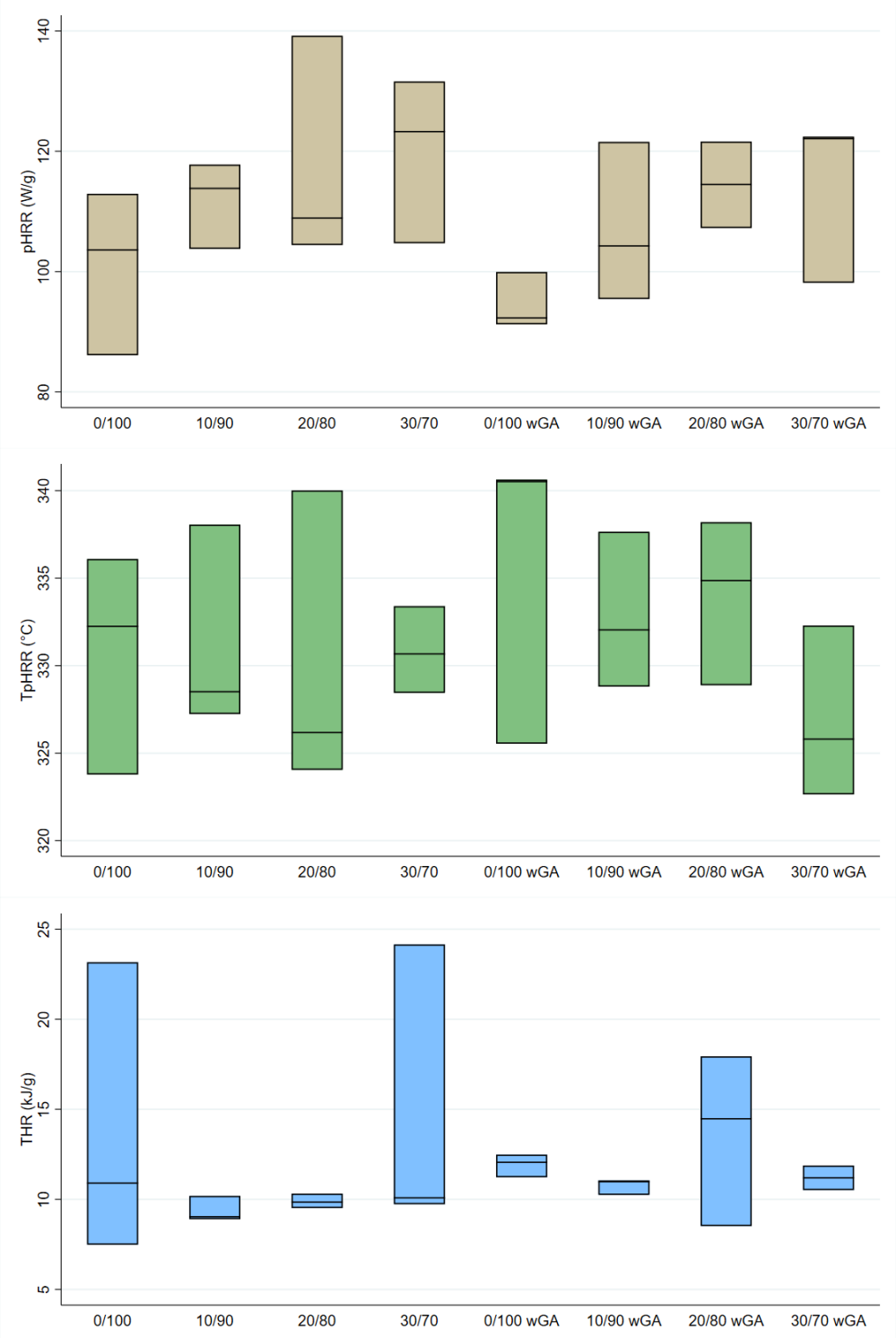

Figure 9: pHRR, TpHRR, and THR boxplots of CFF/SPI resins

Visual inspection of Figure 9 suggests that for pHRR, there is a general increase with the addition of CFF for CFF/SPI resins with and without GA. There is no discernible trend for TpHRR. However, for THR, it can be observed that there are CFF/SPI ratios for which variation is minimized. This large variation in pHRR and TpHRR and the low variation for certain CFF/SPI ratios can be understood from a materials analysis.

Determining flammability using solely MCC data without supplemental characterization techniques such as cone calorimetry must be done carefully. For example, consider the case of the MCC data indicating that the pHRR decreases while the THR increases as an additive is introduced. While the decrease in pHRR may be seen as improvement in flammability, this suggests that the host material was merely consumed at a point prior to the pHRR of the neat resin[76]. At the recorded pHRR of the specimen with the additive included, there was simply less fuel to consume and thus the pHRR was lower. However, the increase in THR illustrates the truth of the matter – that the additive increased the flammability of the material despite the pHRR decrease indicating otherwise.

Another danger of solely relying on MCC data for flammability characterization is its difficulty in considering critical fire retarding mechanisms such as flame inhibition, char production, and intumescing coatings. Flame inhibiting fire retardants decrease the combustion rate and increase the time till ignition by reducing the available oxygen for combustion. This causes the specimen to pyrolyze for longer which is illustrated by a higher reported THR. Thus, it is possible for flame inhibitors to falsely indicate that they increase flammability in MCC characterization by proxy of the higher reported THR. Furthermore, due to the smaller sample sizes used in MCC characterization, charring occurs much more rapidly than in other fire tests. This charring could potentially be so rapid that the entire specimen may char before any

improvement in fire performance can be observed. With factors such as these in mind and considering that the statistical analysis did not show significant changes given the small sample sizes, the following conclusions were drawn regarding the effect of CFF and GA on the flammability of the CFF/SPI resin specimens.

First, the effect of adding CFF to SPI resins was investigated. Figure 10 includes HRR vs temperature typical plots of typical GA-free CFF/SPI resins to demonstrate how the flammability parameters change with the addition of CFF.

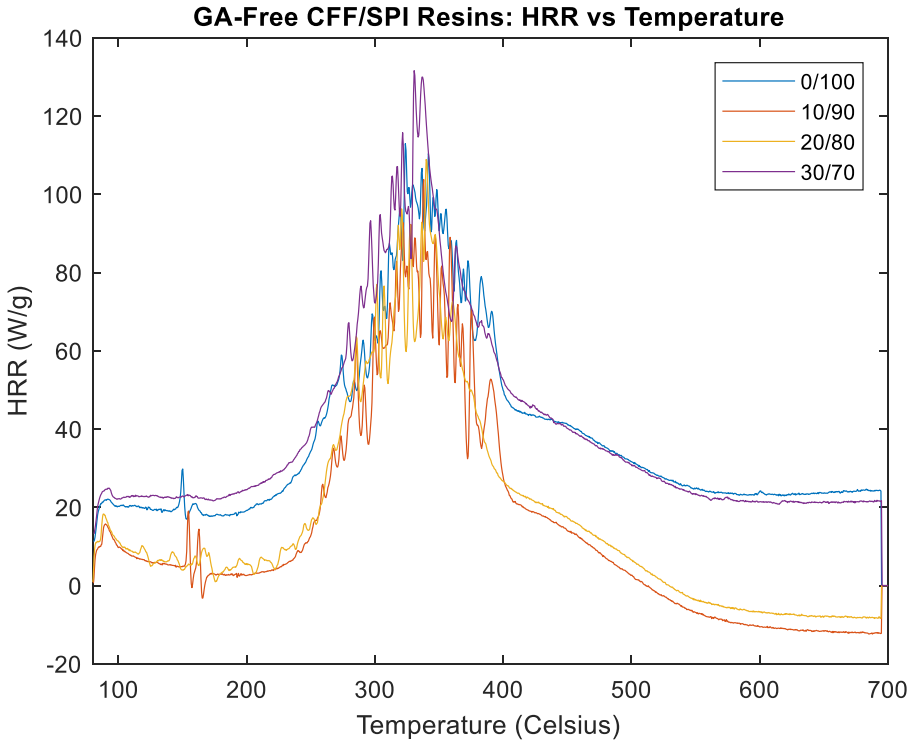

Figure 10: Typical HRR vs temperature plots of GA-free CFF/SPI resins

The plots in Figure 10 show that all CFF/SPI resins, regardless of CFF content, have spikes in HRR through pyrolysis. This behavior can be understood when accounting for the fact that both SPI and CFF are proteins that contain bound nitrogen.[77,78] Nitrogen is an inert, non-

flammable gas that prevents the formation of volatiles and dilutes the released gasses.[75] As the proteins undergo pyrolysis, they release heat and the bound nitrogen gas. Heat release is obviously illustrated by an increase in HRR, and the release of nitrogen would be illustrated by a rapid drop in HRR. Thus, these observed HRR spikes can be explained by the simultaneous release of heat and nitrogen.

The data in Table 4 indicate that for GA-free CFF/SPI resins, adding CFF increased the mean pHRR and the box plots did indicate a trend upwards with the addition of CFF. However, this does not mean that CFF is not a beneficial flame retardant additive. Additives with high heat release rates are known to increase pHRR values in MCC characterization despite cone calorimetry testing indicating that the additive reduces flammability.[76] This was experimentally proven in a study investigating the flammability of PC-siloxane copolymer, and how it changed when diphosphate was added to it.[76] Diphosphate was found to have a higher HRR, and the MCC characterization indicated that as diphosphate was increased from 0 to 100%, pHRR and THR increased from 159 and 9.8 to 400 W/g and 25 kJ/g, respectively. Yet, the cone calorimetry characterization revealed that adding diphosphate significantly reduced the THR and decreased the PHRR after 3.5% diphosphate added.[76]

The authors of the study hypothesized that the reason for this discrepancy was because the additive (PC-siloxane copolymer) most likely improved the char quality of the specimen, which was difficult to observe in the MCC characterization due to the high HRR of the additive.[76] However, by inspecting the THR values in the MCC characterization, the authors were able to identify the beneficial flame retarding features of the additive despite the increase in pHRR. They recognized a decrease in THR which is often tied to an improvement of char quality as the insulating layer would reduce overall heat release.[76]

The “false” pHRR increase described in this earlier study by Zhuge et al. parallels the results observed by adding CFF to SPI in this current work.[76] CFF reduced THR up until a certain ratio after which the pHRR and THR increased dramatically. This is likely due to the char quality developed during pyrolysis. Thus, the reason for the increase in pHRR as CFF is added could be due to the high HRR of CFF but may not necessarily indicate that CFF offer no flame retarding properties for SPI.

Moisture content and absorbance of additives can also influence MCC parameters. Water acts as a heat sink during pyrolysis, diverting the heat energy to evaporating the moisture.[79] This decreases the energy contribution for pyrolysis and is indicated by a decrease in THR and pHRR. However, the SPI used in this work is reported to have a moisture content of 4.8% ± 0.32.[80] In contrast, the various fractions that compose CFF have moisture contents that vary from 8.8 to 12.3%.[39] With regards to moisture absorbance, results presented in Section 4.3.1 will show that adding CFF to GA-free CFF/SPI resins increased moisture absorbance after 72 h of conditioning at 65% RH. Thus, the moisture content and absorbance of CFF is not attributed to the increase in pHRR and in fact may partially explain the decrease in THR.

Visual inspection of the THR boxplots presented in Figure 9 show that at 10 and 20% CFF content, variation is minimized. This can occur when char quality is optimized as the THR becomes consistent. Variability, pHRR, and THR increase past this ratio. The increase in pHRR is attributed to the potentially higher HRR of CFF given the decrease in THR. Since, the pHRR does not decrease with an increase in THR (a warning sign for a false positive correlation), CFF can be attributed to having positive flame retarding abilities for GA-free CFF/SPI resins. The influence of GA in conjunction with CFF is observed in the typical HRR vs temperature plots for CFF/SPI resins with GA shown in Figure 11.

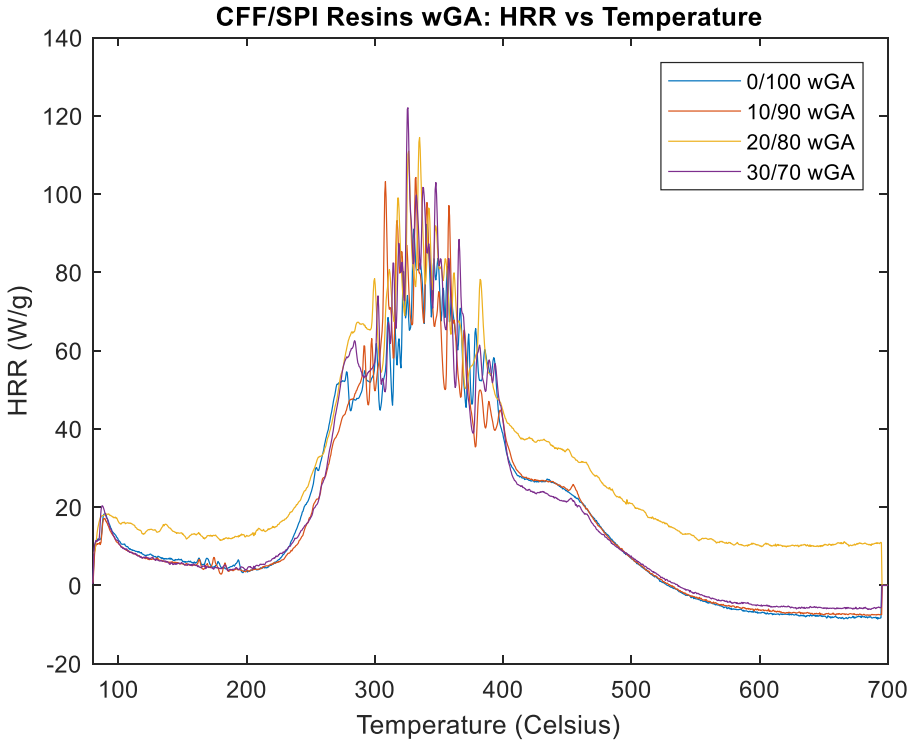

Figure 11: Typical HRR vs temperature plots of CFF/SPI resins wGA

The HRR vs temperature plots presented in Figure 11 mimic their GA-free counterparts in terms of behavior and thus the observed spikes are once again suspected to be due to the release of bound nitrogen.

The influence of CFF on the flammability of CFF/SPI resins with GA also parallel that of GA-free resins. CFF was seen to increase mean pHRR, but lower mean THR up till 10% CFF. As in the case with CFF/SPI resins without GA, 10% CFF was seen as the optimal ratio for CFF/SPI resins with GA. Above 10% CFF, variability, pHRR, and THR increased.

From the boxplots presented earlier in Figure 9 it is clear that there is little variation of THR for 0/100 wGA resins compared to GA-free 0/100. Synergistic crosslinking has been demonstrated in an earlier study to reduce flammability through the formation of compact char

layers that inhibit further combustion and by increasing the complex viscosity of the specimens during heating.[81] Thus, in the present case, GA seems to help improve flammability resistance through mechanisms attributed to synergistic crosslinking. This presents itself in the reduced variation in THR values.

In conclusion, while the small sample size limited the extent of statistical analysis, mean values and box plots gave trends to draw a materials analysis from. By inspection of the THR – which is tied to char quality – it can be observed that CFF and GA individually likely improve char quality. This theory can be given further credence if the MCC results for the JF/(CFF/SPI) composites report a similar trend with the addition of CFF.

4.2.2 MCC Results of JF/(CFF/SPI Resins) Hybrid Composites

Table 5 reports the summary of pHRR, TpHRR, and THR results obtained for JF/(CFF/SPI) hybrid composites.

Table 5: Average MCC results of JF/(CFF/SPI) hybrid composites

	0/100	**10/90**	**20/80**	**30/70**	**0/100 wGA**	**10/90 wGA**	**20/80 wGA**	**30/70 wGA**
N	3	3	3	3	3	3	3	3
pHRR (W/g)								
Mean	83.1	87.7	81.1	94.4	92.8	97.4	86.0	99.3
SD	(1.2)	(4.8)	(1.6)	(9.9)	(6.4)	(20.2)	(8.3)	(2.2)
CV	1.4%	5.5%	2.0%	10.5%	6.9%	20.7%	9.7%	2.2%
TpHRR (C°)								
Mean	336.1	335.8	330.5	328.9	331.6	335.5	331.6	331.9
SD	(0.7)	(1.1)	(4.2)	(4.3)	(5.8)	(3.1)	(3.7)	(5.4)
CV	0.2%	0.3%	1.3%	1.3%	1.8%	0.9%	1.1%	1.6%
THR (kJ/g)								
Mean	8.7	10.7	7.7	18.2	10.4	15.8	8.1	10.2
SD	(1.3)	(2.3)	(0.3)	(8.6)	(0.4)	(10.0)	(0.9)	(0.6)
CV	15.3%	21.6%	3.3%	47.6%	3.5%	63.4%	10.6%	6.2%

For GA-free JF/(CFF/SPI) composites, mean pHRR increased from 83.1 to 87.7 W/g with the addition of 10% CFF, was minimized to 81.1 W/g with 20% CFF and maximized to 94.4 W/g with 30% CFF. Average TpHRR decreased from 336.1 to 328.9 °C as CFF was increased from 0 to 30%. Mean THR increased from 8.7 to 10.7 kJ/g with the addition of 10% CFF, was minimized to 7.7 kJ/g with 20% CFF and maximized to 18.2 kJ/g with 30% CFF.

For JF/(CFF/SPI) composites with GA, pHRR increased from 92.8 to 97.4 W/g with the addition of 10% CFF, was minimized to 86.0 W/g with 20% CFF but maximized to 99.3 W/g with 30% CFF. Average TpHRR increased slightly from 331.6 to 335.5 °C with the addition of 10% CFF but decreased back to 331.9 °C as CFF was increased to 30%. Mean THR increased from 10.4 to its maximum of 15.8 kJ/g with the addition of 10% CFF, was minimized to 8.1 kJ/g with 20% CFF but increased again to 10.2 kJ/g with 30% CFF. None of the differences between the mean parameters reached significance, other than pHRR for 0/100 wGA vs 20/80 wGA ($p = 0.031$). pHRR, TpHRR, and THR box plots included in Figure 12 offer trends on how parameters change as CFF and GA were added.

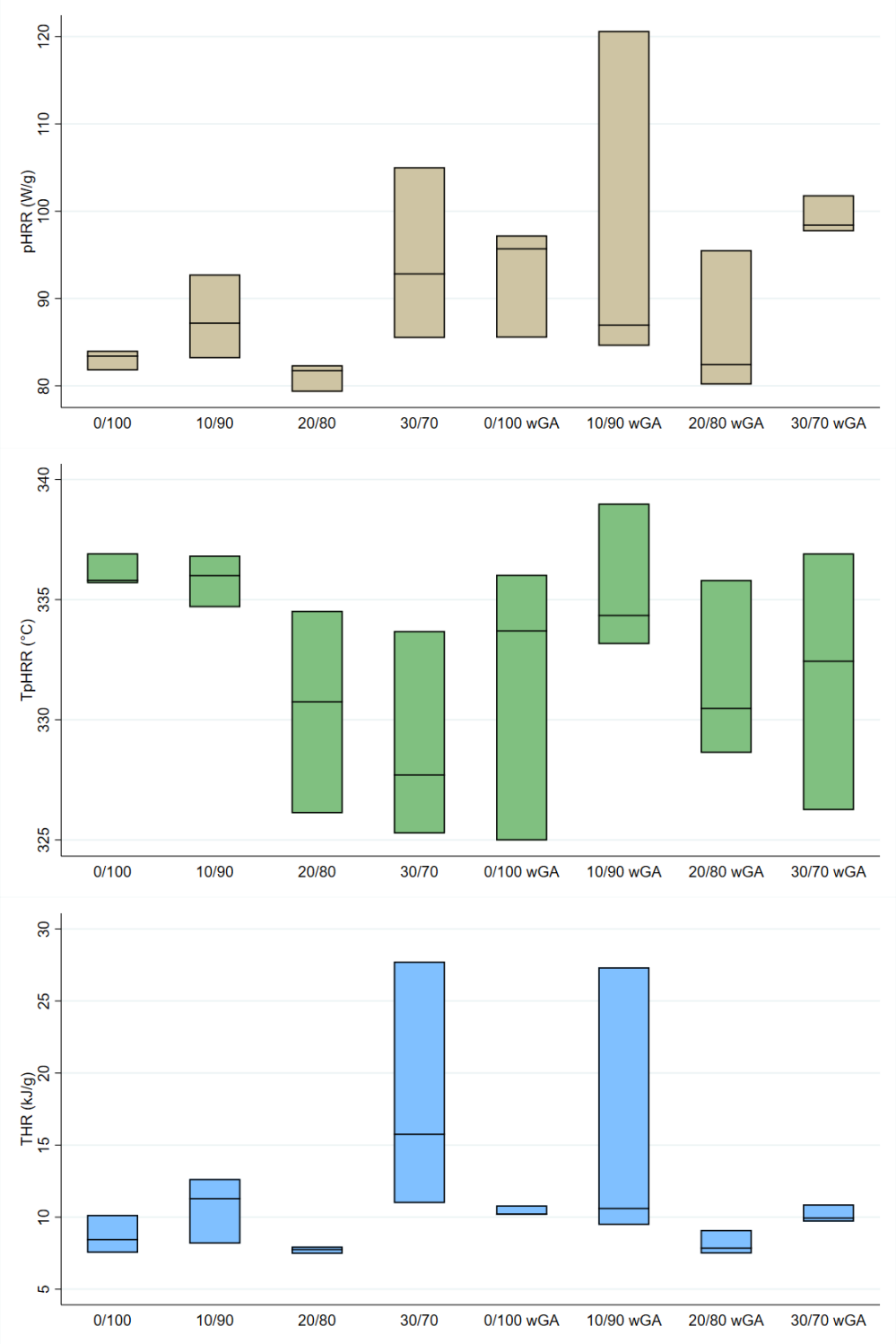

Figure 12: pHRR, TpHRR, and THR boxplots of JF/(CFF/SPI) hybrid composites

Visual inspection of the boxplots demonstrates that despite the statistical analysis not indicating any differences, there are CFF/SPI ratio in which data values do not even overlap – for example, JF/(0/100) vs JF/(0/100) wGA. If the data sets were bigger, the tests would likely have been confident enough to declare these two groups statistically different. With this is mind, the materials analysis will begin starting with the effect of adding CFF to GA-free JF/(CFF/SPI) composites. The HRR vs temperature plots for GA-free JF/(CFF/SPI) composites are included in Figure 12.

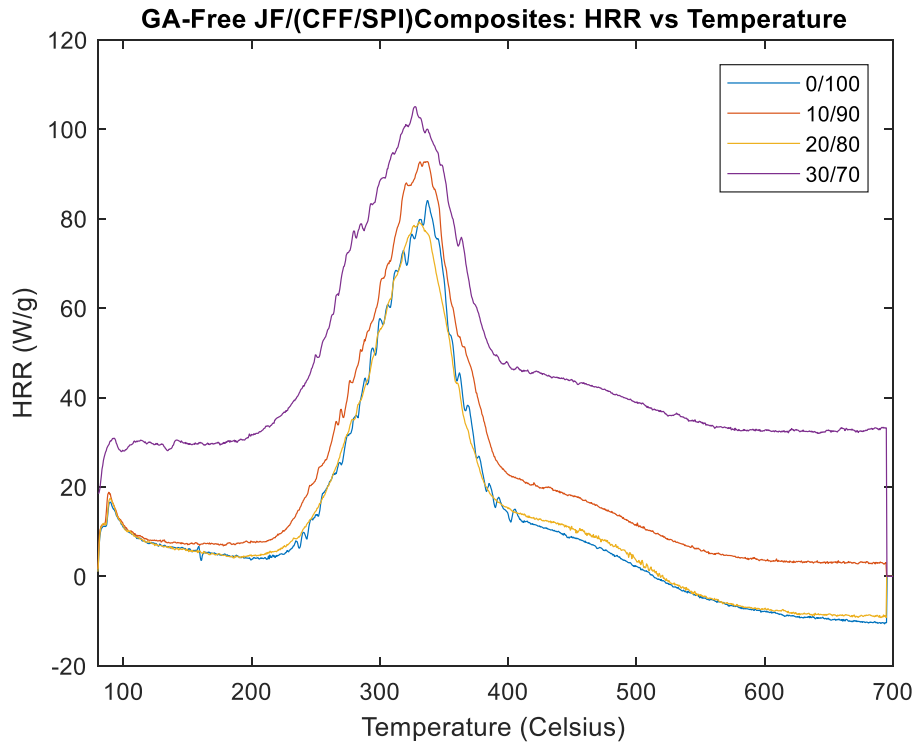

Figure 13: Typical HRR vs temperature plots of GA-free JF/(CFF/SPI) hybrid composites

Compared to the HRR vs temperature plots of the GA-free CFF/SPI resins, the plots of the GA-free composites have less pronounced releases of heat. That is, the HRR spikes observed during pyrolysis for the GA-free resins were more muted for the GA-free composites. This

makes sense since the CFF/SPI resin is only 60% of the total composite by mass (weight). Thus, the spikes, which were characteristic of the protein HRR behavior, were not as noticeable with the incorporation of JF.

CFF, in JF/(CFF/SPI) composites, optimized mean flammability properties (lowest mean pHRR and THR, and smallest variation) at the ratio of 20/80. The mechanism by which it decreases these properties is most likely through the creation of a high-quality char layer with the help of JF. This is likely the case as above 20% CFF content, the mean pHRR and THR, and variation increase which is typical of the char layer quality degrading as mentioned in the previous section.

Compared to the GA-free CFF/SPI resin specimens, the GA-free JF/(CFF/SPI) composites had significantly lower mean pHRR and THR values across respective CFF percentages. Since the composites were prepared with identical resin synthesis, precuring, and hot-pressing conditions with respect to the resin specimens, the thermal properties of the JF and/or the chemical interactions between the JF, CFF, and SPI creating during curing are attributed to the difference between the resins' and composites' flammability behavior.

The moisture content of JF is not attributed to the lower pHRR values reported in the composite specimens since JF only contains about 10% water (of total mass) in the conditioned state.[50] This is higher than the moisture content of SPI but within the range of CFF content. Yet, GA-free JF/(0/100) composites reported an average pHRR of 83.1 W/g and THR of 8.7 kJ/g which are, respectively, 17.8 W/g and a 5.2 kJ/g lower than the average PHRR (100.9 W/g) and THR (13.9 kJ/g) of 0/100 GA-free resins. Furthermore, as CFF is introduced, the composites still maintain lower pHRR and THR values. Thus, either the lignin content of JF, which is known

to increase thermal stability[82], or an interaction with CFF and SPI during curing helped some increase the overall thermal flammability of the composite.

The effect of GA is shown by the HRR vs temperature plots for JF/(CFF/SPI) hybrid composites with GA in Figure 14.

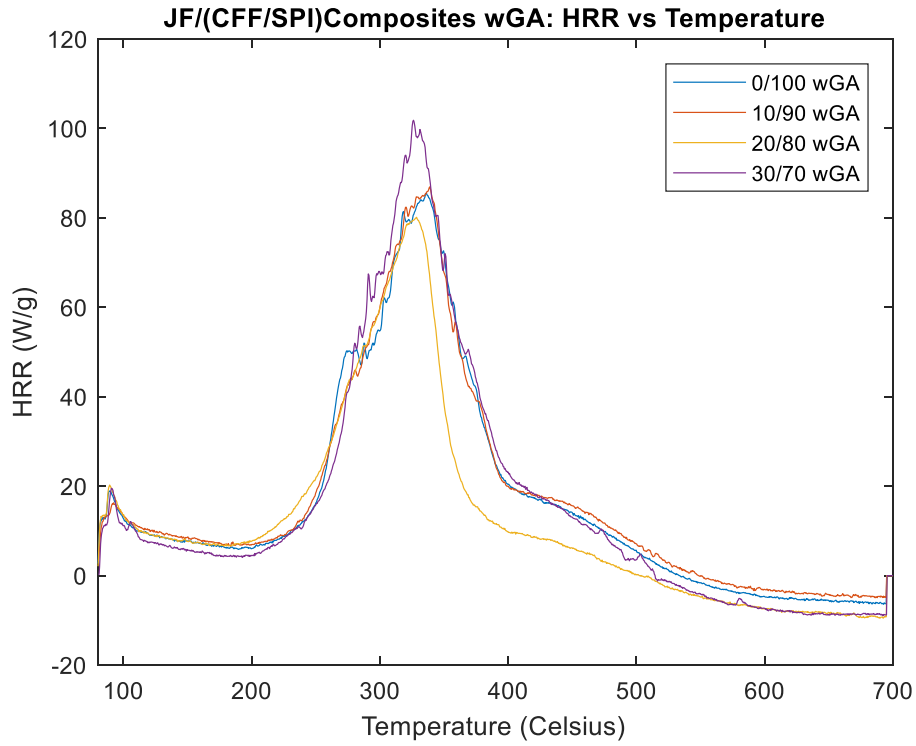

Figure 14: Typical HRR vs temperature plots of JF/(CFF/SPI) hybrid composites wGA

Unintuitively, the JF/(CFF/SPI) composites with GA had worse flammability properties (higher mean pHRR and THR) than GA-free JF/(CFF/SPI) composites despite the fact that results in the previous section indicated that GA crosslinking improved flammability properties of the CFF/SPI resins. There is no literature that has discussed the effect of GA on the flammability of jute. However, GA has been shown to improve thermal stability for chitosan-

based biofilms.[83] While chitosan is a biobased nitrogenous polysaccharide and JF is a lignocellulosic fiber, they share the closest chemical composition found in literature for the purposes of this comparison: 41.27% cellulose, 46% hemicellulose, and 7.4% lignin vs 64.4% cellulose, 12%, hemicellulose, and 11.8% lignin, respectively.[50,83] Although this study did not directly investigate the effect of GA on flammability, the addition of GA should theoretically only serve to benefit JF due to the similar chemical composition and the clear benefit to thermal stability. Thus, chemical modification of JF's thermal properties due to GA is most likely not responsible for the disproportionate increase in flammability observed when incorporating JF with its CFF/SPI with GA matrix. Instead, the most probable answer is that the GA modified JF produces a lower quality char compared to the GA-free JF composites. This decrease in char quality compared to GA-free JF likely resulted in composites with GA to have inferior flammability properties.

Ultimately, JF/(CFF/SPI) composites with and without GA had superior flammability properties compared to the CFF/SPI resins with and without GA, indicating that JF aids in reducing flammability regardless of the inclusion of GA. The introduction of JF and CFF negates the need for GA as GA-free JF/(CFF/SPI) composites had lower mean pHRR and THR values than JF/(CFF/SPI) composites with GA. With a larger sample size, there would likely be statistical proof to reinforce this materials analysis.

4.3 MOISTURE REGAIN RESULTS

4.3.1 Moisture Regain Study of CFF/SPI Resins

Table 6 reports the average masses of CFF/SPI resins before and after conditioning for 72 h at 65% RH and 21 °C to measure the moisture regain (MR).

Table 6: Average moisture regain values of CFF/SPI resins

	0/100	**10/90**	**20/80**	**30/70**	**0/100 wGA**	**10/90 wGA**	**20/80 wGA**	**30/70 wGA**
Average Specimen Mass Pre-Conditioning (g)	1.43	1.53	1.43	1.41	1.68	1.67	1.69	1.57
Average Specimen Mass Post-Conditioning (g)	1.47	1.56	1.47	1.46	1.72	1.70	1.72	1.60
MR (%)	2.77	2.78	2.85	3.78	2.07	1.85	1.81	1.84

The data from Table 6 indicate that for GA-free CFF/SPI resins, MR increased slightly from 2.77% at 0% CFF to 3.78% at 30% CFF. For CFF/SPI resins with GA, MR decreased slightly from 2.07% at 0% CFF to 1.85% with the addition of 10% CFF. Further additions of CFF past 10% CFF did not significantly change the MR for CFF/SPI resins with GA. CFF/SPI resins with GA were observed to be heavier both prior and post conditioning to their GA-free counterparts. This extra mass for CFF/SPI resins with GA is attributed to the additional mass of GA. At 0% CFF, the MR of GA-free resin was 2.77% as compared to 2.07% for the GA crosslinked resin. It can be expected that after crosslinking, the resins become denser, with less space for moisture to diffuse in. In addition, crosslinking reduces the number of polar groups, primarily amine ($-NH_2$), that attract moisture.

From these results it is not obvious what the effect of CFF is on MR for SPI resins, with or without GA. If CFF was simply absorbing more moisture relative to the SPI resin, then the SPI resins with GA should experience increased MR as CFF percentage increased. It is possible for GA-free CFF/SPI resins, the CFF interacted with the SPI in a way that exposed hydrophilic amino groups. Thus, as the CFF percentage increased in GA-free CFF/SPI resins, this hydrophilicity was increased. It is also possible that because of the complex shapes of the CFF, there were more voids within the GA-free resin which can attract and hold water, possibly in

those voids. However, this seems unlikely as the SEM images included in Section 4.7.1 did not reveal any such large voids that would also be applicable to CFF/SPI resins with GA. For the CFF/SPI resins with GA, the CFF, being protein, may have instead interacted with GA and crosslinked in such a manner to disrupt the established structures and bonds present for GA in its aqueous solution. This interaction between the CFF and GA perhaps would not create voids that could potentially formed in GA-free resins. It was observed during resin preparation that the 0/100 resin with GA had a significantly higher viscosity than the GA-free 0/100 resin, as could be expected because of the crosslinking. This viscosity was observed to decrease with addition of more water as well as with the addition of CFF. The mechanism by which CFF decreases viscosity for resins with GA is unclear. However, it could be because as the CFF percentage increases, the SPI percentage decreases, which would mean that the water added to the initial mixture (which is maintained a constant 330 g across all CFF/SPI ratios) would have a proportionally greater impact on decreasing viscosity for the CFF/SPI resin with GA. Higher concentration of GA are known to increase viscosity as a result of increased crosslinking.[61] The former would explain why the MR remained constant for addition CFF content past 10%, as the CFF (according to this theory) would only be interacting with the static 10% GA added across all CFF/SPI ratios with GA. The MR would be limited by the set saturated water produced through the CFF-GA interaction. For CFF/SPI resins with GA, the GA-crosslinked SPI likely does not interact in the same way as the GA-free SPI, which is why MR did not increase.

CFF/SPI resins with GA had lower MR values with respect to their equivalent GA-free CFF/SPI resins (i.e., 10/90 with GA had lower MR of 1.75% than the GA-free 10/90 MR of 2.78%). GA is known to decrease hydrophilicity in soy proteins by reducing hydrophilic groups, particularly the amino groups, as a result of crosslinking.[61]

4.4 MECHANICAL RESULTS

4.4.1 Tensile Results of JF

Table 7 reports the summary of peak tensile fracture stress, tensile strain at peak stress, and Young's modulus results obtained for the JF strips in both warp and weft directions. Typical tensile stress vs strain plots for warp and weft directions are shown in Figure 15. Note that the strain values included are tensile fracture strains at peak loads and not the tensile fracture strains at failure. This is because the criterion for failure was defined as 'the event when the Instron detected a 99% drop in load for one unit of extension'. Consequently, tensile fracture for the strips varied from 10% to up to 110% for both warp and weft directions. Additionally, for much of this duration past 20%, the stress values for the JF strips recorded were close to those at complete failure. Thus, the tensile strain at peak load was chosen as a better parameter for characterization.

Table 7: Average tensile results of jute fabric strips in the warp and weft directions

	Warp	**Weft**
N	8	8
Peak Tensile Stress (MPa)		
Mean	18.2	14.6
SD	(2.6)	(1.7)
CV	14.1%	11.3%
Tensile Strain at Peak Stress (%)		
Mean	7.6	8.0
SD	(0.8)	(0.8)
CV	10.2%	9.7%
Young's Modulus (MPa)		
Mean	332.4	278.0
SD	(45.4)	(42.3)
CV	13.6%	15.2%

The statistical analysis of tensile results of the JF strips indicated that the jute yarns in the warp direction were stronger ($p = 0.004$) and stiffer ($p = 0.026$) than the jute yarns in the weft direction. There was, however, no statistical difference in the strain ($p = 0.359$). This is to be expected, as the warp yarns undergo cyclic tension during fabric weaving and, as a rule, are spun to be stronger than the weft yarns. In addition, since the warp direction typically had more yarns/cm (on average two more yarns than the weft direction for the 2 cm width chosen for the strip test), the warp direction distributed the load among more yarns. This should, theoretically, result in a higher fracture stress along the warp direction. Consequently, the warp direction was chosen when producing composites for tensile and flexural testing.

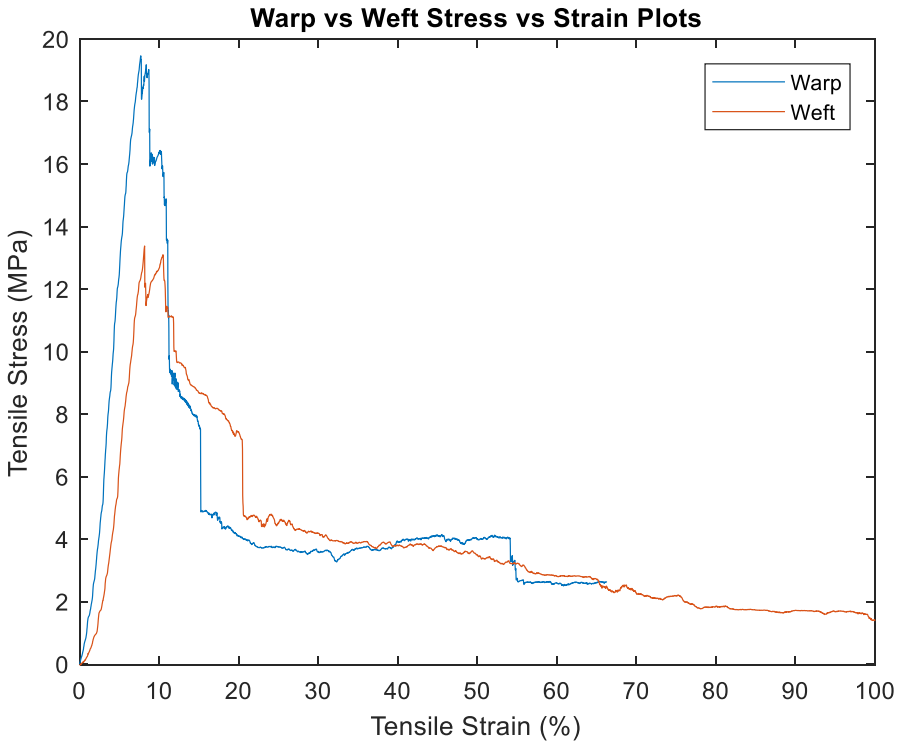

Figure 15: Stress vs strain plots of JF in warp and weft directions

As observed from Figure 15, JF fails in a stepwise manner in both the warp and weft directions. That is, for both directions, the fabric strip is loaded until the initial fracture of the weakest yarn occurs. The load is then transferred onto the remaining yarns which hold the load until the next weakest yarn fractures as the strain continues to increase. This process continues until the maximum load is reached. After enough number of yarns are fractured, the fabric specimen undergoes catastrophic failure. The stress vs strain plots of the fabric in both warp and weft directions clearly show instantaneous changes occurring in the stress values as the yarns break. It should be noted that in spite of the failure of the fabric specimen – as defined and detected by the Instron - the fabric still had a few unbroken yarns, although they had seen stress. Thus, as the composites were made with half the width of these strips, they could be expected to fail at lower strains.

4.4.2 Tensile Results of CFF/SPI Resins

Table 8 reports the summary of tensile fracture stress, tensile fracture strain, and Young's modulus results obtained for all ratios of CFF/SPI resins with and without GA.

Table 8: Average tensile results of CFF/SPI resins

	0/100	**10/90**	**20/80**	**30/70**	**0/100 wGA**	**10/90 wGA**	**20/80 wGA**	**30/70 wGA**
N	11	10	16	13	10	11	10	13
Tensile Fracture Stress (MPa)								
Mean	25.2	17.7	15.3	14.3	17.0	13.1	11.3	10.7
SD	(2.0)	(3.4)	(2.6)	(2.6)	(6.6)	(1.4)	(1.3)	(1.5)
CV	7.9%	19.1%	17.3%	18.5%	38.9%	11.1%	11.7%	14.3%
Tensile Fracture Strain (%)								
Mean	4.0	2.0	1.6	1.4	2.8	1.5	1.2	1.1
SD	(0.5)	(0.5)	(0.5)	(0.3)	(1.8)	(0.2)	(0.2)	(0.2)
CV	11.9%	27.6%	29.5%	19.4%	64.0%	13.2%	14.6%	16.0%
Young's Modulus (MPa)								
Mean	872.0	1125.0	1180.5	1298.2	914.4	1076.3	1164.5	1323.2
SD	(99.4)	(166.3)	(180.7)	(165.0)	(114.2)	(99.8)	(154.3)	(229.4)
CV	11.4%	14.8%	15.3%	12.7%	12.5%	9.3%	13.2%	17.3%

For GA-free CFF/SPI resins, the mean tensile fracture stress decreased from 25.2 to 14.3 MPa ($p = 0$), and average tensile fracture strain from 4.0 to 1.4% ($p = 0$), as the CFF content increased from 0 to 30%. However, the average Young's modulus increased by about 50% from 872.0 to 1298.2 MPa ($p = 0$) as the CFF content increased from 0 to 30%.

CFF/SPI resins with GA saw a similar decrease in mean tensile fracture stress from 17.0 to 10.7 MPa ($p = 0.015$) and mean tensile fracture strain from 2.8 to 1.1% ($p = 0.016$), with the addition of CFF from 0 to 30%. The average Young's modulus increased from 914.4 to 1323.2 MPa ($p = 0$) with the addition of CFF from 0% to 30%. GA-free CFF/SPI resins were statistically stronger and more ductile than CFF/SPI resins with GA. See Appendix A.4 for comparisons between respective groups. Tensile fracture stress, tensile fracture strain, and Young's modulus boxplots are included in Figure 16 to visualize trends.

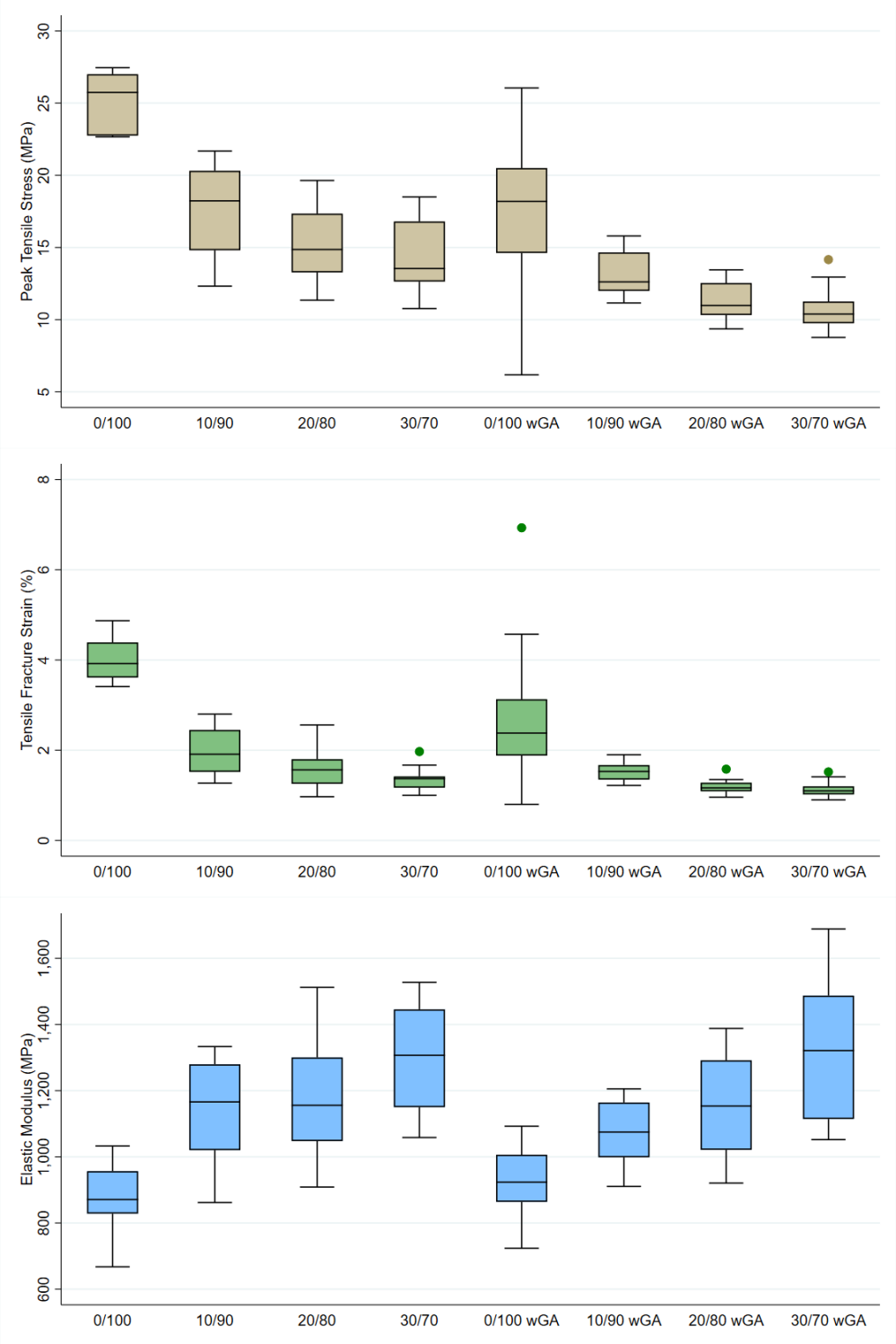

Figure 16: Tensile fracture stress, tensile fracture strain, and Young's modulus boxplots of CFF/SPI resins

Before investigating the effect of CFF and GA, the neat (0/100) SPI resins produced for mechanical testing were analyzed, given the surprising difference with neat SPI resins found in literature.

These results indicated that the methodology detailed in Section 3.2.3 produced neat (0/100) SPI resins that are stronger but more brittle than previous iterations of SPI resins. For example, Lodha and Netravali reported tensile fracture strength, tensile fracture strain, and Young's modulus of 6 MPa, and 204%, 98.7 MPa, respectively, for neat SPI resins containing 30% glycerol (a plasticizer).[11] This difference in mechanical properties is directly tied to the change in procedure as the materials used were the same.

The neat 0/100 (pure SPI) resin prepared as per the procedure described in Section 3.2.3 and tested as described in Section 3.3.6 had more than triple the fracture strength and more than 20 times the Young's modulus of even externally crosslinked traditional SPI resins from literature without the need for GA at all. It should be noted that GA is a toxic chemical compound and avoiding it can preserve the greenness of the resin. Despite its toxicity, GA, may have one advantage. It may prevent the termite and bug attacks on the composites. The resin synthesis procedure detailed by Lodha and Netravali served as a baseline for the pre COVID-19 resin preparation described in Section 3.2.1.[66] The differences between the previous procedure and the ones used in this work are described below.

Instead of glycerol, another polyol plasticizer – D-sorbitol – was used as the plasticizing agent. Resins in this work were prepared with only 10% plasticizer because preliminary resin tensile test results found that satisfactory ductility was achieved with this amount of D-sorbitol. While not directly detrimental to the environment, decreasing the amount of D-sorbitol used can decrease GHG emissions related to its production. Thus, minimizing plasticizer usage was a

design goal for the resin. Pre COVID-19 a slightly higher temperature of 49 °C instead of 35 °C was chosen for pre-curing as the increased number of specimens in the oven meant that a higher temperature was needed for a similar pre-curing time (~24 h). Post COVID-19, the temperature was raised to 80 °C, and the duration spent in the oven to ~46 h. Consequently, the resins produced pre COVID-19 were mechanically similar to those of past studies, but the resins produced post COVID-19 were not.

Figure 17 presents the stress vs strain tensile plots of 30/70 resin specimens prepared using the procedure detailed in Section 3.2.1 (bottom) as well as 3.2.3 (top) to illustrate the difference in mechanical behavior pre and post COVID-19. 30/70 resins are used instead of neat 0/100 resins since there were not enough data values pre COVID-19 for 0/100 resins. However, the difference is comparable. Test parameters were the same for both (specimen width, gauge length, strain rate, etc.), allowing for a valid comparison.

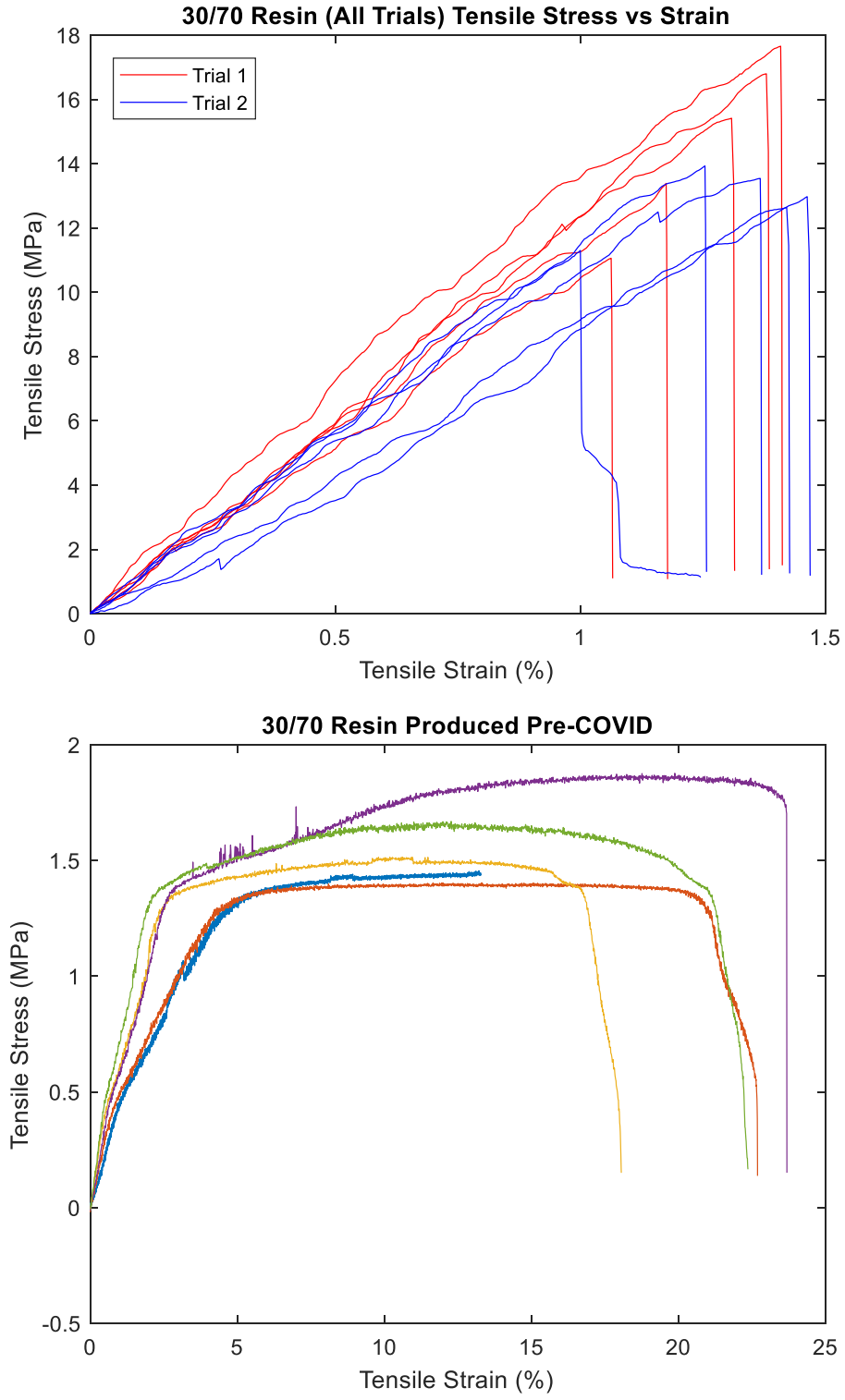

Figure 17: Tensile stress vs strain plots for 30/70 resins produced as per method described in Section 3.2.3 (top) vs that described in Section 3.2.1 (bottom)

As Figure 17 demonstrates, the 30/70 resins produced as per the procedure described in Section 3.2.1 (pre COVID-19) were far weaker (tensile fracture stress averaging 1.33 MPa) and more ductile (tensile fracture strain averaging 20%) than those produced post COVID-19 as per the procedure described in Section 3.2.3 (tensile fracture stress and strain averaging 14.3 MPa and 1.35%, respectively).

Improved tensile properties observed in neat SPI resins can potentially be attributed to two major factors with the new resin procedure: elevated temperature and extended time used for pre-curing. In previous studies resins were pre-cured for roughly 22 h at roughly 35 °C.[11]

As explained in Section 2.2, crosslinking can occur in SP based resins at higher temperatures without any external crosslinking reagent. This could be between –COOH and –OH groups forming ester groups as well as between $–NH_2$ and –COOH groups forming amide groups. The newly developed resin procedure doubled the amount of protein used which required a higher drying temperature of 80 °C as well as longer pre-curing time of 46 h. This fostered a more thermodynamically favorable environment for which some of the various internal crosslinking processes, mentioned above, could potentially occur.

A simpler explanation is that the amount of plasticizer was simply not enough given the CFF/SPI resins for tensile characterization. As mentioned earlier, water is an effective plasticizing agent, and the extended time and elevated temperature detailed in Section 3.2.3 to produced CFF/SPI resins post COVID-19 would have resulted in higher moisture loss compared to the resins produced using the procedure detailed in Section 3.2.1. In addition, previous iterations of SPI resins typically used between 20 to 30% plasticizer.[11,66] The CFF/SPI resins produced in Section 3.2.1 did not need to use as much plasticizer as they were prepared with a higher water:protein ratio and also a shorter, cooler pre-curing period.

Whatever the reason, the resulting neat, GA-free (0/100) resins had a larger tensile fracture stress (25.2 MPa vs 15.8 MPa) and a larger tensile fracture strain (3.99% vs 1.58%) than the 0/100 resins with GA. In fact, at every percentage of CFF added from 0 to 30%, GA-free CFF/SPI resins resulted in higher tensile fracture stresses and strains than the respective CFF/SPI resins with GA.

At first, this appears to contradict common sense, as logically, resins using an external crosslinking agent should be stronger and more brittle than the ones without, simply because of the extra resistance to deformation additional crosslinks provide. However, this behavior can be explained by once again examining the differences in resin preparation between the standard and new procedures. First, the GA-free CFF/SPI resins may have experienced internal crosslinking as previously mentioned. The evidence for crosslinking lies in the browning of GA-free resins produced post COVID-19. As Figure 3 illustrated, Maillard crosslinked SPI resins typically undergo a color change from yellow to brown. Neat SPI resins produced in literature as well as the neat SPI resins produced pre COVID-19 were indeed yellow as seen in Figure 5. However, the neat SPI resins produced post CVOID-19 using the methodology detailed in Section 3.2.3 had a deep brown color very close to that of GA-crosslinked SPI. This similarity in color between 0/100 and 0/100 wGA resins is observed in Figure 22. Possible reasons for crosslinking without the need of an external crosslinker are credited to the change in thermodynamic environment and explored more deeply in the ATR-FTIR analysis in Section 4.5.1. This level of internal crosslinking potentially observed in GA-free CFF/SPI resins might be somewhat comparable if not better than the level of crosslinking generated by adding 10 wt% GA.

Second, it was observed that GA containing CFF/SPI resins suffer far more from warping than GA-free CFF/SPI resins. Hot pressing warped materials results in residual stress

concentration to be introduced into the newly flattened resin. Though not visible to the eye, areas with high residual stress concentrations cause materials to fail prematurely during testing as the specimen bears not just the external load, but the internal stresses as well

For some ratios, such as 0/100 wGA, warping was so significant that hot pressing resulted in shattering in some parts of the resin. For this ratio specifically, fracturing during hot pressing resulted in needing to prepare multiple resin sheets as many of them were unsalvageable after hot pressing. Figure 18 shows what a successful (i.e., to be used for mechanical testing) 0/100 wGA resin post hot pressing looked like.

Figure 18: A 0/100 wGA resin post hot pressing

From the image of the hot pressed 0/100 wGA resin specimen in Figure 18, it is clear that there are regions in which the resin fractured from the main body during hot pressing. This was considered an acceptable resin specimen as there were smooth and visually defect-free areas that could be laser cut to create rectangular specimens for tensile characterization. The tensile stress vs strain plots for the 0/100 wGA resin are shown in Figure 19. These plots demonstrate that this

ratio of resin still suffered from mechanical variability attributed to the residual stresses retained post hot pressing. Note that some tests of the 0/100 wGA resin do illustrate tensile fracture stresses and strains that reach or even exceed the values found in GA-free 0/100 resins.[10,11] However, the average is much lower given the aforementioned residual stresses causing premature failure at lower loads.

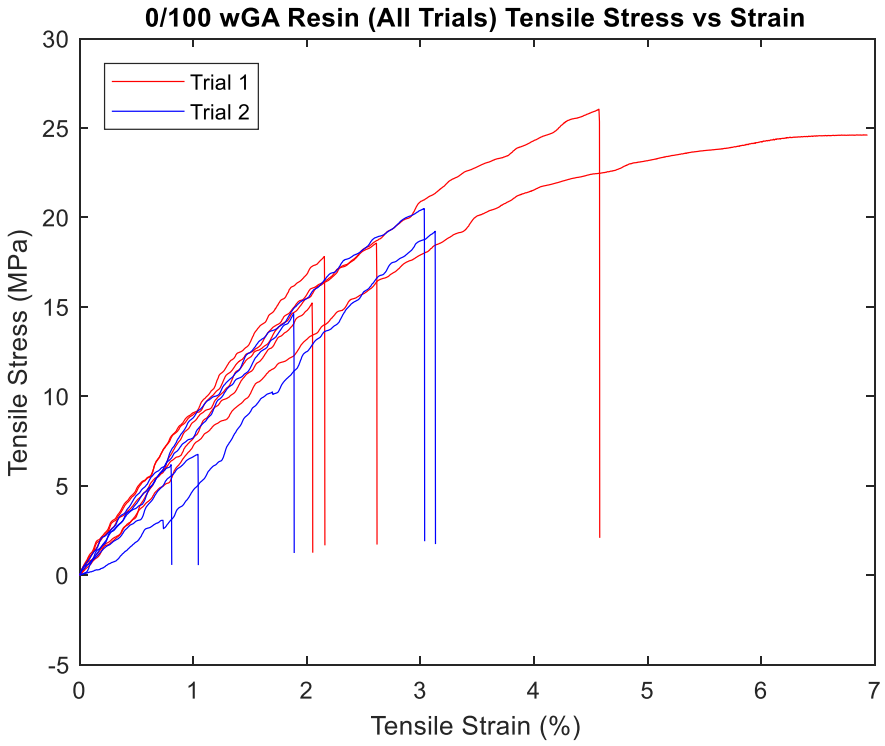

Figure 19: Tensile stress vs strain plots for all 0/100 wGA specimens

GA-free CFF/SPI resins, as well as any CFF/SPI resin with CFF, did not suffer from significant warping and, hence, were easier to hot press which would have minimized residual stresses. Figure 20 shows the tensile stress vs strain plots for the 0/100 CFF/SPI resins. The far

lower variability proves the correlation between warpage and mechanical variability.

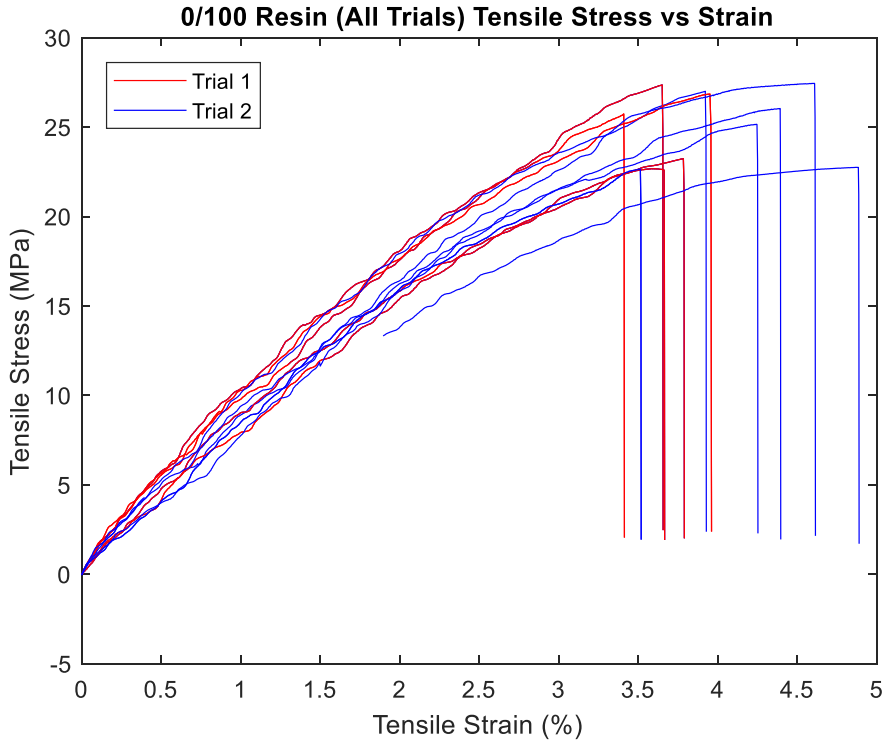

Figure 20: Tensile stress vs strain plots for all 0/100 specimens

The warping observed in CFF/SPI resins with GA is attributed primarily to the resin crosslinking since the GA-free CFF/SPI resins suffered minimal warping, in comparison. A possible explanation for this can be drawn from literature which agrees that while GA is clearly able to crosslink proteins due to nucleophiles being the most reactive side groups, the specific mechanisms under which the crosslinking occurs is still speculated upon.[60] This uncertainty may be partly due to GA not having a singular monomeric form in an aqueous solution. Rather, even under specific and controlled conditions, GA is present in a variety of structures – from a monomeric dialdehyde to several different polymeric structures.[60] From this variance arises argument on which form is predominantly responsible for crosslinking which further adds to the

confusion on identifying exactly what specific mechanisms are driving the crosslinking reaction.[60] Another complication is that GA, including the one used in this study, was commercially supplied in the form of an aqueous solution which introduces further variance in the relative abundances of GA's possible structures.[84]

This variation in GA structure and crosslinking mechanisms ensures that even though the resins were homogenously mixed and cast onto Teflon® sheets prior to being placed in the oven, there could exist a random distribution of GA crosslinking behavior, e.g., regions with different crosslink densities, throughout the resin. Furthermore, it has been noted that the introduction of GA does not result in the sole act of crosslinking, rather, there is a parallel aldol condensation process that occurs as well, producing water as a byproduct.[60] In addition, the ester and amide reactions mentioned earlier also produce water as condensate. Ultimately, this leads to an uneven drying across the resin, which is what is attributed to causing the significant warping present in the GA containing CFF/SPI resins.

Other factors contributing to overall warping experienced include uneven shrinkage that occurs during drying due to the temperature difference through the thickness of the resin, and mold restraint. These two reasons are why the GA-free neat resins also experienced slight warping. Temperature difference through the thickness is caused by the fact that only the top of the resin is open and exposed and, hence, experiences a different rate of cooling than the bottom of the resin, which is constrained by the mold. This differential causes the top side to shrink more than the bottom, leading to warping. Similarly, the mold that the resin was pre-cured in prevented shrinkage in that plane, resulting in more shrinkage through the thickness and causes stresses to accumulate on the surface of the resin, which eventually relaxes to cause warping.

Further analysis of the tensile parameters presented in Table 8 also appears to indicate that CFF has no beneficial contribution to the mechanical properties of the CFF/SPI resins with and without GA except the linear increase in the Young's modulus. Once again, delving into the resin preparation answers, at least in part, the reason behind these results.

As mentioned earlier, the neat, GA-free SPI resins (0/100) produced for tensile testing were far more brittle than resins prepared using the traditional procedure described earlier by Lodha and Netravali.[11,66] This brittleness was only further exacerbated by the addition of CFF. Standard knowledge on fiber-reinforced polymers state that typical composites employ a low strength, but ductile matrix reinforced by a much higher strength fibers to produce a composite material with the aggregate properties.[29]

Because the SPI matrix was so brittle and strong already, adding CFF did not increase tensile fracture strength. Furthermore, the CFF procured for this experiment was randomly chopped resulting in discontinuous, i.e., short fibers, that behave more as particulates and carry no significant load. CFF acting in this manner would still contribute to the observed increase in Young's modulus by restricting the movement of polymer chains, but this restriction in movement would decrease ductility and cause failure at lower strains. Despite not increasing the tensile strength, CFF does, in fact, help in producing superior CFF/SPI resins.

One noticeable benefit of incorporating CFF into both GA containing and GA-free CFF/SPI resins is the decreased extent of warping. Since fibers, unaffected by the crosslinking reaction, do not shrink or grow (stretch) during pre-curing or curing, they constrain the resin polymeric chains that would otherwise relax and result in resin warpage. This characteristic is rather helpful. Figure 21 illustrates the difference between a 0/100 wGA and 10/90 wGA resins prior to hot pressing.

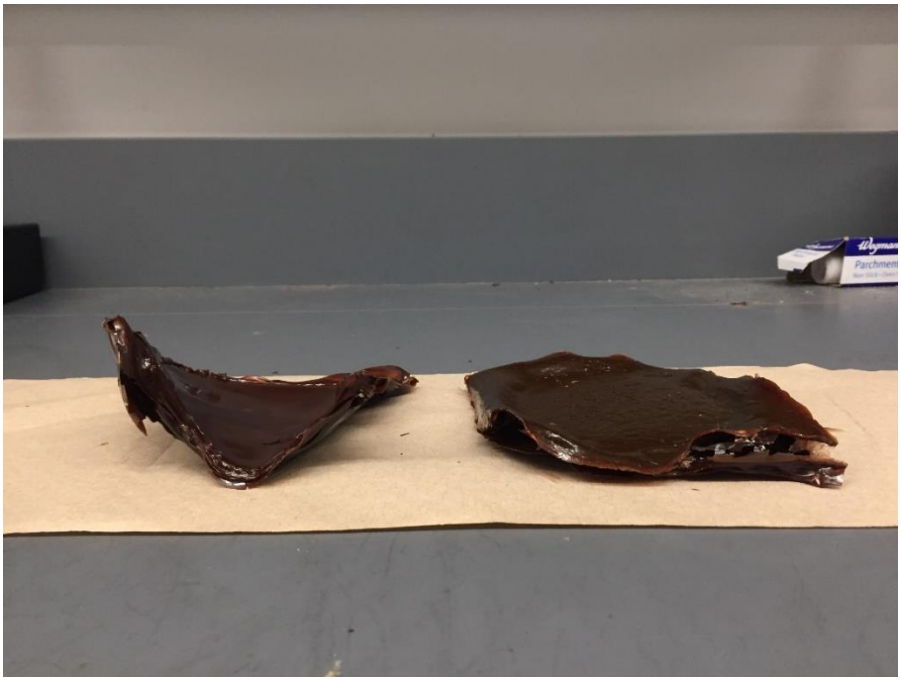

Figure 21: CFF/SPI resin specimens prior to hot pressing: (left) 0/100 wGA and (right) 10/90 wGA

After hot pressing, all CFF/SPI resins are initially flat and free of warping. However, post 72 h conditioning at ASTM conditions of 65% RH and 21 °C, the residual stresses that were retained post processing cause the neat resins to deform, the CFF/SPI resins with GA more so. Figure 22 shows the shadows of the warped resin specimens that give a good idea about the differences between a 0/100, 10/90, and 0/100 wGA tensile specimens after conditioning and just prior to testing.

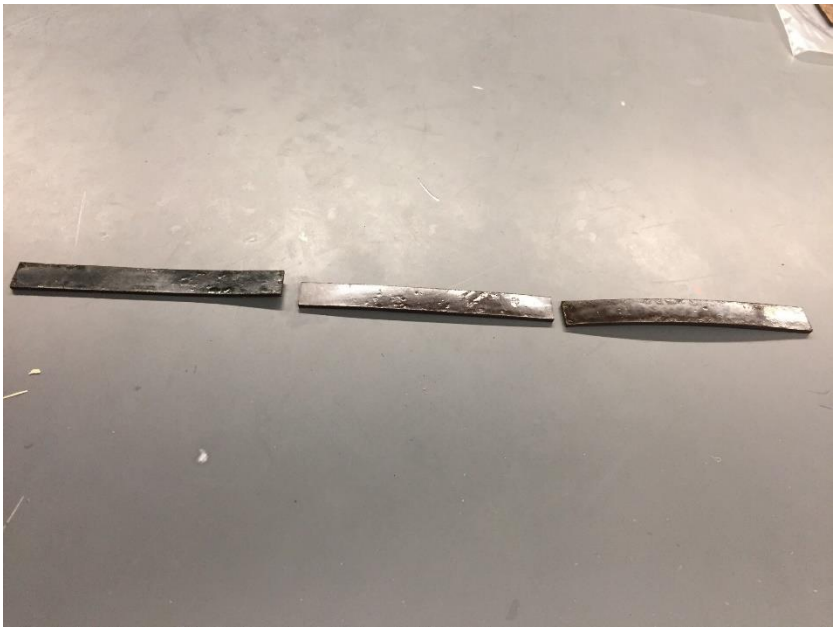

Figure 22: Tensile specimens showing warping. From left to right: 0/100, 10/90 wGA, 0/100 wGA

Pictures presented of warped tensile specimens in Figure 22 clearly show the differences observed among different resins. Controlling or eliminating warping is critical for green plastics and composites to be viable alternatives to commercially established petroleum-based resins/composites and, thus, the loss of tensile strength and strain may be considered a worthwhile sacrifice. Observations suggest that for GA-free CFF/SPI resins, just 10% CFF was enough to eliminate warping, while 20% CFF was needed for CFF/SPI resins with GA. However, once warping – and by proxy mechanical variability – was eliminated with 20% for CFF/SPI resins with GA, GA-free resins still reported higher fracture stresses and strains. Thus, processing cannot fully account for why GA-free CFF/SPI resins had better mechanical properties. It could be due to the theorized internal crosslinking, or perhaps due to CFF disrupting GA from crosslinking SPI.

The final piece of analysis that can be drawn from the data presented in Table 8 is that for some CFF/SPI ratios, the resin has a higher fracture strength than the JF strips. Also, for all CFF/SPI ratios, the resins had a lower fracture strain and significantly higher modulus than the JF. This meant that the CFF/SPI matrix would always be more brittle and stiffer than the weaker and more ductile reinforcing JF yarns. The composites that were tested in the following sections were thus expected to follow different behavior from conventional composites that employ a lower strength, ductile matrix and a stiffer, stronger reinforcing fiber.

4.4.3 Tensile Results of JF/(CFF/SPI) Hybrid Composites

Table 9 reports the summary of the peak tensile stress, tensile fracture strain, and Young's modulus results obtained for all ratios of JF/(CFF/SPI) composites with and without GA. Peak tensile stress was chosen instead of fracture as at higher percentages of CFF (20,30%), specimens would yield but not fail until much lower stresses. As a result, peak stresses were considered to be more comparable.

Table 9: Average tensile results of JF/CFF/SPI) hybrid composites

	0/100	**10/90**	**20/80**	**30/70**	**0/100 wGA**	**10/90 wGA**	**20/80 wGA**	**30/70 wGA**
N	8	8	8	9	8	9	9	9
Peak Tensile Stress (MPa)								
Mean	26.6	28.4	24.5	22.0	34.7	21.3	26.5	18.6
SD	(2.7)	(1.8)	(2.2)	(3.7)	(5.1)	(1.5)	(2.8)	(2.0)
CV	10.1%	6.4%	8.8%	16.6%	14.8%	7.0%	10.6%	10.8%
Tensile Fracture Strain (%)								
Mean	4.3	6.7	5.2	5.8	9.3	8.2	7.8	7.8
SD	(1.3)	(1.3)	(0.7)	(2.3)	(1.7)	(1.8)	(1.2)	(1.2)
CV	29.4%	18.9%	13.3%	38.7%	17.8%	21.8%	15.3%	15.0%
Young's Modulus (MPa)								
Mean	1278.7	1298.2	1321.2	1284.8	1129.5	1064.3	1213.3	1046.1
SD	(236.4)	(161.1)	(134.3)	(178.4)	(266.5)	(88.1)	(231.2)	(239.8)
CV	18.5%	12.4%	10.2%	13.9%	23.6%	8.3%	19.1%	22.9%

For GA-free JF/(CFF/SPI) composites, the mean peak tensile stress decreased from 26.6 to 22.0 MPa ($p = 0.01$). The average tensile fracture strain and Young's modulus did not change from 4.3 to 5.8% and 1278.7 to 1284.8 MPa, as the CFF content increased from 0 to 30%.

For JF/(CFF/SPI) composites with GA mean tensile fracture stress and mean tensile fracture strain decreased from 34.7 to 18.6 MPa ($p = 0$) and 9.3% to 7.8% ($p = 0.054$) respectively, with the addition of CFF from 0% to 30%. The average Young's modulus did not change significantly from 1129.5 to 1047.1 MPa as CFF was added.

Note that the statistical differences mentioned above are comparing overall trends, i.e., 0% vs 30% CFF. Appendix A.5 provides all statistical changes between respective groups. Peak tensile stress, tensile fracture strain, and Young's modulus boxplots are included in Figure 23 to visualize trends.

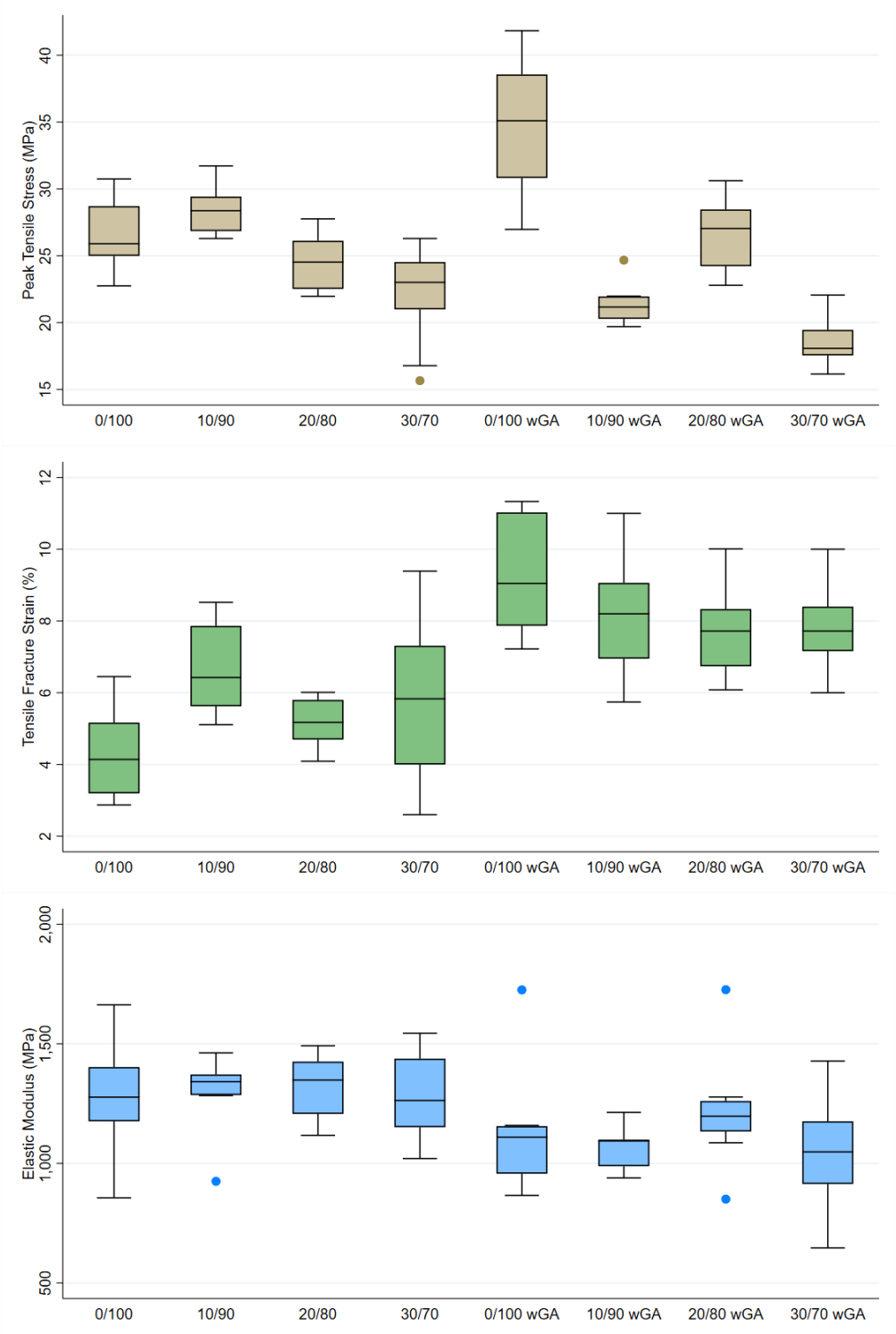

Figure 23: Peak tensile stress, tensile strain at peak tensile stress, and Young's modulus boxplots of JF/(CFF/SPI) hybrid composites

Comparing the tensile results presented in Table 9 for JF/(CFF/SPI) composites to those of the CFF/SPI resins provided in Table 8, it can be observed that despite preparing the JF/(CFF/SPI) composites in an almost identical manner to the CFF/SPI resins (only difference was thickness), their respective tensile behaviors was quite dissimilar.

Firstly, there was no clear correlation between the CFF percentage and the tensile parameters for JF/(CFF/SPI) composites with or without GA. For the CFF/SPI resins with or without GA, it was shown that with every consequent addition of CFF (0 to 10%, 20 to 20%, etc.) the tensile fracture strength and strain decreased, and Young's modulus increased.

Although the overall trend (from 0 to 30% CFF) remained same for GA-free composites, this was not true for JF/(CFF/SPI) composites with GA. In addition, tensile strength and strain were maintained with some addition of CFF. For example, for GA-free JF/(CFF/SPI) composites, mean peak tensile stress was maximized at 28.4 MPa with 10% CFF and tensile fracture strain increased as CFF was added. This retention of mechanical properties can be explained by comparing the tensile properties of the CFF/SPI resins used as the matrix at every percentage of CFF.

At 0% CFF, the GA-free 0/100 resins reported a higher peak tensile fracture stress (25.2 MPa) than that obtained for JF strips (18.2 MPa). This would mean that matrix for the GA-free JF/(0/100) likely was holding majority of the load, not the JF. Once the 0/100 matrix failed, the entire JF/(0/100) composite should instantaneously fail given that the JF was too weak to carry the load. This is reinforced by the data showing that the JF/(0/100) fails at 26.6 MPa and 4.3% strain, very close the 0/100 resin failure at 25.2 MPa and 4.0% strain. Figure 25 shows the fracture of a JF/(0/100) tensile specimen to further prove this point. As a reminder, "failure" was defined and enforced by the Instron when a 99% drop in load for one unit of extension is

detected. Figure 24 display the tensile plots for GA-free JF/(0/100) and GA-free JF/(30/70) composite tensile specimens respectively to further provide proof of the difference in failure behavior as CFF content is increased.

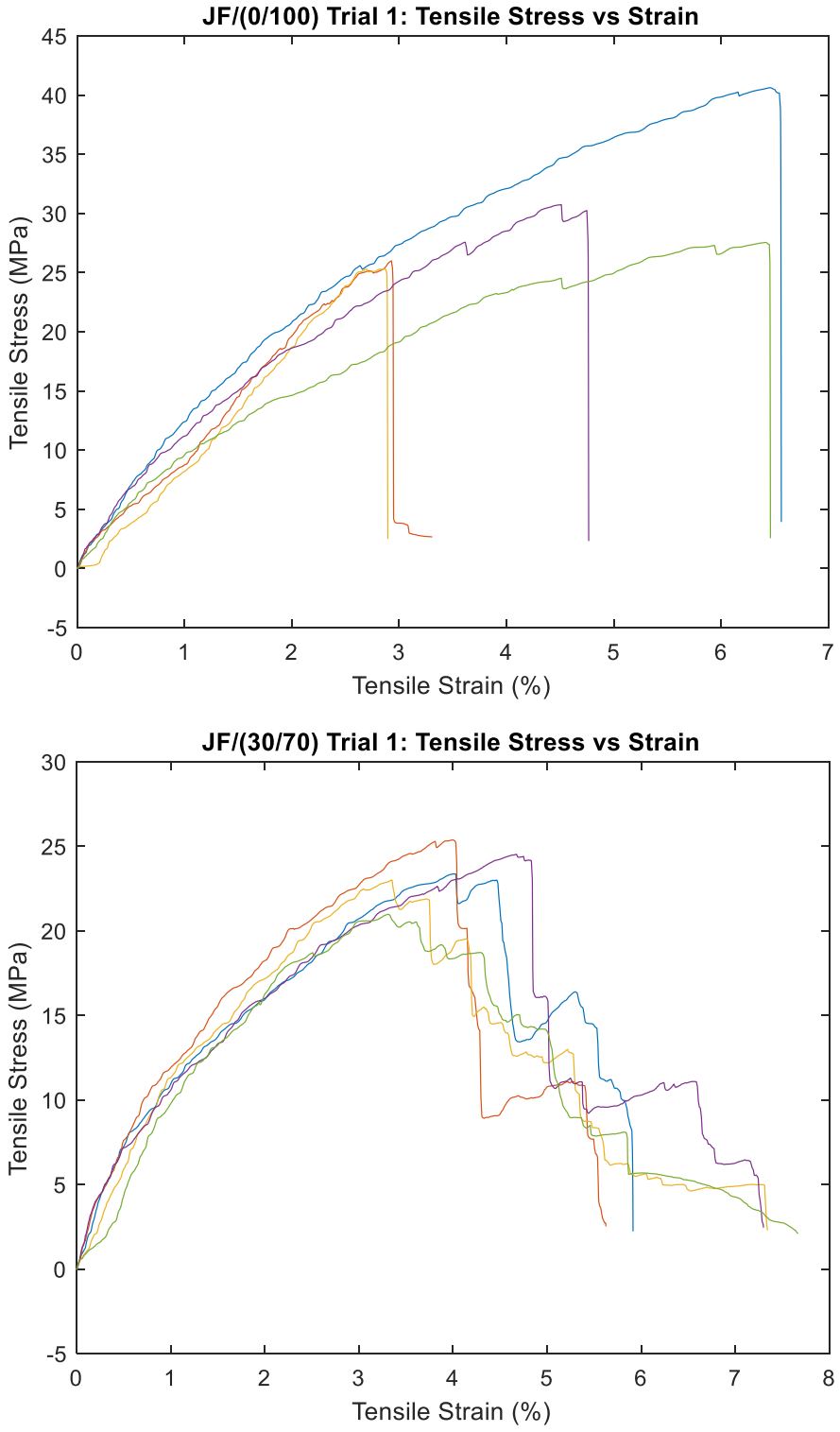

Figure 24: Tensile stress vs strain plots of JF/(0/100) (top) and JF/(30/70) (bottom) hybrid composite specimens

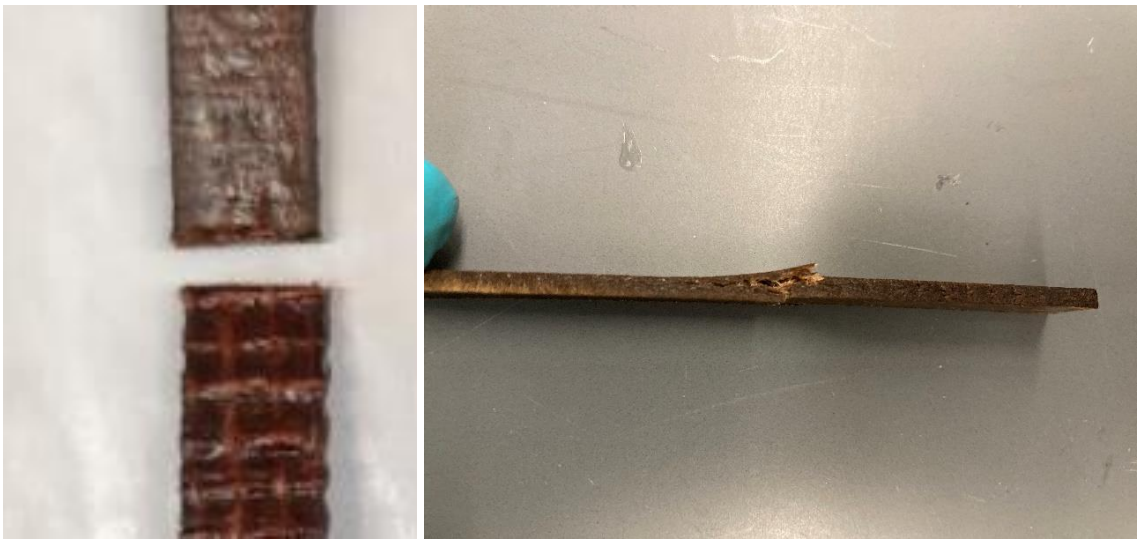

Figure 25: Tensile fracture of a JF/(0/100) wGA hybrid composite (left) and tensile fracture of a GA-free JF/(30/70) hybrid composite (right)

From Figures 24 and 25 it is clear (from both numerical and visual analysis) that CFF content influences failure mode. At 30% CFF, the (30/70) resin is weaker (tensile fracture stress of 14.3 MPa) than the JF strip (tensile fracture stress of 18.2 MPa). At this CFF%, the JF/(30/70) composite fails at 22.0 MPa and 5.8% fracture strain, which is closer to the tensile properties of JF strips: tensile fracture stress of 18.2 MPa and tensile fracture strain of 7.6%. Obviously, the CFF/SPI resin contribution and the addition of multiple JF layers explain the composites still fail at slightly higher stress levels than the individually tested JF strips. Thus, at higher (20-30) percentages of CFF, the CFF/SPI resin fails before the JF yarns. Furthermore, at 0% CFF the composite fails like its resin counterpart, i.e., in a singular brittle fracture. At 30% CFF, it is clear that the composite fails like the JF strips, i.e., in a stepwise fracture. Since the 30/70 resin is not stronger than the JF strip, it cannot support the same max loads that the 0/100 resin can.

The second difference in tensile behavior between the CFF/SPI resins and JF/(CFF/SPI) composites was the difference in tensile behavior at 0% CFF. The JF/(0/100) wGA composites

showed significantly higher tensile fracture strength of 34.7 MPa ($p = 0.002$) compared to its GA-free counterpart which had a tensile fracture strength of 26.6 MPa. This is in contrast with CFF/SPI resins in which the 0/100 resins had higher tensile fracture stresses than the 0/100 wGA resins. This change can be understood when evaluating the tensile results of the 0/100 wGA resin and observing that while some 0/100 wGA resin specimens had similar tensile values to 0/100 resin specimens, many 0/100 wGA specimens failed prematurely due to the excessive warping in the 0/100 wGA resin observed pre hot pressing. Since the JF/(0/100) wGA composites were prepared by impregnating the JF with the 0/100 wGA resin, the 0/100 wGA resin was constrained by the JF during pre-curing and did not significantly warp prior to hot pressing. Thus, the 0/100 wGA resin was able to perform free of residual stress concentration and avoiding premature failure, which potentially led to a higher tensile fracture strength. However, JF/(CFF/SPI) composites with GA did not retain this mechanical advantage over GA-free JF/(CFF/SPI) composites with the addition of CFF.

From 10 to 30% CFF, GA-free JF/(CFF/SPI) composites had better tensile fracture stresses than JF/(CFF/SPI) composites with GA. Much like the CFF/SPI resins with GA, it is possible that the introduction of CFF disrupted GA crosslinking SPI in JF/(CFF/SPI) composites with GA. This would explain why the tensile fracture stress values of JF/(CFF/SPI) composites with GA lose the initial mechanical advantage observed at 0% CFF.

The third difference in tensile behavior between the CFF/SPI resins and JF/(CFF/SPI) composites was that CFF/SPI resins with GA had lower fracture strains than GA-free CFF/SPI resins while JF/(CFF/SPI) composites with GA had noticeably larger fracture strains than GA-free JF/(CFF/SPI) composites. However, the tensile results for the CFF/SPI resins with GA explain why JF/(CFF/SPI) composites with GA have larger fracture strains. As previously

mentioned, residual stresses induced during processing caused many 0/100 wGA tensile specimens to fail prematurely. However, among the many tested 0/100 wGA specimens there were a few that had tensile fracture strains above 8%. Thus, at 0% CFF, JF/(0/100) composites with GA report high tensile fracture strains compared to GA-free JF/(0/100) composites because the 0/100 wGA matrix can support that level of load and elongation. As CFF is introduced, and the JF begins to bear more of the applied load, the tensile fracture strain of the JF/(CFF/SPI) composites with or without GA shifts to that of JF. This difference in tensile fracture strain between the JF/(CFF/SPI) composites with GA and those without GA decreased as CFF% increased. Initially, the JF/(0/100) wGA composites reported a tensile fracture strain of 9.3% compared to 4.3% of the JF/(0/100) composites, roughly a 5% difference ($p = 0$). However, at 30% CFF, the tensile fracture strain for the JF/(0/100) wGA (7.8%) was only 2% more ($p = 0.039$) than its GA-free counterpart (5.8%).

The fourth and final difference between the CFF/SPI resins and JF/(CFF/SPI) composites was that CFF increased Young's modulus for the CFF/SPI resins while the statistical difference for the JF/(CFF/SPI) composites was not significant. This is primarily due to the introduction of JF. For the CFF/SPI resins, CFF helps restrict polymer chain movement, improves stiffness. However, since JF is also carrying part of the load, the CFF is not solely responsible for restricting movement and thus predicting Young's modulus becomes more difficult.

Despite these differences, JF/(CFF/SPI) composites did share one key aspect with their CFF/SPI resin counterparts: the reduction of warping with the addition of CFF. While this reduced warpage was not as significant in the JF/(CFF/SPI) composites, due to JF helping restrain the matrix during processing, it was observed that like the CFF/SPI resins there was a minimum amount of CFF% needed to prevent warping post conditioning. Like the CFF in

CFF/SPI resins, CFF in JF/(CFF/SPI) composites would prevent warping by restraining the SPI matrix during conditioning through fiber geometry and characteristics. For GA-free JF/(CFF/SPI) composites the CFF amount needed to prevent warping was 10% while for JF/(CFF/SPI) composites with GA this was at 20% CFF. Note that this is the same observed CFF percentages for GA-free CFF/SPI resins and CFF/SPI resins respectively. This suggests that while JF prevents warping pre hot pressing (which reduces residual stresses), CFF still helps prevent warping post conditioning in both CFF/SPI resins and composites.

4.4.4 Flexural Results of JF/(CFF/SPI) Hybrid Composites

Table 10 reports the summary of flexural stress, flexural strain at the peak flexural stress, and flexural modulus results obtained for JF/(CFF/SPI) composites with and without GA. Note that peak flexural stress was reported rather than flexural fracture stress because fracture was found to be a variable parameter for reasons that are explained later in this section. In contrast, peak flexural stress occurred within a tighter interval and was additionally observed to be a more useful tool when identifying composite failure in flexion.

Table 10: Average flexural test results of JF/(CFF/SPI) hybrid composites

	0/100	**10/90**	**20/80**	**30/70**	**0/100 wGA**	**10/90 wGA**	**20/80 wGA**	**30/70 wGA**
N	8	9	7	8	8	8	7	8
Peak Flexural Stress (MPa)								
Mean	46.8	39.5	40.9	39.7	28.2	31.3	32.1	32.3
SD	(6.1)	(3.1)	(3.5)	(5.3)	(5.4)	(3.8)	(7.3)	(5.8)
CV	13.1%	7.9%	8.6%	13.5%	19.0%	12.3%	22.6%	18.1%
Flexural Strain at Peak Flexural Stress (%)								
Mean	3.4	2.7	1.9	2.2	4.3	3.7	2.9	1.7
SD	(1.1)	(1.0)	(0.2)	(1.2)	(1.0)	(1.0)	(1.5)	(0.4)
CV	31.8%	35.6%	12.8%	53.6%	23.6%	27.6%	51.5%	21.7%
Flexural Modulus (MPa)								
Mean	3321.3	3806.7	4210.0	4623.1	1553.4	2231.2	3210.6	3854.8
SD	(633.6)	(856.6)	(809.2)	(1252.3)	(289.9)	(651.8)	(1453.5)	(887.6)
CV	19.1%	22.5%	19.2%	27.1%	18.7%	29.2%	45.3%	23.0%

For GA-free JF/(CFF/SPI) composites, the mean peak flexural stress was the highest at 46.8 MPa with 0% CFF, but remained statistically unchanged (p-value > 0.05) at roughly 40 MPa for all percentages of CFF from 10 to 30%. Average flexural strain at peak flexural stress decreased from 3.4 to 2.2% ($p = 0.042$) with the addition of CFF from 0 to 30% CFF. The mean flexural modulus saw an increase with the addition of CFF from 3321.3 MPa to 4623.1 MPa ($p = 0.025$) from 0 to 30% CFF.

Unlike their GA-free counterparts, JF/(CFF/SPI) composites with GA did not see any change in mean peak flexural stress as CFF% was increased. However, the average flexural strain at the peak flexural stress decreased from 4.3 to 1.7% ($p = 0$) with the addition of CFF from 0 to 30% CFF. The mean flexural modulus, increased from 1553.4 to 3584.8 MPa ($p = 0$) as CFF was increased from 0 to 30%. Note that these comparisons are overall trends for 0% CFF vs 30% CFF. Statistical differences between various groups are presented in Appendix A.6.

GA-free JF/(CFF/SPI) composites were, in general, stronger and stiffer than JF/(CFF/SPI) composites with GA. Box plots included in Figure 26 describe overall trends as CFF and GA are added.

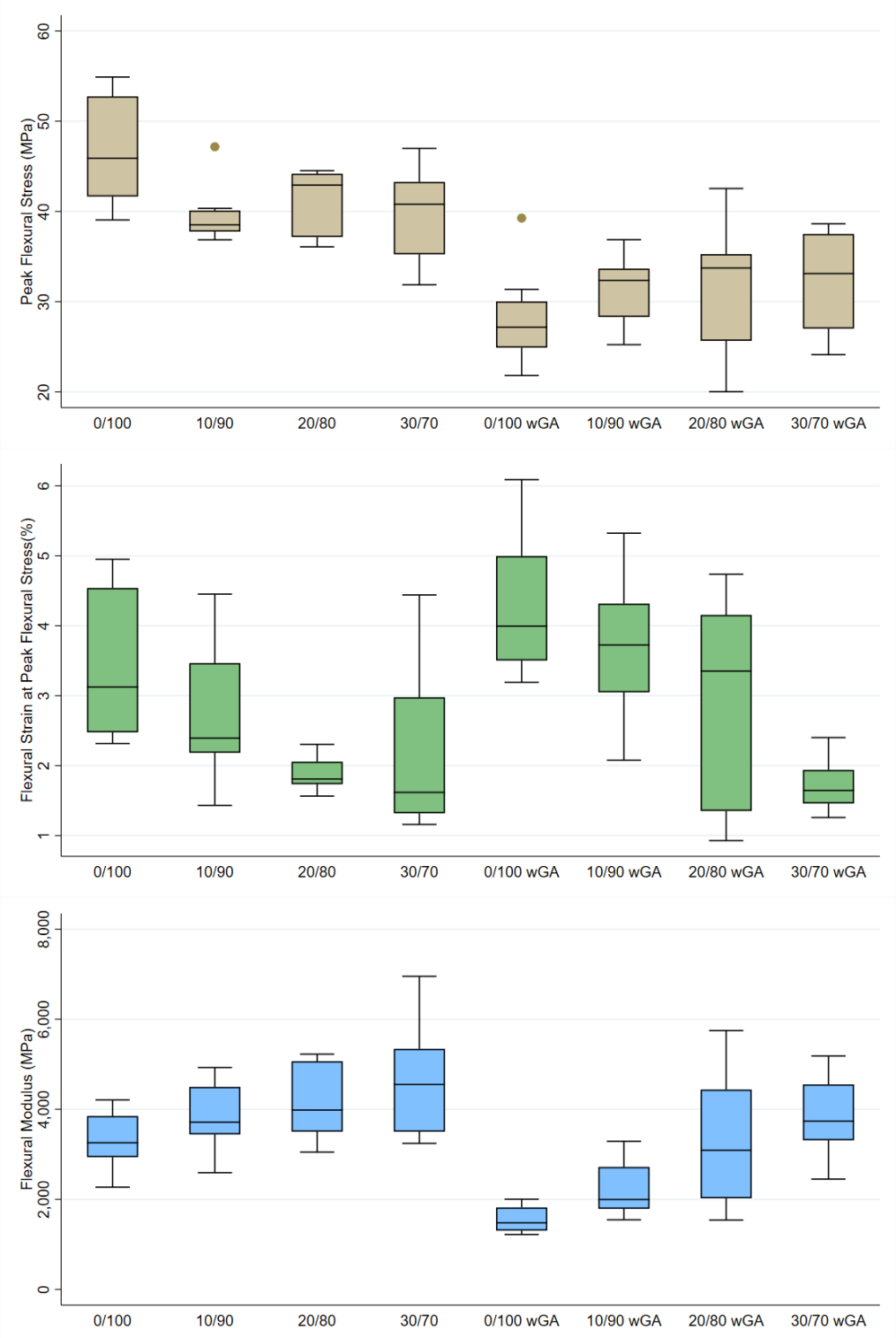

Figure 26: Peak flexural stress, flexural strain at peak flexural stress, and flexural modulus boxplots of JF/(CFF/SPI) hybrid composites

Composites can fracture in flexural mode in a few different ways, the most common being either stepwise (one layer at a time) or catastrophically (all at once). Figure 27 contains flexural stress vs strain plots for the five specimens from the first JF/(0/100) composite sample and showcases this variability in fracture.

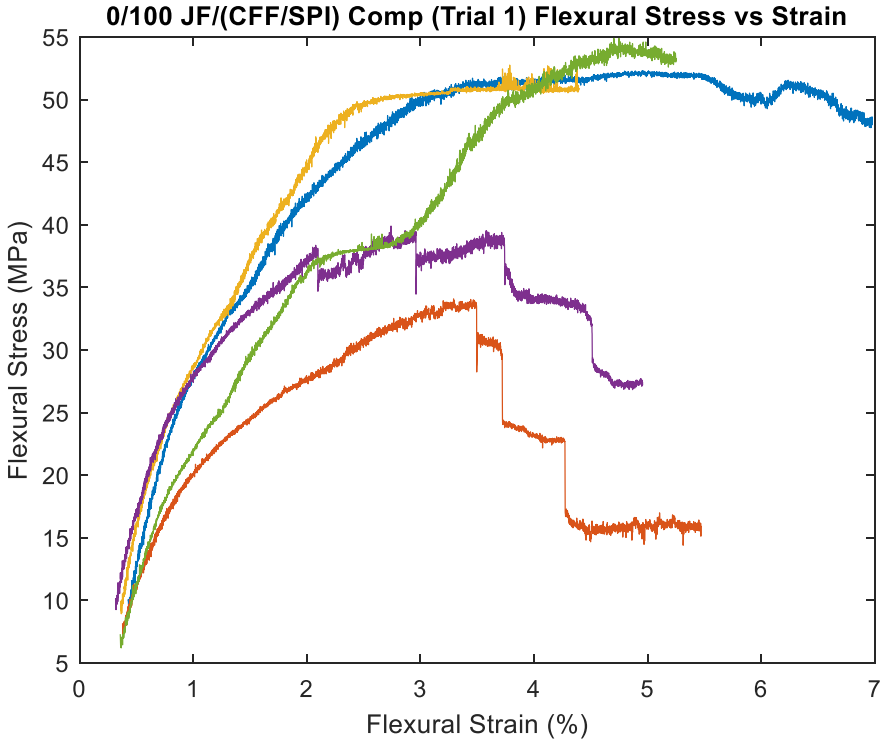

Figure 27: Flexural stress vs strain plots for GA-free JF/(0/100) hybrid composite specimens

From Figure 27 it can be seen that three specimens (shown in blue, yellow, and green) failed as a whole unit, catastrophically, while the other two (shown in purple and red) failed layer by layer. Failure of an individual laminae is demonstrated by the stepwise vertical drops in stress during loading. Each failed lamina meant that the composite had fewer layers to support the

continued loading, which is why these specimens naturally had lower maximum flexural stress values.

Another observation derived from the flexural test plots shown in Figure 27 is that the variability in failure mode is not a result of the heterogeneity caused by adding CFF as these specimens had 0% CFF. Furthermore, when looking at tensile data presented in Section 4.4.2 regarding 0/100 resins, it seems unlikely that this variability is caused by the resin. The fiber/matrix interface was also unlikely to be responsible as there was no observed delamination between any layers during testing for any of the JF/(CFF/SPI) composites, with or without GA. Thus, it seems most probable to attribute the application of resin during composite fabrication to this variability. While care was taken to distribute an equal amount of resin to each side of the jute mat, the hand-layup process used could have led to a nonuniform resin distribution throughout the four laminae. Thus, while there was no observable delamination, there could potentially be excess resin in between two layers which could have created differing failure methods.

In any case, the binding part of the composite consists solely of the SPI – that is the CFF does not aid in holding the composite together. Thus, for increasing contents of CFF, the available SPI binder naturally decreases. This can then lead to more brittle composites in the flexural direction. This is supported by the data from Table 10 which show that the flexural strain at maximum flexural stress decreased with the addition of CFF.

For each CFF/SPI ratio, GA-free JF/(CFF/SPI) composites were found to be superior to composites with GA with respect to both maximum flexural stress and flexural modulus across all ratios of CFF/SPI. In fact, the weakest ratio of the GA-free JF/(CFF/SPI) composites - JF/(10/90) – had a maximum flexural stress of 39.7 MPa. This is higher than the strongest ratio

of the composites with GA – JF/(30/70) – which had a maximum flexural stress of 32.3 MPa. The 10% GA used can be observed to have no flexural benefit for the composites outside of a small increase in flexural strain at maximum flexural stress.

CFF was shown to increase the flexural modulus for both JF/(CFF/SPI) composites with and without GA. This is likely due to the stiff CFQ resisting flexural deformation. While it may have been too short to carry load in axial tension, its stiffness would help, regardless of geometry, in flexural mode. GA-free JF/(CFF/SPI) composites only saw a decrease of roughly 6-7 MPa in maximum flexural strength as CFF content was increased while becoming significantly stiffer in flexure mode. For JF/(CFF/SPI) composites with GA, adding CFF also improved flexural strength. This is most likely because the GA crosslinked JF/(CFF/SPI) composites were shown to be more ductile through tensile testing, and thus would likely be less stiff in flexure as well.

From this analysis, it is demonstrated that GA-free JF/(CFF/SPI) composites are superior in two of the three flexural parameters; namely, maximum strength and modulus, and only falling slightly behind in the strain compared to JF/(CFF/SPI) composites with 10% GA.

When considering the tensile and flexural results, it is evident that using the methodology described in Sections 3.2.3 and 3.2.4, GA-free CFF/SPI resins and JF/(CFF/SPI) composites can be created to mechanically outperform CFF/SPI resins and JF/(CFF/SPI) composites with 10% GA.

4.5 CHEMICAL RESULTS

4.5.1 ATR-FTIR Results of CFF/SPI Resins

Figures 28-A and 28-B present ATR-FTIR spectra for two SPI resins found in literature.[9,66] Figure 28-A includes ATR-FTIR spectrum for a typical SPI resin in black.[66] Figure

28-B includes the ATR-FTIR spectrum for a typical non-crosslinked and a typical crosslinked SPI resin (SPI crosslinked with oxidized sucrose).[9] In both studies, the resins were pre-cured at temperatures between 30-40 °C which is an important metric to consider when comparing it to the resins produced as per the process discussed in Section 3.2.3 which were pre-cured at 80 °C. Apart from precuring temperature, the use of D-sorbitol for plasticization in this work, instead of the previously used glycerol, was the only other notable difference in the preparation methodology.

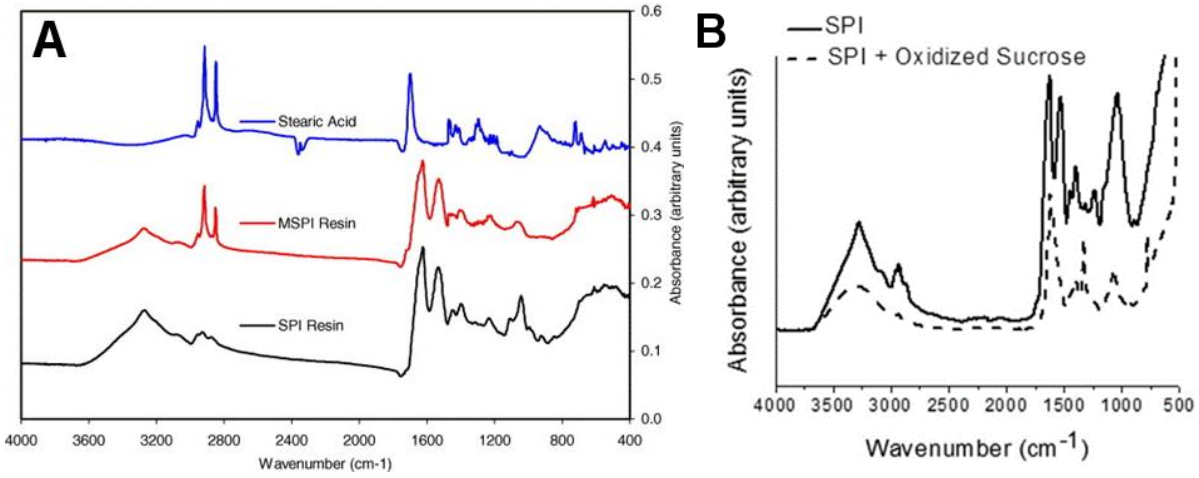

Figure 28: ATR-FTIR spectra of SPI resins from literature[9,66]

Figure 29 shows the ATR-FTIR spectra for typical 0/100 CFF/SPI resins with and without GA produced using the methodology detailed in Section 3.2.3. The ATR-FTIR spectra of the SPI resins produced as per Section 3.2.3 were found to be very similar to spectra of past SPI resins, with the key difference of having two absorption bands unique to this work. The crosslinked spectra of the resins produced in this work had a similarly dampened absorption

spectrum, showing same broad absorption band at 3250 cm^{-1} wavenumber that was noticeably rounder than the non-crosslinked SPI resins.

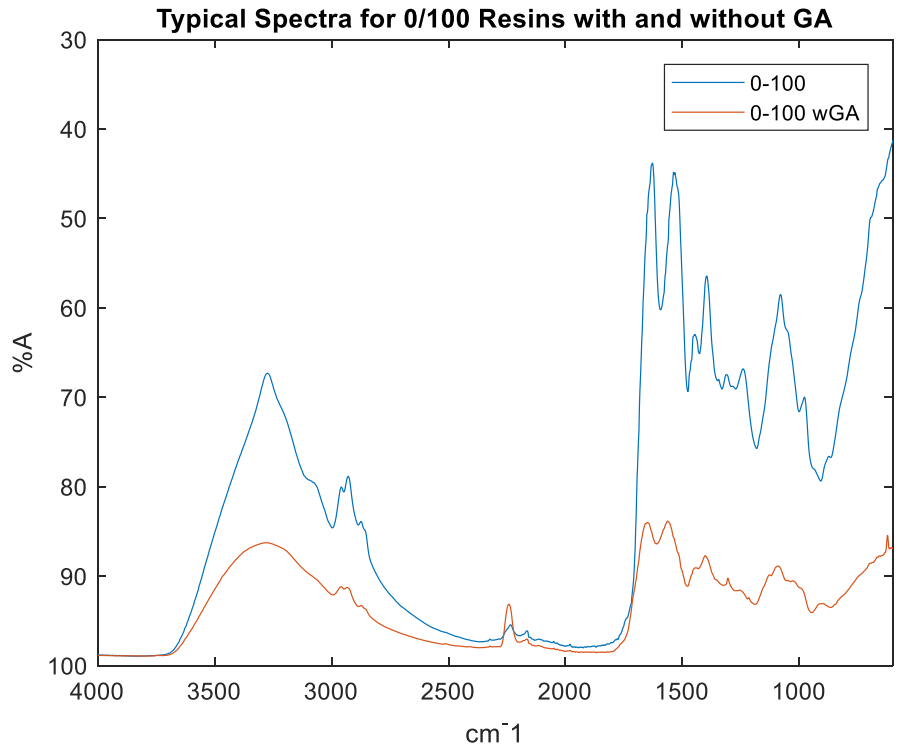

Figure 29: Typical ATR-FTIR spectra of a 0/100 resin with and without GA

The two absorption peaks unique to this work correspond to carbon-carbon triple bonds, specifically the carbon-carbon stretching present in disubstituted alkyne groups for the absorption band 2260-2190 cm^{-1} as well as the carbon-carbon stretching present in monosubstituted alkyne groups for the band 2140-2100 cm^{-1}.

Given the novelty of the presence of these bonds compared to past work, care was taken to ensure that this was not caused by contamination during resin synthesis or due to residue left

on the instrument. After it was confirmed that this was not the case, a few explanations were explored but without great success.

The simplest (but not necessarily correct) reason for these bands being present in this work and not in previous spectra is due to the use of D-sorbitol rather than glycerol. The primary mechanism by which D-sorbitol is theorized to plasticize proteins is by disrupting hydrogen bonding between polymers and, thus, increasing intermolecular distance which results in improved flexibility.[85] Being a small molecule, D-sorbitol also brings in a large amount of free volume into the resin system and improves molecular mobility. As a hydrophilic additive, D-sorbitol exposes the hydroxyl groups of the proteins it interacts with, increasing moisture absorption, which further plasticizes the resin.[86] Consequently, the introduction of D-sorbitol in and of itself would likely not introduce new bands around in the carbon-carbon triple bond region by proxy of new bonding mechanisms.

However, at high temperatures and alkalinity perhaps the hydroxy groups react with the hydrogen in the backbone in a condensation reaction to produce water while forming a carbon-carbon triple bond as seen in Figure 30.

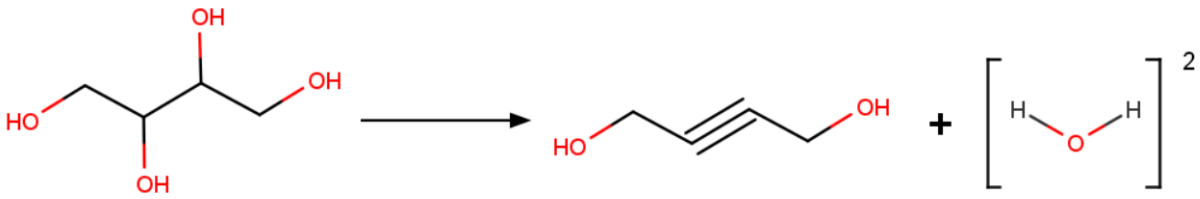

Figure 30: Possible triple bonding pathway through condensation reaction of D-Sorbitol

Figure 31 displays FTIR spectrum of D-sorbitol to illustrate that these absorption bands are not simply associated with unreacted D-sorbitol either.[87]

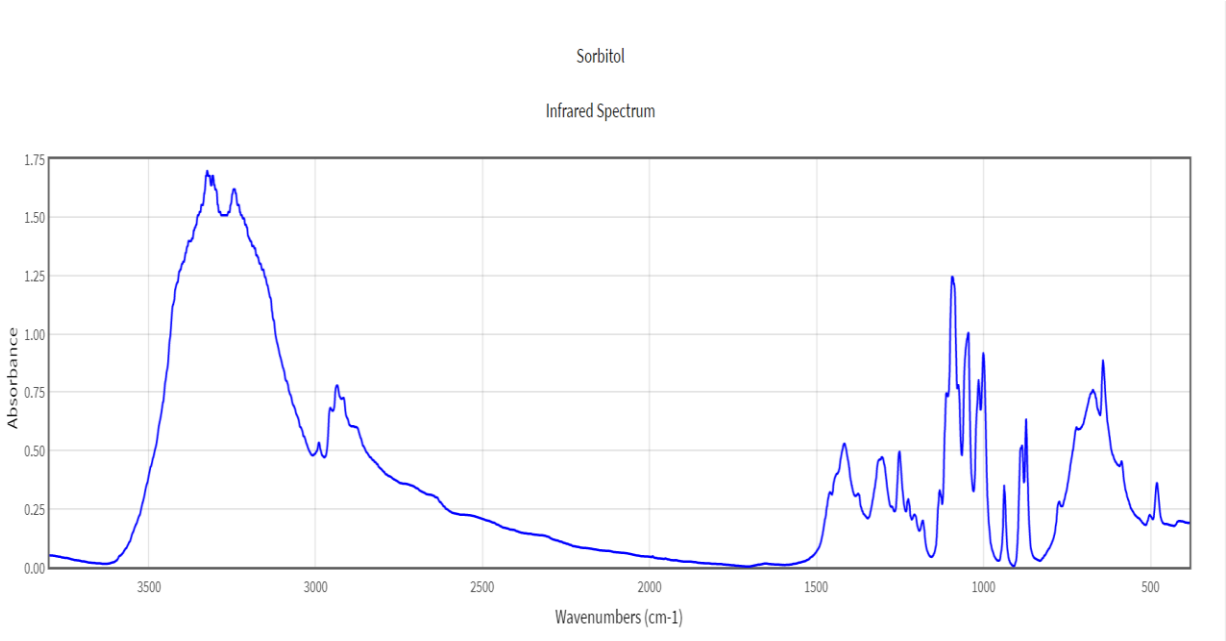

Figure 31: FTIR spectrum of D-sorbitol[87]

If D-sorbitol did not contribute to these absorption bands, another possible explanation is that these carbon-carbon triple bonds formed as a result of internal crosslinking due to the difference in resin procedure used in this work. Specifically, the increased temperature in conjunction with time during the pre-curing phase. As Ghosh-Dastidar and Netravali have noted, it is difficult to judge crosslinking extent through ATR-FTIR data.[9] There are various chemical ways in which SPI can crosslink, and the Maillard reaction is only one of them.[11,44,88] For example, hydroxyl groups in SPI can react with carboxyl groups forming ester groups and with amine groups to form amide groups.[88] Internal crosslinking through lysinoalanine formation

caused by high heat and alkalinity – as this work suggests – is another.[44] However, internal crosslinking by this mechanism would only create a carbon-carbon double bond, not a triple bond.[44]

CFF was shown to not introduce any new absorption bands and thus it follows that CFF does not introduce new types of bonding, including the observed carbon-carbon triple bonding, to the SPI resin. FTIR spectra from a study on chicken feather treated with various surfactants are shown in Figure 32 to demonstrate that CFF and SPI share an identical spectra mapping.[89] Both SPI and CFF are proteins and contain approximately same amino acids.

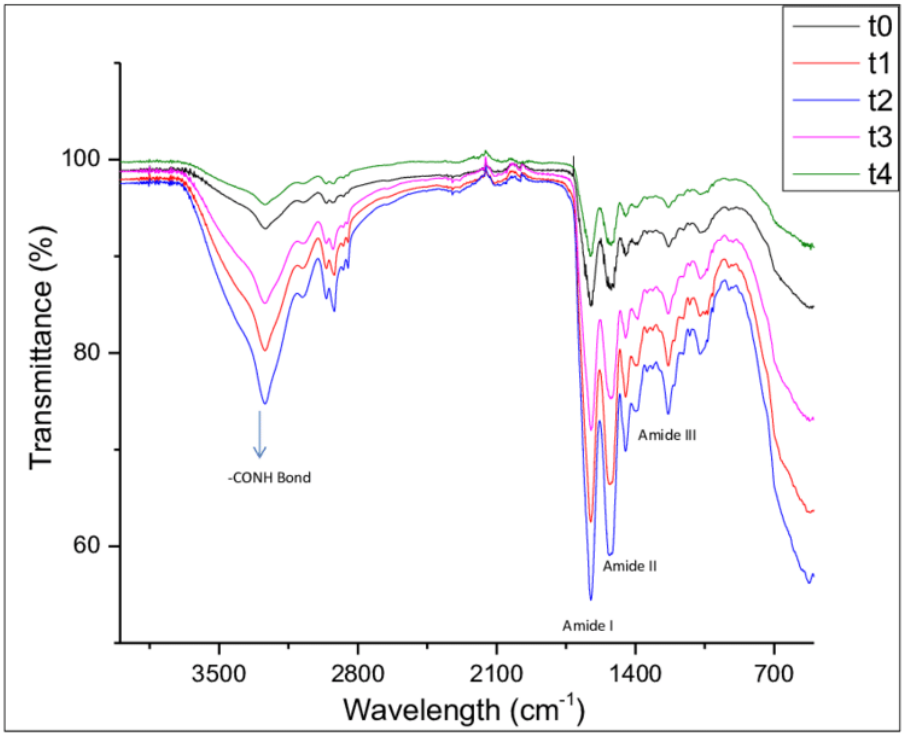

Figure 32: FTIR spectra of CFF treated with various surfactants: unwashed (t0), washed (t1), treated via SDS (t2), treated via CTAB (t3), treated via PEG (t4)[89]

Figure 32 presents FTIR spectra of CFF treated with various surfactants.[9] As the spectra in Figure 32 illustrate, the absorbance percentage is clearly affected by the surfactant treatments. Because of the variations obtained as a function of treatment, the CFF used in this work was not characterized through ATR-FTIR. To have an accurate characterization, the CFF used in ATR-FTIR characterization would have to be exposed to the same chemicals and undergo the same heat treatment as the CFF used in resin synthesis. This was deemed as unnecessary after characterizing all CFF/SPI ratios and observing no new bands. Figure 33 shows typical spectra obtained for GA-free CFF/SPI resins.

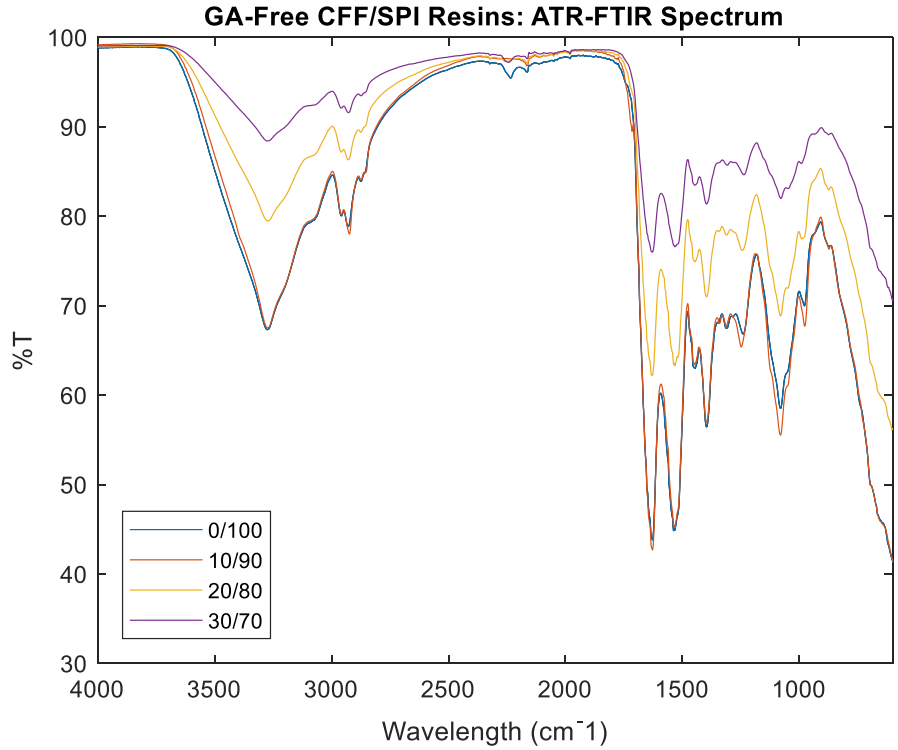

Figure 33: Typical ATR-FTIR spectra of GA-free CFF/SPI resins

The only notable effect of CFF on the ATR-FTIR spectra in this work was to decrease the absorbance percentage. This decrease can potentially be attributed to the increased coarseness of the resin surface at higher CFF percentages, perhaps reducing the contact with the crystal as well as internal reflection of IR. For hard materials such as the resins prepared in this work, a coarse surface results in air pockets between itself and the ATR crystal, which results in a weaker absorbance signal. This can also explain why the 10/90 resin spectra was shown to be almost identical to the 0/100 spectra, as at this percentage the CFF did not create a coarse enough surface. Additionally, IR is not sensitive at very low concentrations of chemical groups. The effect of GA in conjunction with CFF on ATR-FTIR spectra is observed in Figure 34.

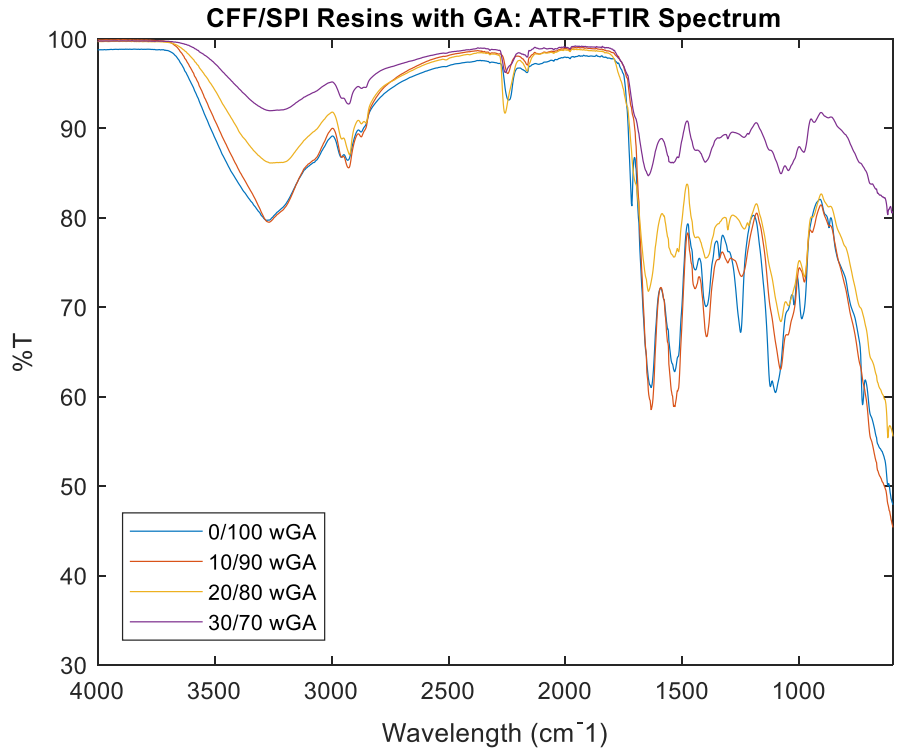

Figure 34: Typical ATR-FTIR spectra of CFF/SPI resins with GA

CFF was observed to affect the ATR-FTIR results for resins with GA in a similar manner to that of the GA-free resins. No new bond types were observed as a result of any potential GA and CFF interactions.

Peak normalization was the final avenue from which the presence of these carbon-carbon triple bonds was investigated. The aliphatic C-H peak at 2924 cm should not undergo any change due to crosslinking. Thus, it was chosen to normalize the two carbon-carbon peaks to determine how these peaks were affected by CFF and GA. The normalized plots of GA-free CFF/SPI resins are included in Figure 35.

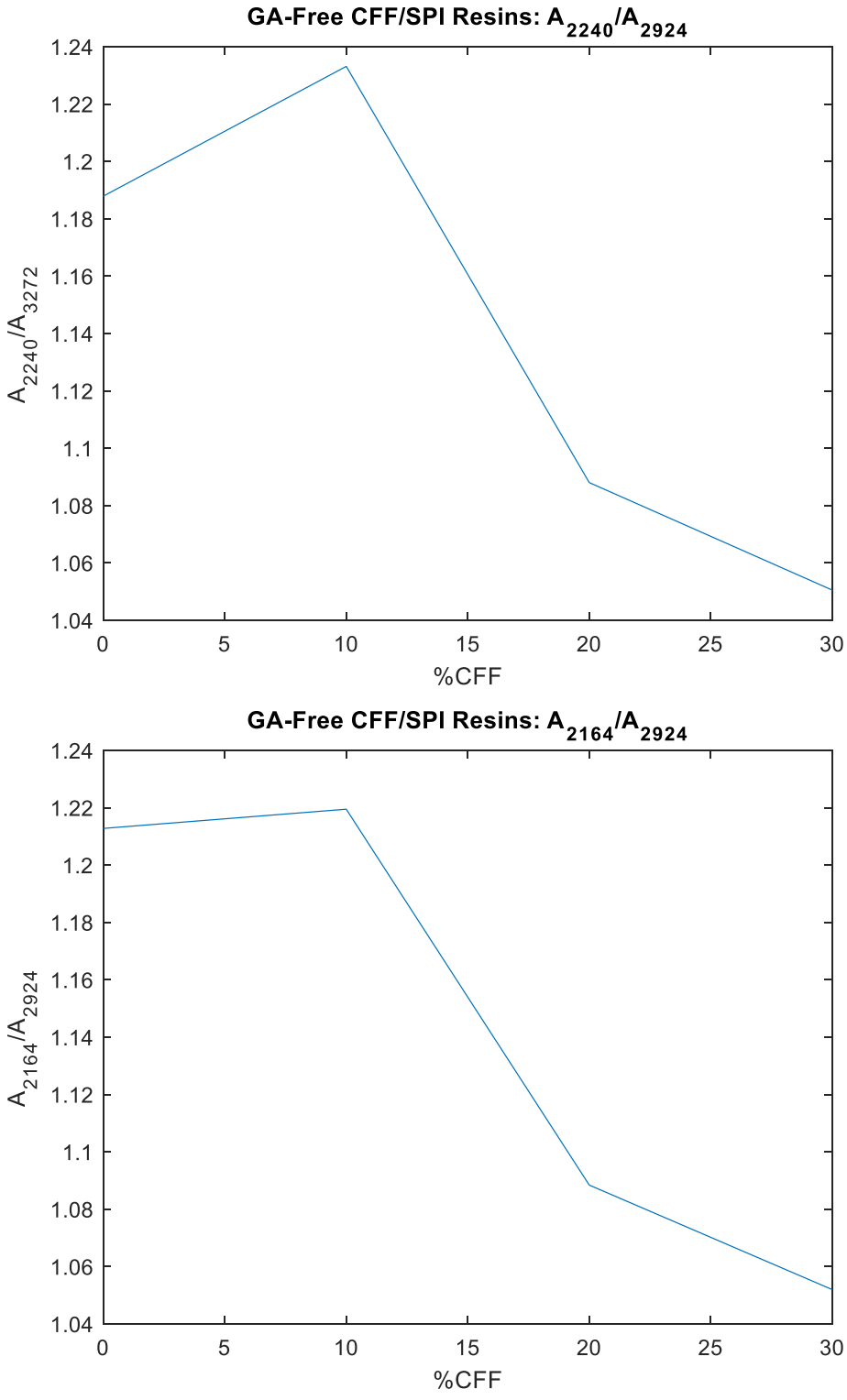

Figure 35: Relative absorbance peaks for GA-free CFF/SPI resins

From the plots in Figure 35 it is clear that increasing CFF content from 0 to 30% reduced the presence of these carbon-carbon triple bonds, despite an initial increase at 10% CFF. The overall trend indicated that as the SPI content decreased, the number of carbon-carbon bonds decreased, meaning that these carbon-carbon triple bonds are products of the unique SPI resin preparation detailed in Section 3.2.3. If this is the case then the D-Sorbitol condensation reaction is not likely to be the cause, but rather the aforementioned internal crosslinking or semi-crystallization. The discrepancy at 10% CFF may be due to optimal dispersion of SPI resin amongst CFF which could have led to better internal crosslinking or semi-crystallization of SPI. Crosslinking and crystallization are both difficult to assess using FTIR techniques so confirming this is difficult to do.[9,90] The effect of GA of the carbon-carbon triple bonds are observed in the relative absorbance peaks in Figure 36.

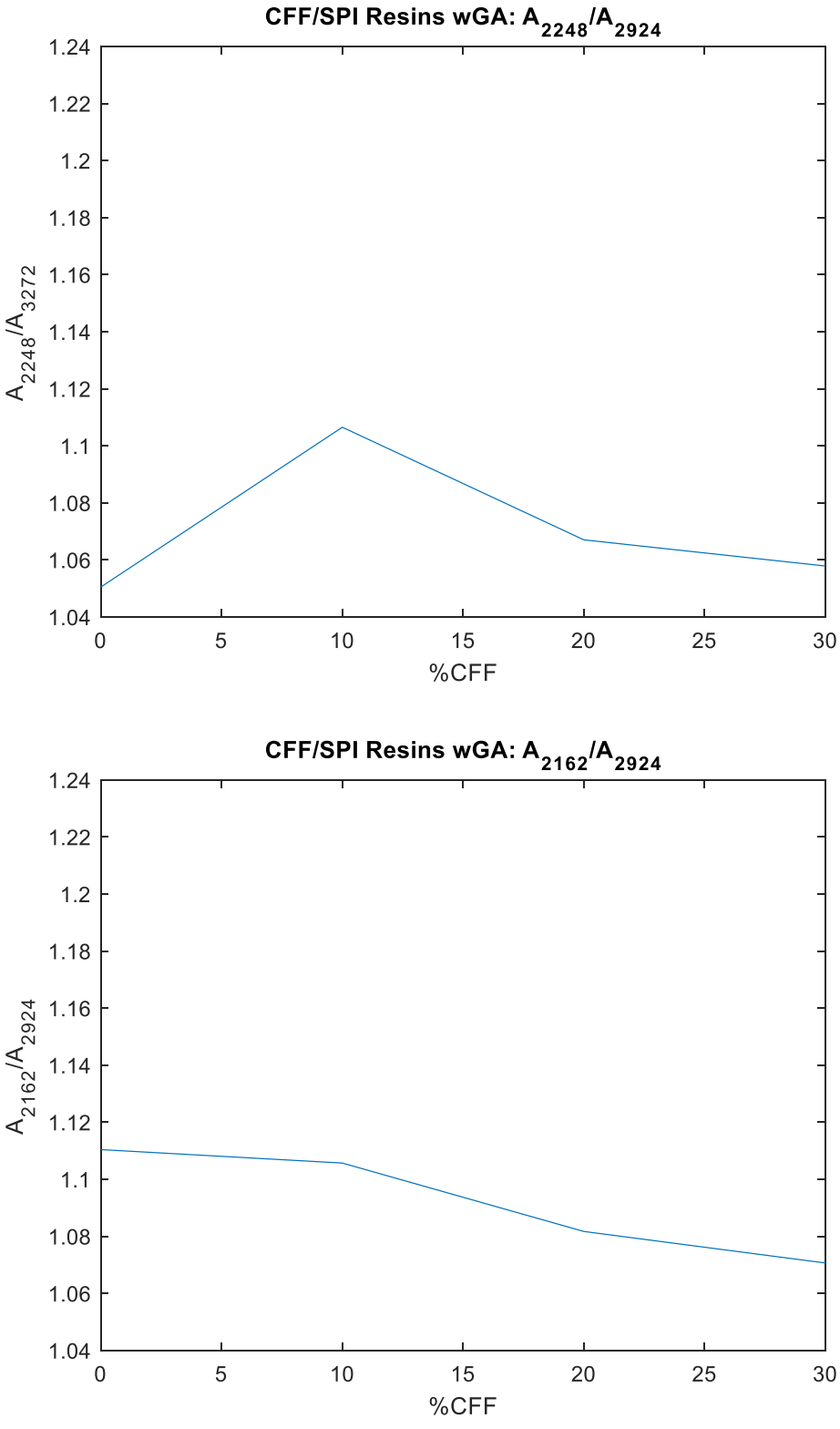

Figure 36: Relative absorbance peaks for CFF/SPI resins with GA

The relative absorbance peaks of CFF/SPI resins with GA seen in Figure 36 illustrate that the addition of GA decreases the presence of these carbon-carbon triple bonds. GA is shown in literature to primarily crosslink through a methylene bridge or disulphide linkages.[9,62] Thus, the smaller relative presence of the carbon-carbon triple bonds for CFF/SPI resins with GA compared to GA-free CFF/SPI resins can be expected and also be seen as further evidence of a unique mechanism that the GA-free CFF/SPI resins must undergo.

While the exact cause for the carbon-carbon triple bonds were not confirmed, sufficient analysis has revealed the probable causes.

4.6 THERMAL RESULTS

4.6.1 TGA Results of CFF/SPI Resins

Table 11 reports the summary of the temperatures of local maxima at the two observable degradation peaks (hereafter referred to as Peak I and Peak II respectively) for CFF/SPI resins.

Table 11: Average TGA results of CFF/SPI resins

	0/100	**10/90**	**20/80**	**30/70**	**0/100 wGA**	**10/90 wGA**	**20/80 wGA**	**30/70 wGA**
N	2	2	2	2	2	2	2	2
Peak I Temperature (°C)								
Mean	173.8	172.5	183.4	192.8	196.2	189.4	192.8	199.1
SD	(4.2)	(9.0)	(4.1)	(1.4)	(2.4)	(1.2)	(1.2)	(2.3)
CV	2.4%	5.2%	2.3%	0.7%	1.2%	0.6%	0.6%	1.2%
Peak II Temperature (°C)								
Mean	299.5	318.5	319.8	317.1	309.5	318.2	321.7	320.0
SD	(6.4)	(3.6)	(0.2)	(0.8)	(1.7)	(3.3)	(1.7)	(3.3)
CV	2.1%	1.1%	0.1%	0.3%	0.5%	1.0%	0.5%	1.0%

For GA-free CFF/SPI resins, the mean temperature at Peak I increased from 173.8 to 192.9 °C ($p = 0.074$) as the CFF percentage is increased from 0 to 30%. The mean temperature at Peak II increased from 299.5 to 317.1 °C as the CFF percentage is increased from 0 to 30%. Mean parameters had a few significant differences between groups that can be seen in Appendix A.7.

For CFF/SPI resins with GA, the mean temperatures at Peak I increased from 196.2 to 199.1 °C as the CFF percentage increased from 0 to 30%. The mean temperature at Peak II increased from 309.5 to 320.0 °C as the CFF percentage increased from 0 to 30%. The only significant difference in mean parameters was for Peak II temperature between 0/100 and 20/80 ($p = 0.018$)

At 0% CFF, Peak I temperature for 0/100 resins was statistically lower than that of 0/100 wGA resins ($p = 0.039$). For comparisons between other groups, see Appendix A.7. Boxplots are shown in Figure 37 to indicate the general trends.

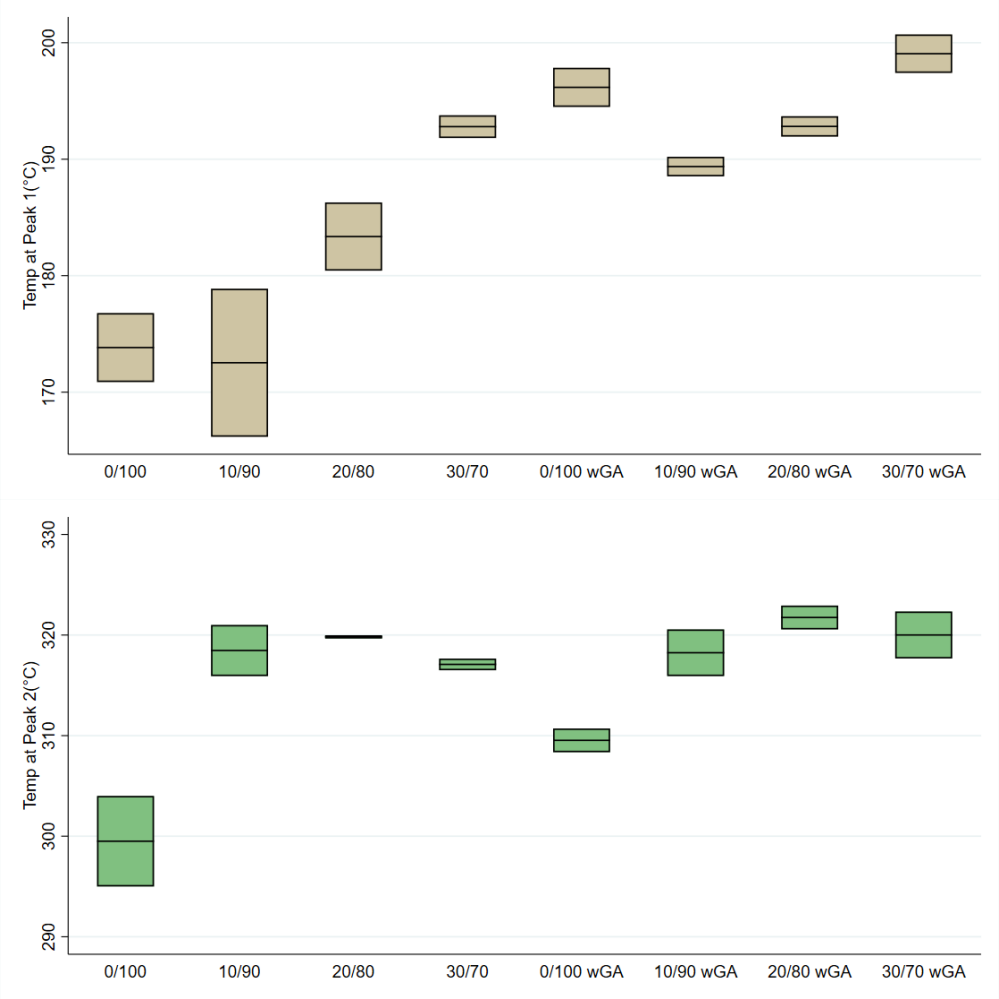

Figure 37: Peak I and II temperature boxplots of CFF/SPI resins

Visual inspection of Figure 37 demonstrates that while the small sample size may have prevented concrete statistical differences, there are clearly observable trends with the addition of CFF and GA. For GA-free CFF/SPI resins, Peak I increased with the addition of CFF. Peak II, however, jumps up with 10% and maintains the same general range of values for 10 to 30% CFF. Unlike the GA-free CFF/SPI resins, Peak I initially decreased with 10% CFF for CFF/SPI resins with GA, before climbing again. However, Peak II behaves similarly, as both groups observe a jump with 10% CFF, that is maintained with further addition of CFF. At 0% CFF it is clear that

both Peak I and II are higher for 0/100 wGA resins despite the statistical analysis only indicating Peak I being higher. Furthermore, with the addition of CFF, Peak II is roughly the same with or without GA. To understand these trends, material analysis must be conducted, beginning with the effect of CFF on CFF/SPI resins without GA.

Peak I, as it is around the 100 to 190 °C, is likely tied to specimen moisture loss, as studies on SP resins and CFF support.[10,43] Analysis of Peak I for GA-free CFF/SPI resins shows that as CFF% increases, the peak associated with moisture loss is shifted to a higher temperature and the weight percentage change occurs less rapidly. This suggests that adding CFF either decreased moisture absorbed or that the moisture was prevented from diffusing out during pyrolysis.

The former reason cannot be true, as the moisture regain study discussed in Section 4.3.1 showed that increasing CFF increased the water absorbance for GA-free CFF/SPI resins during conditioning. The latter reason is supported by the MCC study discussed in Section 4.2.1 in which the results showed that adding CFF likely formed a high-quality char layer that worked as thermal insulation. A thicker and insulating char layer would indeed prevent moisture from diffusing out, which would explain the slower change in weight percentage as well the higher temperature needed to observe the moisture peak – Peak I. Unlike the GA-free CFF/SPI resins prepared using pre COVID-19 procedure detailed in Section 3.2.1 used for MCC characterization, there was no observed loss of properties with continued addition of CFF to GA-free resins used in TGA characterization. This is likely because the CFF/SPI resins produced as per the procedure described in Section 3.2.3 are markedly different than those produced as per the procedure described in Section 3.2.1, and consequently would produce a char layer with different characteristics. Furthermore, CFF is known to experience mass loss due to moisture

losses in the 23 to 230 °C range.[43] However, this is not a sharp peak rather a gradual wt loss as both free water, i.e., loosely bonded water, and chemically bonded water would be released across the broad temperature range from 23 and 230 °C. As a result, the peak is not localized at a particular temperature. This could be another reason as to why the moisture peak is seen to have a decreasing slope.

Analysis of Peak II indicates that when 10% CFF was added, the peak temperature shifted upwards from 300 to 318 °C. Further addition of CFF did not significantly change Peak II temperature. However, the derivative wt% change continued to increase. This is because while SPI has been reported to begin thermal degradation in this interval[10], CFF begins partial degradation of the keratin at a higher temperature, around 230 to 280 °C[43]. The fluctuation in Peak II temperature as CFF is increased could be a byproduct of the variance between the thermal degradation values of the different parts of CFF. Thermal studies of CFF have demonstrated that the CFB, CFQ and whole feather do not have the same TGA values.[43] This variation prevents an accurate assessment of TGA data since a random amount of each feather fraction was added to the specimens. The fluctuation could also be explained as being within the statistical deviation.

Note that TGA characterization of CFF was not performed in this work for two reasons. First, the CFF was unable to reach the minimum mass threshold for characterization due to its low density. The small TGA pan was unable to reach even 0.2 g before the volume of CFF was too much to hold. Second, any form of air convection, e.g., nitrogen flow, resulted in CFF flying from the pan. Thus, even if a smaller than recommended mass of CFF were used for characterization, the thermograms would show random and sudden changes in mass. Figure 38

includes the TGA thermograms for GA-free CFF/SPI resins to illustrate how CFF influences thermal stability.

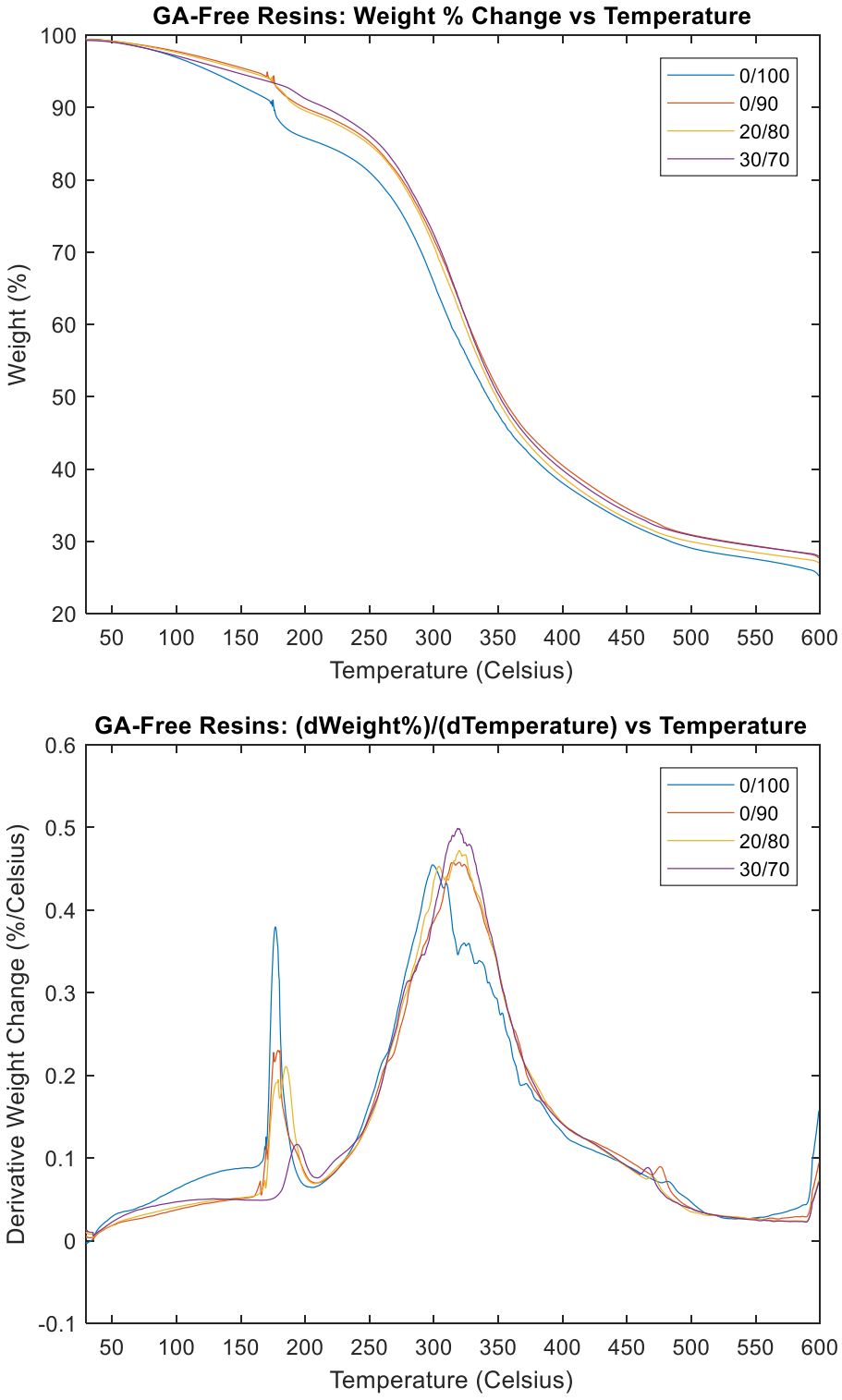

Figure 38: Typical TGA thermograms (top) and derivative curves (bottom) of GA-free CFF/SPI resins

Typical thermograms of GA-free CFF/SPI resins illustrate that throughout the duration of the heating cycle, GA-free CFF/SPI resins with CFF had a higher wt% than the neat GA-free 0/100 resin. This means that CFF improved thermal stability for the GA-free CFF/SPI resins most likely through formation of a higher quality char layer. The influence of CFF in conjunction with GA was observed by Figure 39 which showed the TGA thermograms for CFF/SPI resins with GA.

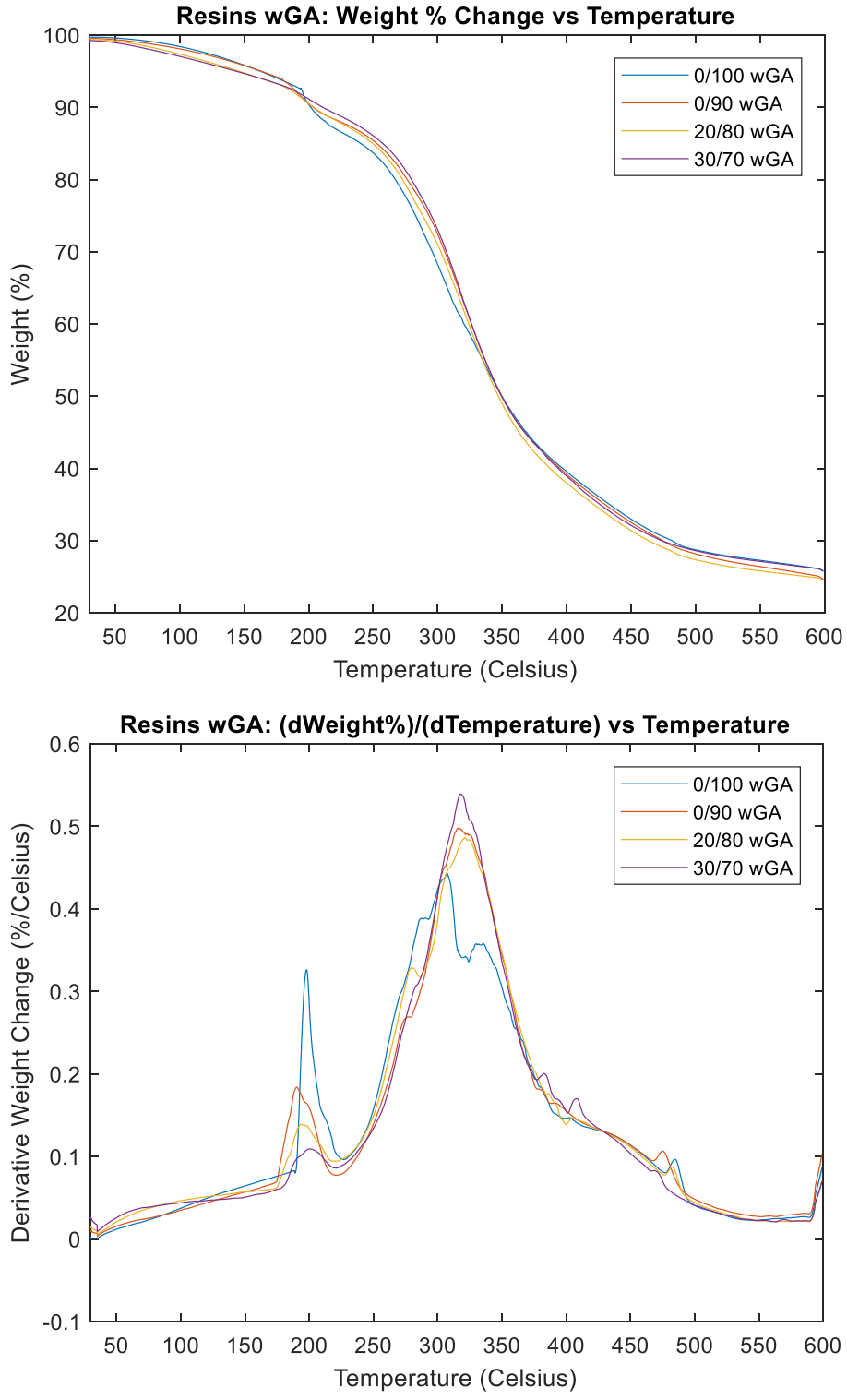

Figure 39: Typical TGA thermograms (top) and derivative curves (bottom) of CFF/SPI resins wGA

Analysis of Peak I indicates that adding GA further shifts the moisture loss to a higher temperature. At 0% CFF, the moisture loss peak at 0/100 wGA resin was at 196.2 °C which is roughly 22 °C higher than that obtained for 0/100 resin. The moisture regain study for CFF/SPI resins as discussed in Section 4.2.1 showed that CFF/SPI resins with GA absorb less water than GA-free CFF/SPI resins and absorb even less with the addition of CFF. This is supported by the DSC data which showed that addition of CFF continued to shift Peak II to the right (higher temperature) for CFF/SPI resins with GA. Thus, the comparative lack of moisture found in CFF/SPI resins with GA in conjunction with the char forming properties of GA and CFF as discussed in the MCC study in Section 4.2.1, are the probable causes for the higher Peak I temperatures compared to GA-free CFF/SPI resins.

Analysis of Peak II between 0/100 and 0/100 wGA resin specimens indicates that GA-crosslinked SPI has a higher degradation temperature. This makes sense as crosslinks improve thermal stability by requiring additional energy to degrade. Furthermore, synergistic crosslinking improves char quality which improves thermal stability as well. However, with the addition of CFF, Peak II for CFF/SPI resins wGA shifted to that of GA-free CFF/SPI resins. This means that CFF has an even higher degradation temperature than that of GA-crosslinked SPI.

As the thermograms for CFF/SPI resins with GA indicate, unlike GA-free CFF/SPI resins, CFF only decreases weight loss between 200 to 340 °C. Furthermore, while the weight percent of 0/100 wGA remained higher than 0/100 at every point during the heating cycle (indicating that GA-crosslinked 0/100 SPI has higher thermal stability the GA-free 0/100), the addition of CFF allowed GA-free CFF/SPI resins to retain comparable weight percentages to

CFF/SPI resins with GA. Thus, CFF was able to negate the need for GA to be used for enhanced thermal stability.

In conclusion, CFF was shown to have prevented moisture diffusion during pyrolysis, degraded at a higher temperature than SPI, and improve thermal stability, all likely through the formation of a high-quality char layer as suggested by the MCC results in Section 4.2.1. GA-crosslinked SPI (0/100 wGA) had a higher degradation temperature than neat SPI (0/100) but adding CFF to SPI resins with GA only improved thermal stability in the range of 200 to 340 °C. Adding GA also further shifted the moisture peak (Peak I) to a higher temperature.

4.6.2 TGA Results of JF/(CFF/SPI) Hybrid Composites

Table 12 reports the summary of the temperatures of the local maxima at the two observable degradation peaks as well as the derivative weight percentage changes calculated at the respective peaks for JF/(CFF/SPI) composites. Unlike the CFF/SPI resins there were no clear Peak I's for JF/(CFF/SPI) composites and thus Peak I was excluded from Table 12.

Table 12: Average TGA results of JF/(CFF/SPI) hybrid composites

	0/100	**10/90**	**20/80**	**30/70**	**0/100 wGA**	**10/90 wGA**	**20/80 wGA**	**30/70 wGA**
N	2	2	2	2	2	2	2	2
Peak II Temperature (°C)								
Mean	319.2	321.3	327.2	329.8	322.8	324.9	327.3	328.2
SD	(3.0)	(5.4)	(3.4)	(1.4)	(2.8)	(1.5)	(3.7)	(1.2)
CV	0.9%	1.7%	1.0%	0.4%	0.9%	0.5%	1.1%	0.4%

For GA-free JF/(CFF/SPI) composites, the mean temperature at Peak II increased from 319.2 to 329.8 °C as the CFF percentage was increased from 0 to 30%.

For JF/(CFF/SPI) composites with GA, the mean temperature at Peak II increased from 322.8 to 328.2 °C as the CFF percentage was increased from 0 to 30%. No statistical significance was found between groups. The p-values can be found in Appendix A.8. The mean temperature at Peak II of the JF/(CFF/SPI) composites were higher than those observed for CFF/SPI resins for all CFF percentages, but this difference diminished with the addition of CFF. Boxplots of Peak II temperature are included in Figure 40 for observing trends as CFF and GA are added.

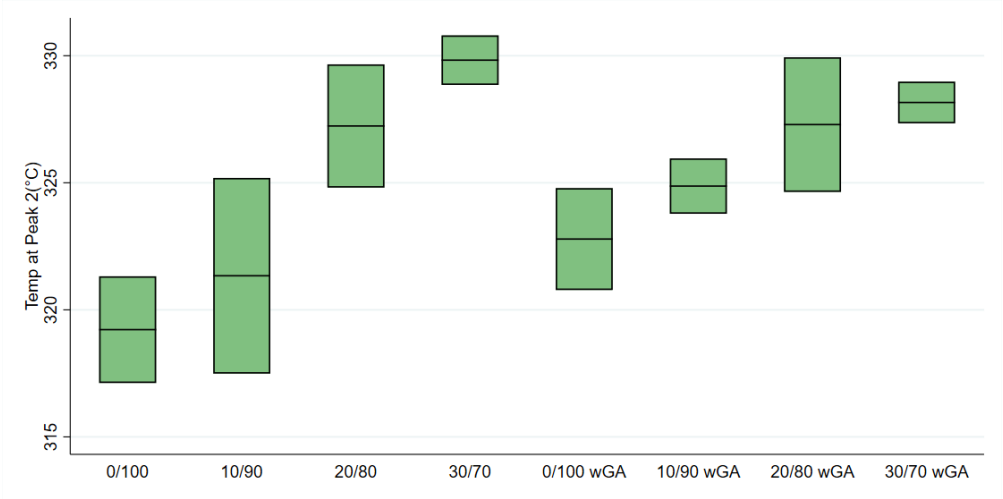

Figure 40: Peak II temperature boxplots of JF/(CFF/SPI) hybrid composites

The boxplots indicate an increase in Peak II temperature with the addition of CFF despite the statistical analysis not suggesting significance. This, once again, may be due to small sample size. With this is mind, material analysis has been conducted, beginning with the effect of CFF for GA-free JF/(CFF/SPI) composites. Figure 41 includes TGA thermograms for GA-free JF/(CFF/SPI) composites.

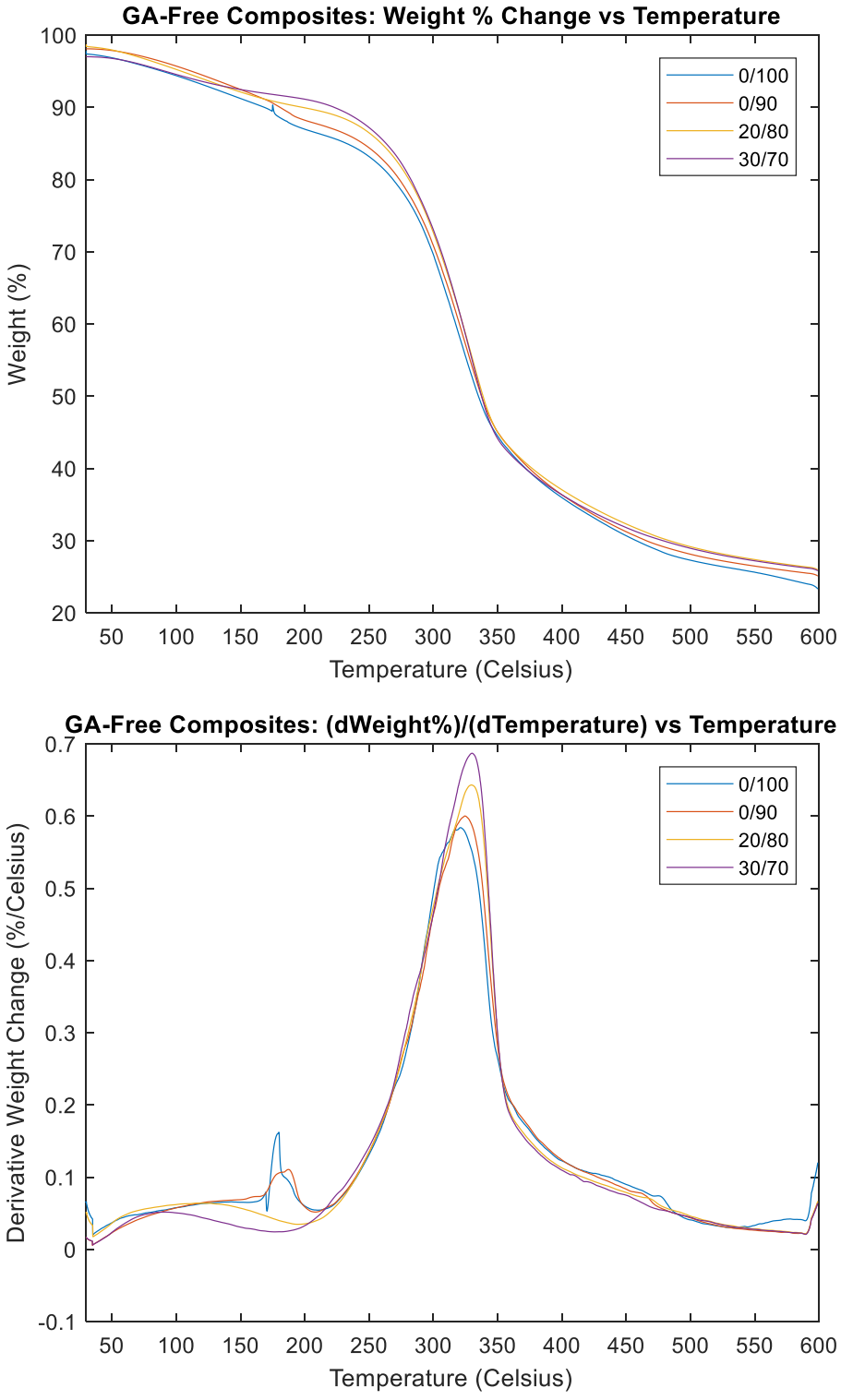

Figure 41: Typical TGA thermograms (top) and derivative curves (bottom) of GA free JF/(CFF/SPI) hybrid composites

Before analyzing the effect of CFF, the lack of Peak I for JF/(CFF/SPI) composites with or without GA must be addressed. The disappearance of a Peak I indicated that moisture loss is not as prevalent in JF/(CFF/SPI) composites with or without GA. As mentioned in Section 4.6.1, the lack of a moisture peak is not likely due to lack of moisture absorbance. Rather, a high-quality char layer likely preventing outward water diffusion. Thus, the TGA results parallel the MCC results finding of the inclusion of JF likely improving char quality. The higher Peak II temperature for JF/(CFF/SPI) composites is attributed to the cellulose component of JF, which degrades around 310 to 350 °C.[53,91] Similar to the resins, as the SPI component decreased in percentage, Peak II temperature increased as the components with higher degradation temperatures – CFF and JF – became the majority.

From the typical thermograms of GA-free JF/(CFF/SPI) composites, it is clear that the addition of CFF improved thermal stability since the wt% of typical GA-free JF/(CFF/SPI) composites with CFF were higher than the typical GA-free, neat JF/(0/100) composite. The influence of JF in conjunction with GA was observed by Figure 42 which shows the TGA thermograms for JF/(CFF/SPI) composites with GA.

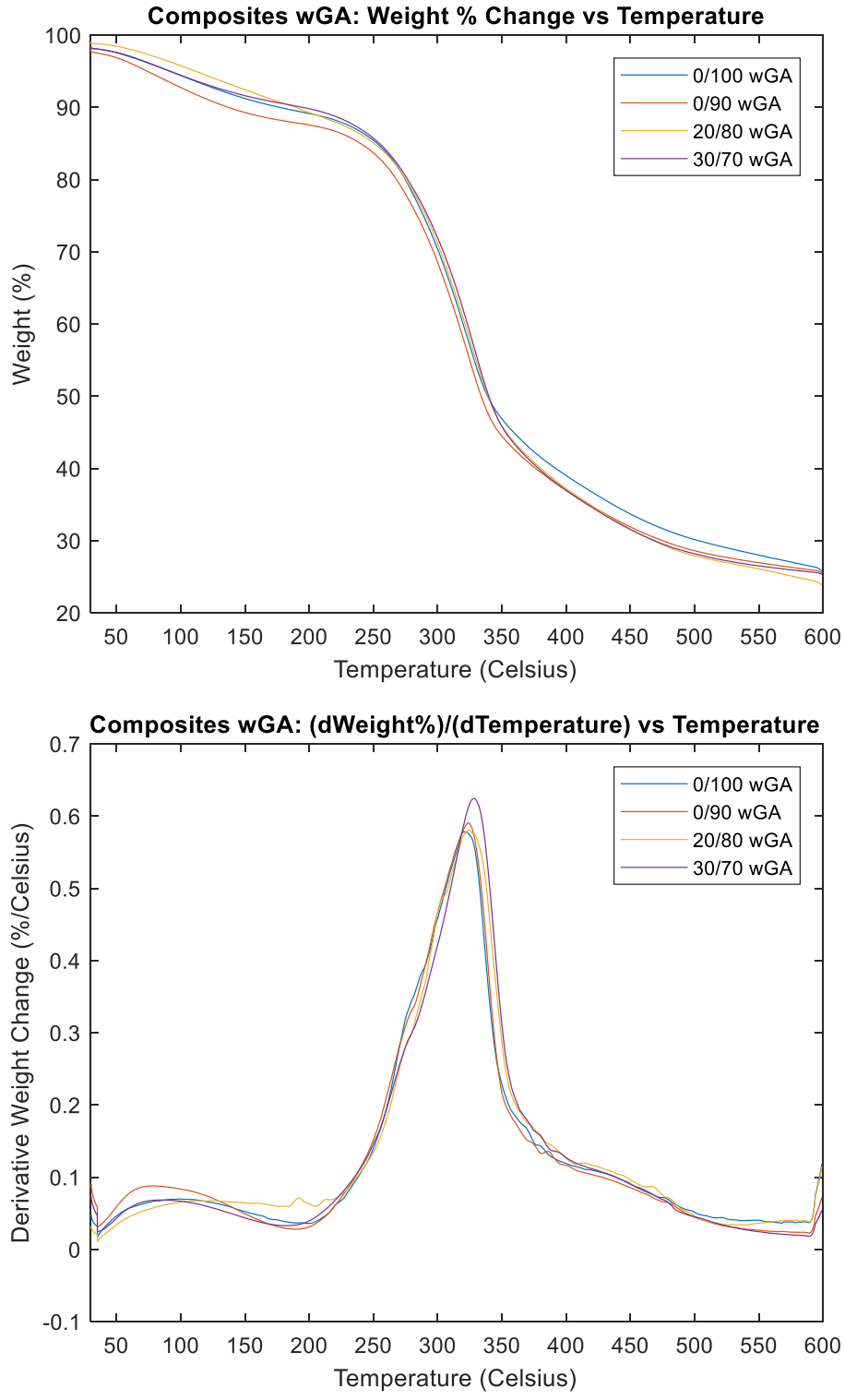

Figure 42: Typical TGA thermograms (left) and derivative curves (right) of JF/(CFF/SPI) composites wGA

JF/(CFF/SPI) composites with GA showed comparable Peak II temperatures among all CFF/SPI ratios which indicated that JF is more important in reducing thermal degradation than GA. As the MCC study in Section 4.2.2 indicated, JF when added to CFF/SPI improved flammability properties, likely through the formation of an even superior char layer. This should allow for composites to be crafted without using GA - a toxic crosslinking agent – while maintaining thermal stability.

4.6.3 DSC Results of CFF/SPI Resins

CFF and GA were added to SPI to determine their individual, as well as their cumulative, effect on the melting enthalpy change/enthalpy of fusion (ΔHf) and peak melting temperature (Tm). A larger ΔHf indicates that the specimen had a larger crystalline percentage that needed to be absorbed in order to change phases. A higher Tm is indicative of greater thermal stability as it means that the specimen needs to reach a higher temperature to melt. However, as per the summary statistics presented in Table 13, there was not a clear correlation between the addition of CFF and GA with these thermal properties. Mean Tm was not seen to significantly change with addition of CFF and/or GA, indicating that the net effects of these two additives did not significantly affect thermal stability. Meanwhile, mean ΔHf was observed to initially increase with the addition of CFF but fluctuate significantly after. GA was not observed to effect average ΔHf or Tm significantly. P-values can be found in Appendix A.9. The only statistically significant difference reported was for ΔHf, between 10/0 wGA and 30/70 wGA ($p = 0.006$).

Table 13: Average DSC results of CFF/SPI resins

	0/100	**10/90**	**20/80**	**30/70**	**0/100 wGA**	**10/90 wGA**	**20/80 wGA**	**30/70 wGA**
N	2	2	2	2	2	2	2	2
ΔHf (J/g)								
Mean	77.3	156.1	109.7	140.9	88.6	157.3	135.2	78.5
SD	(70.7)	(3.1)	(25.2)	(16.9)	(70.4)	(1.8)	(22.9)	(3.7)
CV	91.4%	2.0%	23.0%	12.0%	79.5%	1.1%	16.9%	4.7%
Tm (°C)								
Mean	206.3	199.0	203.2	198.7	203.1	204.4	203.7	215.7
SD	(1.2)	(5.9)	(0.4)	(6.7)	(4.9)	(8.8)	(1.8)	(11.4)
CV	0.6%	3.0%	0.2%	3.4%	2.4%	4.3%	0.9%	5.3%

The large variations in the results are visually illustrated by the boxplots of reported ΔHf and Tm values of CFF/SPI resins with and without GA in Figure 43.

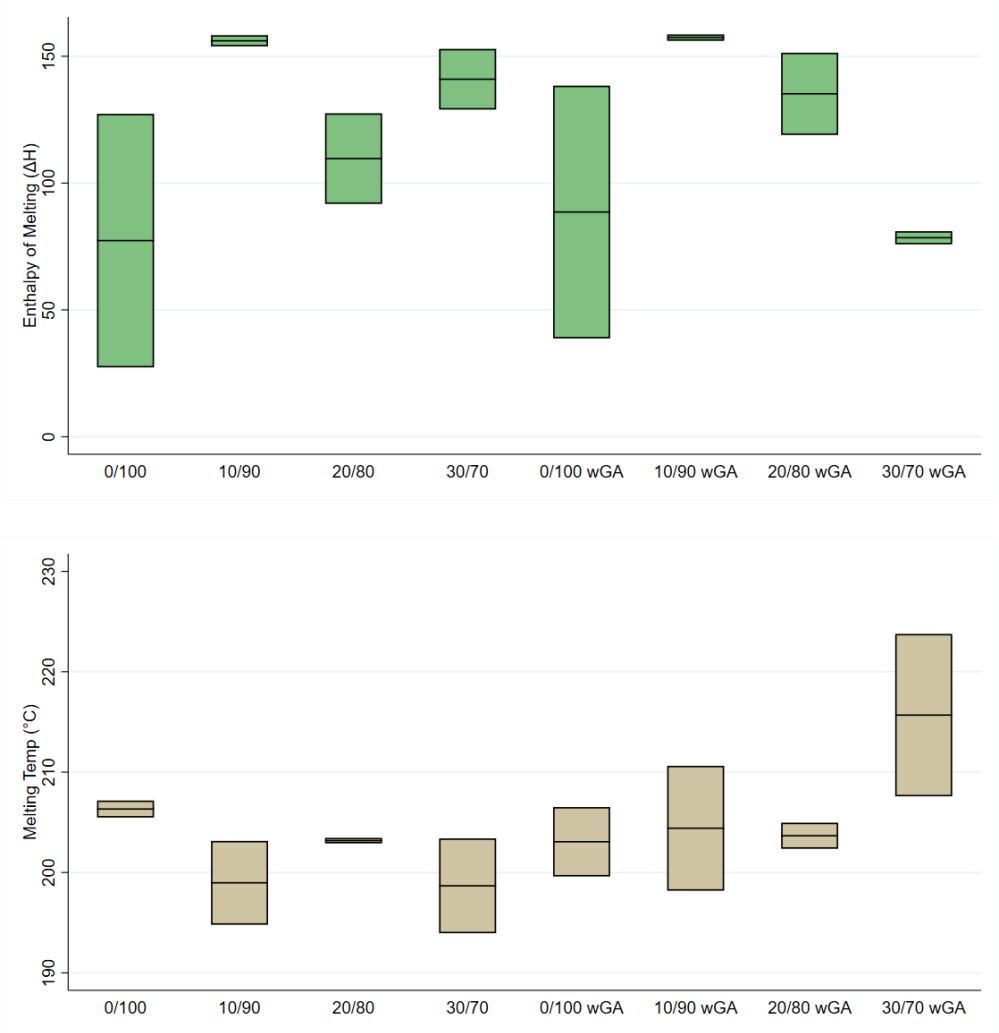

Figure 43: ΔHf and Tm boxplots of CFF/SPI resins

It should be noted that despite this variation in reported mean Tm and ΔHf values, the DSC thermograms of the neat (0/100) SPI resins produced in this work are remarkable in that they are completely unlike those of previous iterations of neat SPI resins.[10,66,68] Namely, previous iterations of neat SPI resins did not have any endothermic peaks at all.

The source of the observed endothermic peaks in this study are not attributed to protein unfolding as the various globulins were caustically (NaOH) and thermally unfolded during resin

preparation. Furthermore, the main globulins (7S and 11S) have Tm values of respectively, far lower than the reported average Tm of 206.3 °C for the 0/100 resin produced in this work. Water is unlikely to be the cause either as if that was the case, the Tm should have been lower, closer to 100 °C.

Ultimately, this peak may in fact be due to partial crystallization of the SPI. Crystallization requires both nucleation and growth of crystals and is facilitated by a favorable thermodynamic environment – longer time and higher temperature. Both these parameters were introduced in the CFF/SPI resins and JF/(CFF/SPI) composites produced post COVID-19. This partial crystallization of the SPI offers an alternative reason apart from internal crosslinking for the change in the mechanical and optical behavior of the neat SPI resins produced in this work. Partially crystalline polymers have increased strength and reduced ductility as the presence of crystalline structures restricts polymer chain movement. Opacity would also be increased, leading to a darkening in observed color. However, this theory is not without argument, as endothermic peaks were also observed in GA-crosslinked CFF/SPI resins. Typically, crosslinking increases amorphous behavior and thus would decrease ΔHf. Regardless of the mechanism that produced the endothermic peak, it was demonstrated that this peak was difficult to analyze due to large variations.

The unclear behavior of ΔHf can be understood by investigating the DSC thermograms presented in Figure 44 of two 0/100 resin specimens. Note that both specimens were derived from 0/100 resins prepared on the same day, hot pressed within moments of each other, and conditioned for the exactly same time. While all resins naturally followed the same preparation methodology, these two were specifically prepared together, further reducing potential differences.

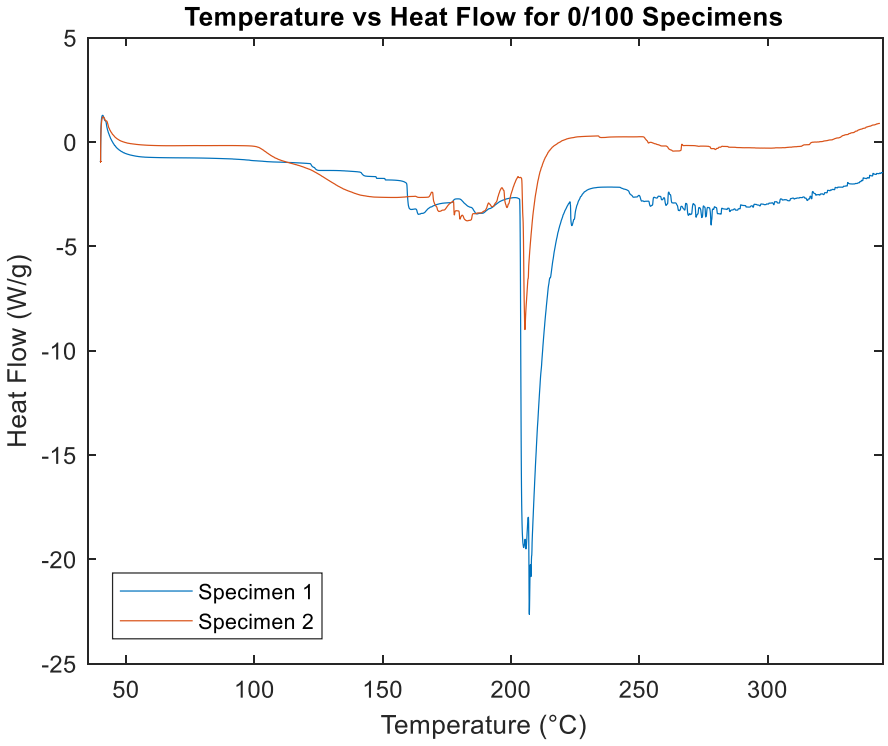

Figure 44: DSC thermograms of 0/100 GA-free resins

DSC thermogram of specimen 2 shows a much broader and shallower melting peak that begins earlier compared to the melting peak of specimen 1. A broader melting peak is indicative of a greater variation in crystallinity, and the broad size distribution amongst the crystals leads to a range of absorbed endothermic energy during melting. This means that despite being prepared and conditioned identically, there was a significant amount of variation in crystallinity between the two specimens even in the absence of CFF and GA. Thus, the effects of CFF and GA on the SPI's thermal properties are more difficult to ascertain.

This variability in reported Tm and ΔHf was further complicated when considering the nature of the chopped CFF used in this work. Since the CFF in this work consists of CFB and

CFQ, DSC tests were performed on both to determine their respective differences in melting enthalpy and melting temperature contributions. Figure 45 presents DSC thermograms for typical CFQ and CFB specimens. As a reminder CFQ refers to the rachis (quill) which serves as the primary "trunk" from which the secondary barb "branches" are located. CFQ is primarily arranged in β sheet conformation, while CFB is primarily arranged in α helix conformation.

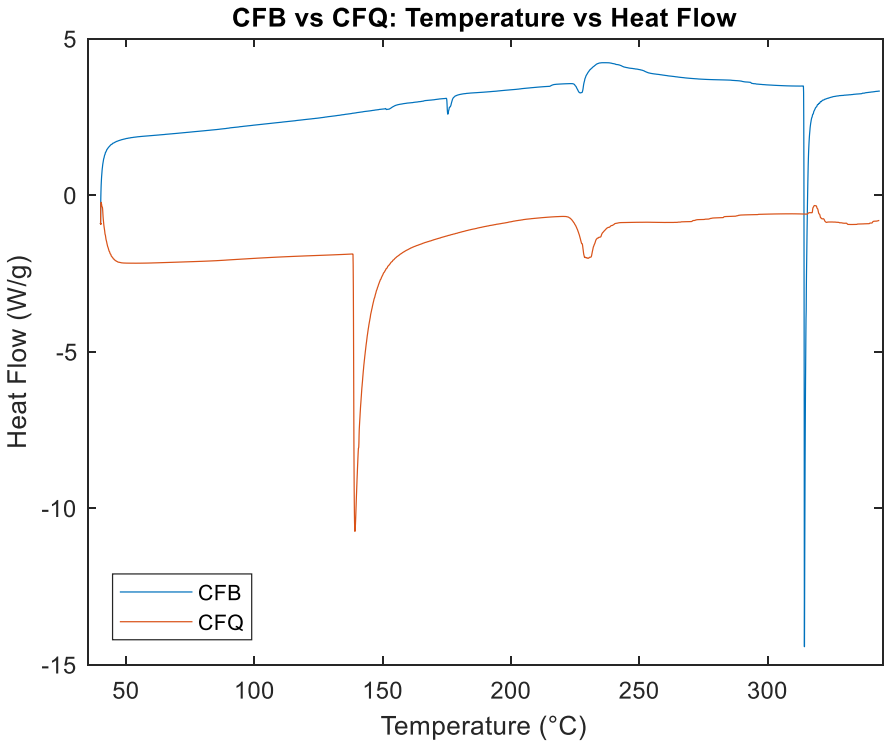

Figure 45: Typical DSC thermograms of CFB and CFQ

As can be observed from Figure 45, the CFB had a higher Tm of 314.0 °C compared to the CFQ's Tm of 138.9 °C. The higher Tm for CFB is most likely due to its higher α helix content with respect to the predominantly β conformed CFQ. Compared to the β sheet conformation, α helices have a higher packing efficiency, meaning they require a greater amount

of energy to break apart the bonds which consequently correlates to a higher thermal stablity.[43] Since the exact amount of CFB and CFQ varied specimen to specimen, a characterized specimen could have further variation in its reported Tm values.

The effect of CFF on ΔHf is not a linear one. That is, from 0 to 10% CFF the ΔHf increases from 77.3 to 156 J/g for GA-free CFF/SPI resins and from 89 to 157 J/g for CFF/SPI resins with GA. However, after this initial increase, the mean ΔHf fluctuates around 150 J/g. This is likely because as CFF is added, the amount of SPI decreases, which allows for more thermodynamically favorable crystallization. However, the exact amount will fluctuate as the amount of crystallization present in each specimen will vary.

GA's influence on ΔHf and Tm is not clear. Comparing the 0/100 CFF/SPI resins with and without GA, the ΔHf values indicate higher crystallinity for 0/100 resins with GA (77.3 J/g for GA-free 0/100 vs 88.6 J/g for 0/100 wGA) while the Tm values indicate similar thermal stability (206.3 °C vs 203.1 °C). This is contrary to the belief that crosslinked resins should have lower ΔHf values as repeatedly mentioned. Crosslinking has a complicated relationship with Tm and ΔHf. It generally reduces ΔHf and Tm since the added crosslinks decrease crystallinity. However, lower polymer chain flexibility – an effect of crosslinking – increases Tm.[29] Ultimately, perhaps the benefits offered by GA-induced crosslinking were diminished by the cons, as the DSC data and statistical analysis does not indicate that GA improved Tm or ΔHf.

4.6.4 DSC Results of JF/(CFF/SPI) Hybrid Composites

Table 14 reports the reports the summary of ΔHf and Tm values for JF/(CFF/SPI) composites with and without GA.

Table 14: Average DSC results of JF/(CFF/SPI) hybrid composites

	0/100	**10/90**	**20/80**	**30/70**	**0/100 wGA**	**10/90 wGA**	**20/80 wGA**	**30/70 wGA**
N	2	2	2	2	2	2	2	2
ΔHf (J/g)								
Mean	176.1	180.8	122.7	120.8	166.1	146.5	195.0	116.5
SD	(28.9)	(69.7)	(74.1)	(6.3)	(10.4)	(80.3)	(31.1)	(18.0)
CV	16.4%	38.6%	60.4%	5.2%	6.3%	54.8%	16.0%	15.4%
Tm (°C)								
Mean	186.8	191.3	205.5	201.3	188.2	182.4	191.4	200.0
SD	(11.5)	(18.5)	(25.3)	(6.9)	(8.1)	(21.1)	(10.4)	(3.6)
CV	6.2%	9.7%	12.3%	3.4%	4.3%	11.6%	5.4%	1.8%

The values from Table 14 show no discernable trends or behaviors apart from showing that JF/(CFF/SPI) composites with and without GA have comparable values, with large variations. The p-values, included in Appendix A.10, did not indicate any difference between the groups. The mean ΔHf values are on average larger than those of CFF/SPI resins, indicating that the JF/(CFF/SPI) composites had a higher degree of crystallization than the CFF/SPI resins. This is likely because cellulose, which makes up a large percentage of JF, is semi-crytalline.[92] However, at 0% CFF, the average Tm values for JF/(CFF/SPI) composites with and without GA are lower than 0/100 and 0/100 wGA resins. The mean Tm difference between the resins and composites decreased with the addition of CFF, suggesting that CFF perhaps improved thermal stability for the JF/(CFF/SPI) composites. Given the large variations, this observed trend cannot be concretely proven. However, overall trends are observed, in Figure 46 which includes boxplots of ΔHf and Tm.

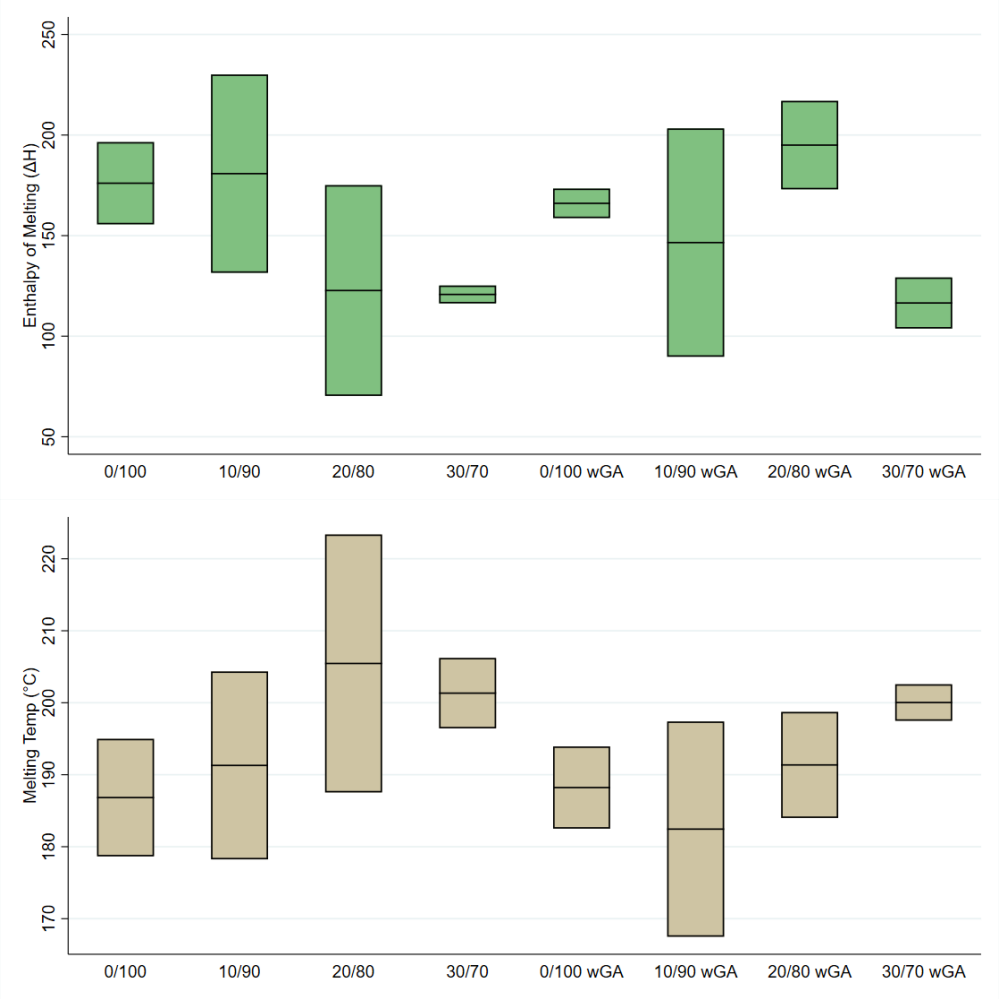

Figure 46: ΔHf and Tm boxplots of JF/(CFF/SPI) composites

Visual inspection of the boxplots does not reveal any clear trend for Peak I temperature and include a slight trend upwards for Peak II temperature. Figure 47 shows a DSC thermogram of jute fibers after conditioning for 72 h in conditioning room at 21 °C and 65% RH.

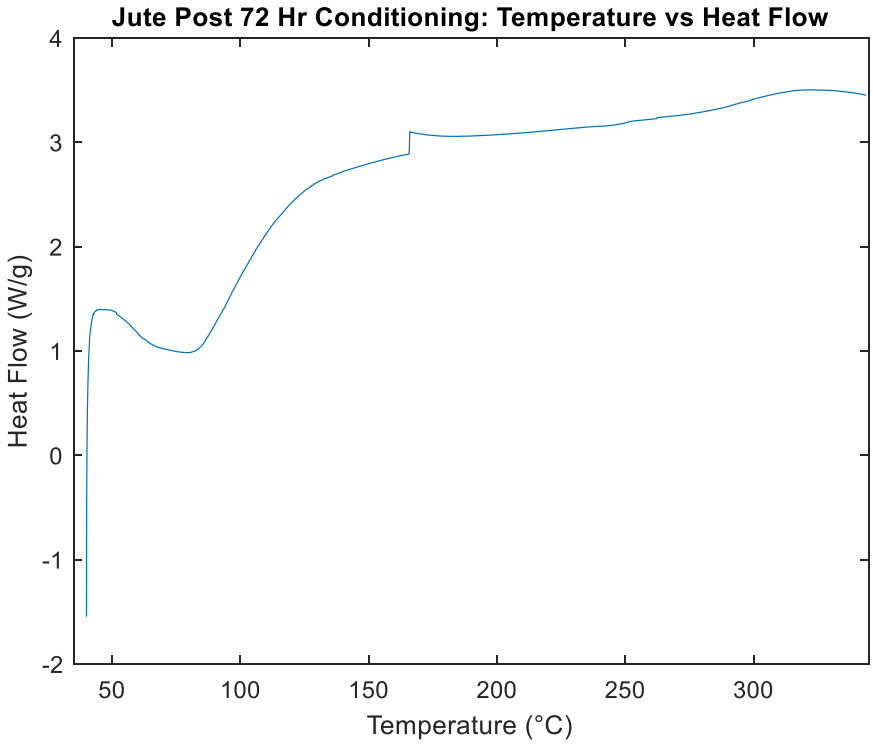

Figure 47: DSC thermogram of conditioned jute yarn

An earlier study reported that untreated jute fibers had enthalpy values of roughly 230 J/g that more or less stays the same with alkali treatment (5% NaOH) over several hours.[53] Thus, the jute component of the composite tested – which would have been exposed to caustic conditioning for many hours – can be estimated to have an ΔHf value around this level. This provides evidence for why the JF/(CFF/SPI) composites have higher ΔHf values on average than the CFF/SPI resins. The DSC data did not indicate that JF improved thermal stability as the mean Tm values for JF/(CFF/SPI) composites are on average were lower than those of the CFF/SPI resins. This suggests that the reason why JF/(CFF/SPI) composites had better flammability properties was due to the production of a high-quality char and not because of the intrinsic thermal properties of JF.

The same issues that prevented a reasonable conclusion about the influence of CFF on the thermal properties - variability in SPI crystallinity as well as unpredictability in the characterized blend of CFB/CFQ – seem to be relevant here as well. Accurate analysis is further hindered by the variable amount of JF present in each tested specimen. However, unlike the CFF/SPI resins, CFF does not generally increase the ΔHf for the JF/(CFF/SPI) composites as the JF contribution appears to be the dominating factor.

GA was not seen to affect the thermal properties of the JF/(CFF/SPI) composites. This is likely due to the same reasons (imprecise nature of crosslinking on DSC values) outlined in Section 4.6.3.

4.7 FRACTURE SURFACE IMAGING RESULTS

4.7.1 SEM Images of CFF/SPI Resin Fracture Surfaces

Figures 48 (A-D) display typical SEM images of the fracture surfaces post tensile testing of GA-free 0/100, 10/90, 20/80, and 30/70 CFF/SPI resins, respectively.

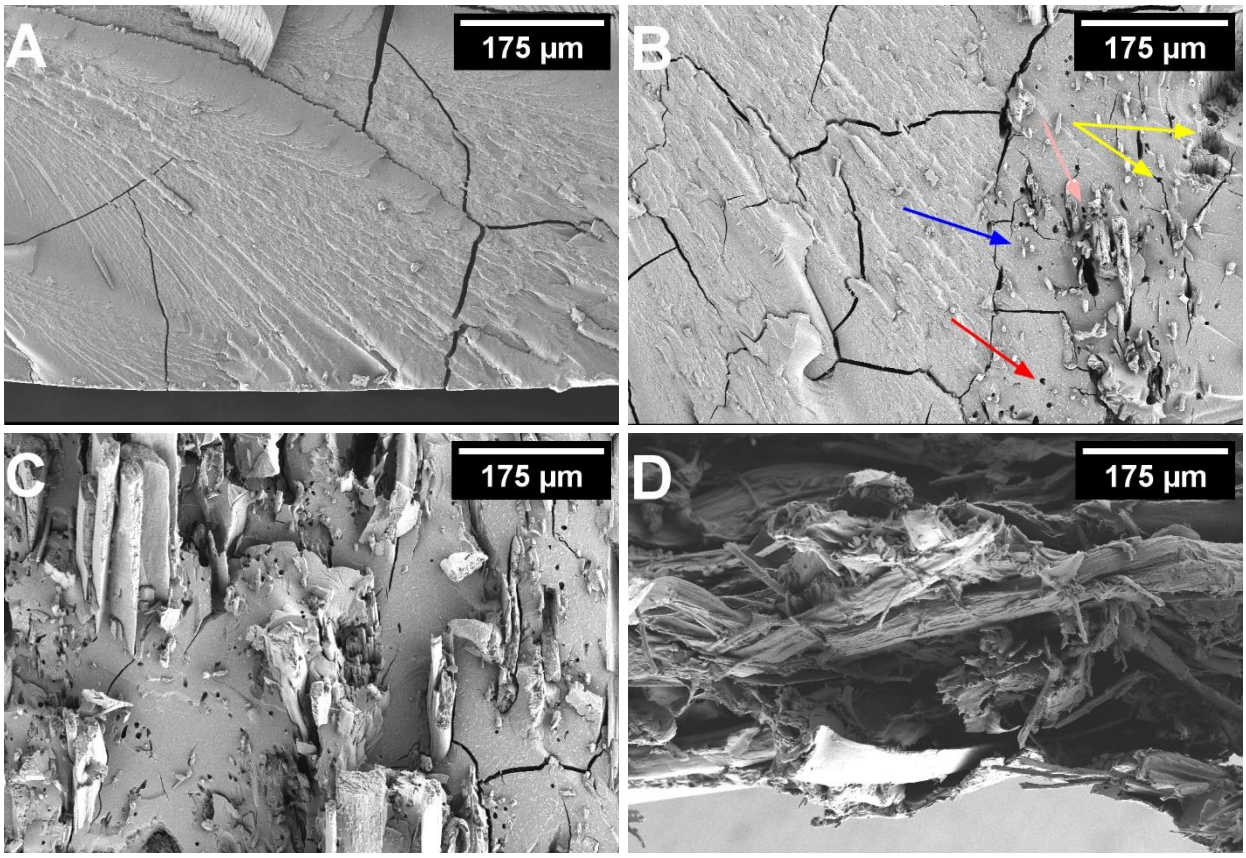

Figure 48: Typical SEM images of fracture surfaces for A: 0/100, B: 10/90, C:20/80, D: 30/70 GA-free CFF/SPI resins

The SEM image of a typical fracture surface of a 0/100 resin, as seen in Figure 48-A, can be used as a baseline to understand how adding CFF as well as GA to SPI impact the resin's tensile fracture.[93] The fracture surface of the neat SPI resin is seen to be planar, with large cracks throughout, indicative of a brittle failure. The presence of some rough texture on the surface suggests that there is some element of ductility, but not enough to produce a "dimpled" surface that is typically associated with full ductile failure.[93] This indicates that the resin did not fail below its yield strength, but still had a primarily brittle failure which reinforces conclusions drawn from the tensile resin characterization documented in Section 4.4.2.

The typical SEM image of the fracture surface for a 10/90 resin, seen in Figure 48-B**,** reveals how the addition of CFF affects the composition of the overall resin as well as how it

influences its failure. The fracture surface shows areas with higher SPI concentration (SPI-rich) and areas with higher CFF concentration (CFF-rich). A CFF rich area is identified by a pink arrow. Thus, despite the thorough homogenizing effort during resin preparation, CFF tends to aggregate or get entangled in small clumps during curing, resulting in somewhat of a heterogenous end product. CFF can be seen embedded in and protruding out of the SPI matrix throughout the fracture surface. One such CFF is shown by a blue arrow. Some voids are also observed on the fracture surface, and as their diameters match that of CFF, these voids are attributed to CFF pullout during tensile characterization rather than pockets of air or voids formed during resin preparation. An example of a void caused by CFF pullout is shown by following the red arrow. The surrounding area around these voids are seen to be flush with the planar SPI fracture surface. This could mean that the adhesion between the SPI and CFF was not stronger than the tensile force, causing CFF to be pulled out from the resin, leaving a void. If the fiber/resin interface was stronger, the surface area around the void should have appeared as "dimpled" and raised. Note that if the CFF was weaker than the force needed to pull CFF out, it could also break at the fracture surface.

Alternatively, the CFF could have been too short or had too low of an aspect ratio, to be held by the SPI resin. Either way, the SEM images suggest that the CFF was unable to perform the role of a typical fiber reinforcement and acted more as a filler. The image provides evidence that the cluster of voids caused by CF fiber pullout can act as stress concentrations and reduce specimen fracture strain which is detrimental to material strength. Inspection of the fracture surfaces shows micro-cracks surrounding some CFF voids. Many of these microcracks also appear to propagate to another CFF void, resulting in a larger observed void. Yellow arrows shown in Figure 48-B point to some microcracks and their propagation during fracture. This, in

turn, can become an even greater site of stress concentrations and induce catastrophic failure. Thus, the decrease in tensile strength with the addition of CFF as reported by the tensile tests can be understood through SEM analysis of Figure 48-B.

The SEM images of the fracture surfaces for 10/90 and 20/80 resins seen in Figure 48-B and 48-C, respectively, also show that the SPI fraction of the resin (i.e. the matrix) breaks in an increasingly brittle manner as CFF is added. This can be observed by the SPI fracture surface becoming smoother as the CFF percentage increases. This may seem counterintuitive as the SEM images show the surfaces becoming increasingly corrugated with the addition of CFF. However, this topography is tied to the increase of CFF creating CFF clusters, i.e., larger CFF-rich zones to be separated from the SPI-rich zones which results in the rougher fracture surfaces. This happens because the clusters do not exist in one plane but are spread through the resin. The SPI-rich areas, however, are observably smoother as expected and, thus, since the SPI constitutes the matrix, means that the resins are becoming more brittle with the addition of CFF. This confirms the GA-free resin characterization discussion presented in Section 4.4.2. In fact, as the SEM image of the 30/70 resin seen in Figure 48-D shows, with 30% CFF, the resin's actual fracture surface can no longer be observed as the failure at the CFF aggregation. Thus, adding 30% or more of CFF using the specific resin preparation methodology detailed in Section 3.4 is not recommended. This SEM analysis gives credence to the observed inability to form a cohesive resin past 30% CFF during early trials of resin preparation using lab equipment. Industrial mixers might help in dispersing the CFF more evenly.

Figures 49 (A-D) display typical SEM images of fracture surfaces post tensile testing of 0/100, 10/90, 20/80, and 30/70 CFF/SPI resins with GA, respectively.

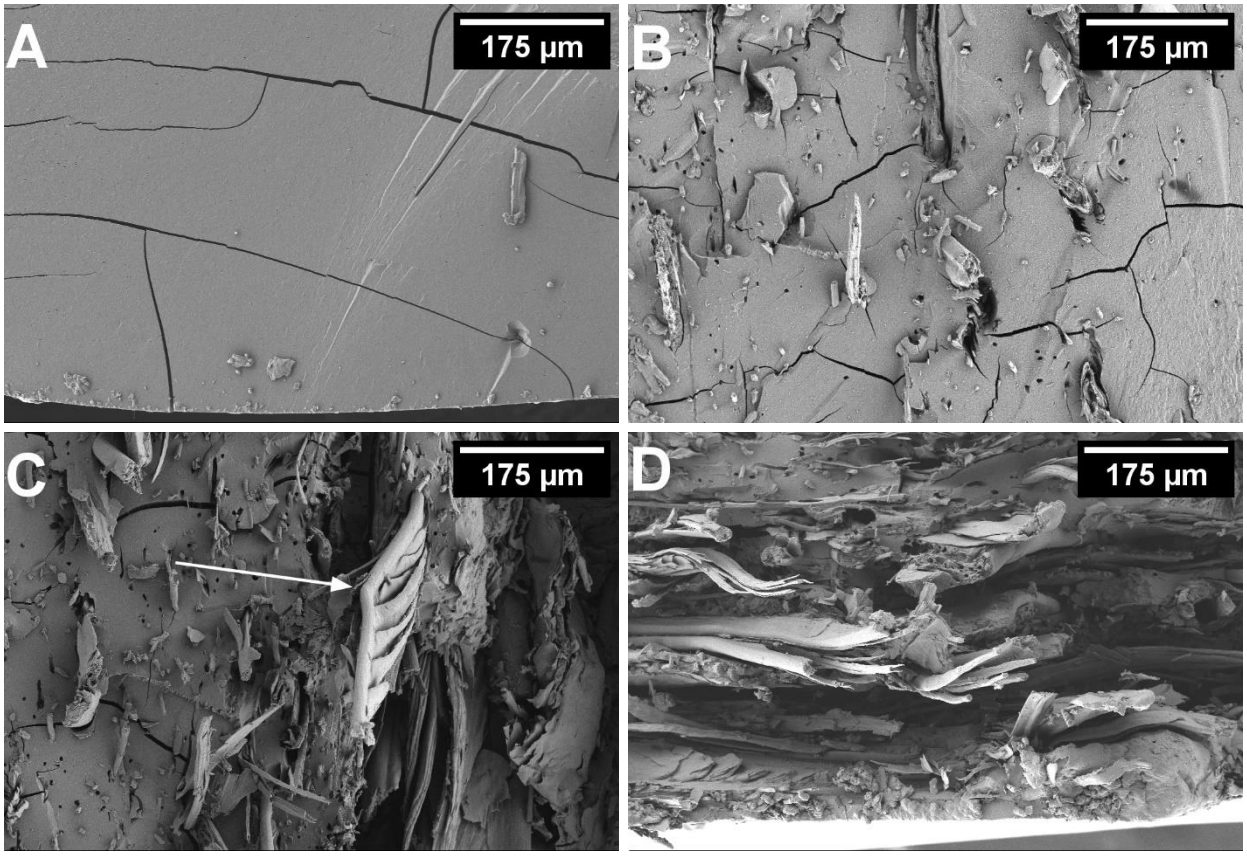

Figure 49: Typical SEM images of fracture surfaces for A: 0/100, B: 10/90, C:20/80, D: 30/70 CFF/SPI wGA resins

These SEM images illustrate that the CFF/SPI resins with GA fail in a similar manner with respect to their GA-free counterparts. Comparing the SEM images of the fracture surfaces for a 0/100 GA-free resin and a 0/100 wGA resin using Figures 48-A and 49-A, respectively, it appears that GA leads to an even more brittle fracture. This is expected because of the crosslinking provided by GA and is evidenced by the comparatively smoother and even more planar fracture surface of the 0/100 wGA resin compared to the 0/100 GA-free resin. Failure analysis using the SEM images support the tensile test results which found the resins with GA to be more brittle than the GA-free ones. The increasing addition of CFF, and its consequence on the fracture plane, as seen in the SEM images for 10/90, 20/80, and 30/70 wGA resins in Figures 49-B, 49-C, 49-D, respectively, mimic their respective GA-free counterparts.

Another parallel to the GA-free resins is that as CFF content is increased, the fracture surface is once again becomes more obscured and/or rough until, as the SEM image of the fracture surface for the 30/70 wGA resin seen in Figure 49-D shows, the resin is no longer visible within the majority of the image and only the CFF can be seen.

The SEM image of the fracture surface for a typical 20/80 wGA resin is seen in Figure 49-C, with a white arrow pointing to a quill piece with attached barbs. The presence of this pristine looking piece demonstrates that the NaOH added to the resin did not dissolve or alter the structure of the chopped CFF in any way. This, in turn, confirms that the lower mechanical properties reported for SPI/CFF resins with higher CFF% are not due to the destruction of the fiber morphology but perhaps due to the brittle nature of the SPI resin and its below-desired adhesion to the CFF and defects formed by clustering of CFF.

4.7.2 SEM Images of JF/(CFF/SPI) Hybrid Composite Fracture Surfaces

Figures 50 (A-D) display typical SEM images of various sections of the fracture surfaces, post tensile testing, of GA-free 0/100, 10/90, 20/80, and 30/70 JF/(CFF/SPI) hybrid composites, respectively.

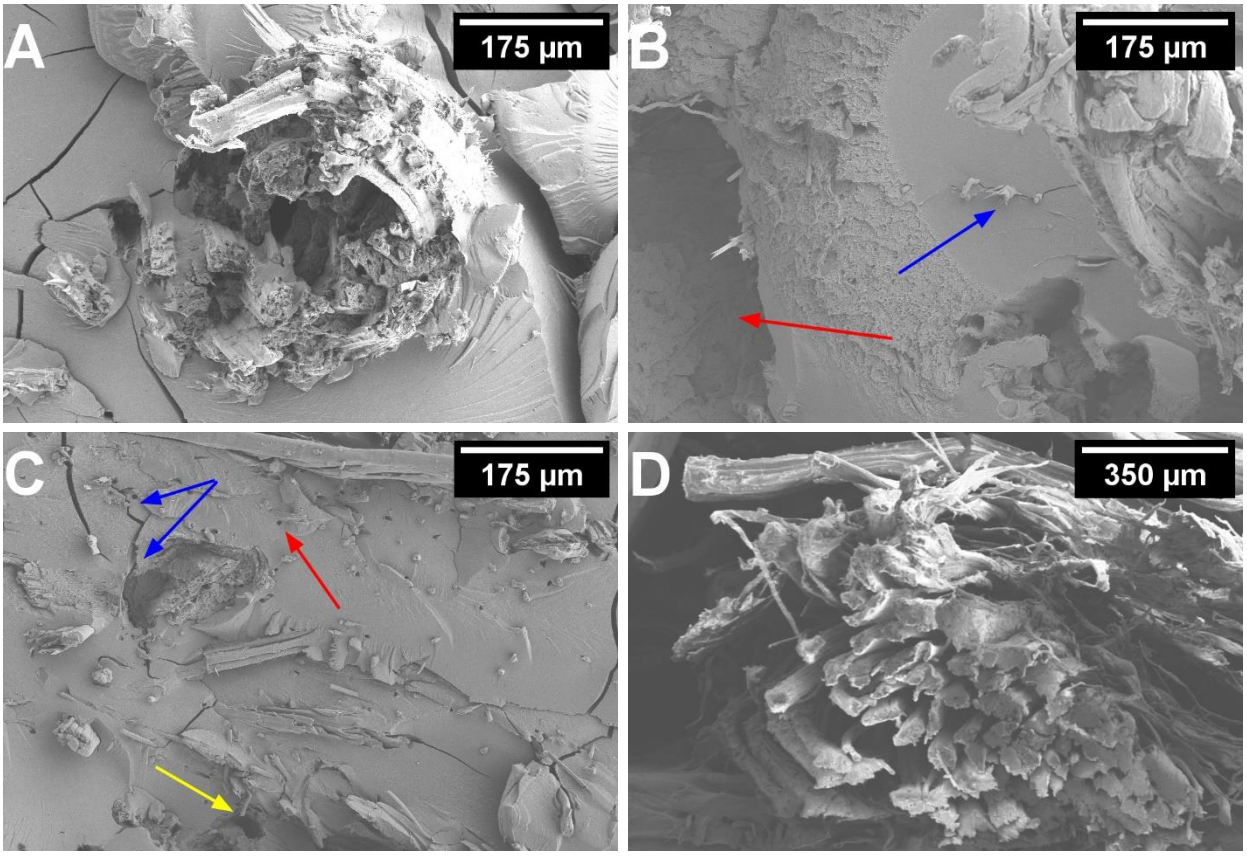

Figure 50: Typical SEM images of fracture surfaces for A: 0/100, B: 10/90, C:20/80, D: 30/70 GA-free JF(CFF/SPI) hybrid composites

Using the scale bar, jute yarns were measured to have a diameter in the range of 300-700 µm, most frequently in the 500-700 µm range. Figure 50-A shows what a typical fracture surface for a JF/(0/100) GA-free composite looks like. From this image, the cross-section of a broken jute yarn can be seen, embedded in the SPI matrix. The SPI matrix itself contains similar large cracks observed in 0/100 GA-free resins but has a smoother fracture surface compared to respective resins. As mentioned in the analysis for the jute tensile tests in Section 4.4.1, the jute yarns are more ductile and less strong than the neat 0/100 GA-free resin. This explains why the matrix in JF/(0/100) GA-free composites is shown to have failed in a brittle manner despite the overall higher ductility compared to the 0/100 GA-free resin.

The SEM image of the fracture surface for a typical 10/90 GA-free composites seen in Figure 50-B shows what the addition of CFF looks like in the composite as well as what a void caused by jute yarn pullout looks like. A red arrow points to this type of void. CFF is seen embedded in the SPI matrix in a similar manner to its resin counterpart by a blue arrow. Figure 50-C focuses on a matrix section of the 20/80 JF/(CFF/SPI) GA-free composite to confirm that the CF fibers still leave voids that act as stress concentrations. A void caused by CFF pullout is pointed to by the red arrow. Microcrack propagation is shown by following the blue arrows, and a CFF-rich area is indicated by a yellow arrow. Figure 50-D focuses on a cross section of a fractured jute yarn in a 30/70 JF/(CFF/SPI) GA-free composite to observe the individual fractured jute fibers that the yarn is composed of. However, the fracture surface is obscured by the increased presence of CFF (as previously mentioned).

Figures 51 (A-D) display SEM images of fracture surfaces of various sections post tensile testing of 0/100, 10/90, 20/80, and 30/70 JF/(CFF/SPI) hybrid composites with GA, respectively.

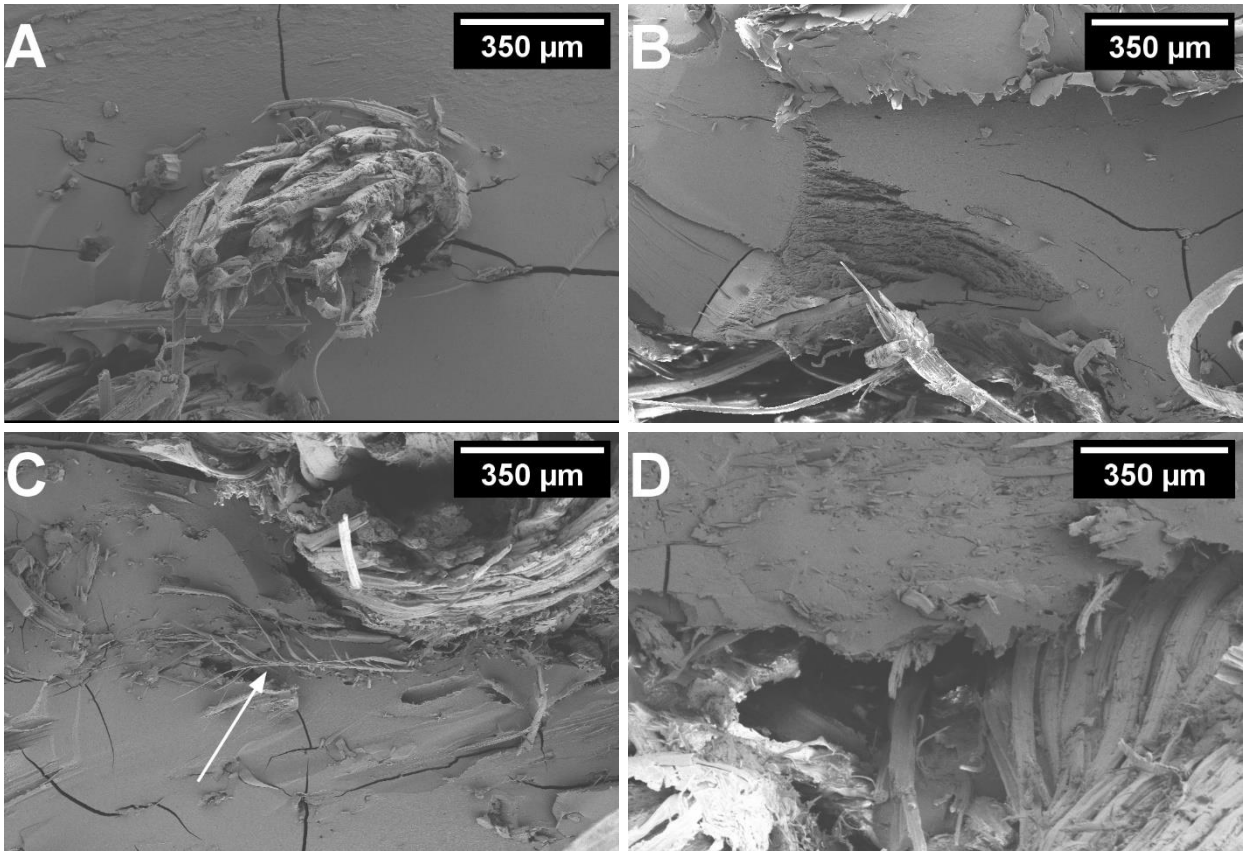

Figure 51: Typical SEM images of fracture surfaces for A: 0/100, B: 10/90, C:20/80, D: 30/70 JF/(CFF/SPI) wGA hybrid composites

These images only serve to confirm that they mimic the GA-free composites discussed above, in their behavior. In the SEM image of a fracture surface for a 20/80 GA (SPI/CFF)/JF composite shown in Figure 51-C, a CF quill and its barbs are seen embedded in the SPI matrix near a fractured jute yarn, confirming that once again, the CFF morphology is preserved through the composites manufacturing process.

Chapter 5

CONCLUSIONS

In this research, CFF, SPI, and JF were used to fabricate green, non-toxic, and biodegradable CFF/SPI resins and JF/(CFF/SPI) hybrid composites. While GA was used to crosslink these resins and composites, experiments were carried out to investigate whether GA-free CFF/SPI resins and JF/(CFF/SPI) composites could have competitive properties without the use of any external crosslinkers. All specimens were characterized for their tensile, thermal, flammability (fire resistance), and fracture surface (post tensile testing) properties. Additionally, resins underwent moisture regain and ATR-FTIR characterization and composites underwent flexural characterization.

Results indicated that the addition of CFF improved the properties of CFF/SPI resins with and without GA in the following ways: eliminating warping both pre-hot pressing and post conditioning, and increasing elastic stiffness (Young's modulus). For CFF/SPI resins without GA, adding CFF improved thermal stability and flammability likely through the formation of a higher quality char layer. For CFF/SPI resins with GA, thermal stability and flammability were generally better without CFF as CFF probably compromised the high-quality char layer formed from GA crosslinks. CFF additionally decreased moisture regain for CFF/SPI resins with GA.

The introduction of JF created hybrid composites with and without GA that had better tensile properties (higher peak tensile stress, higher ductility, greater stiffness) and were less flammable (lower pHRR and THR) than the CFF/SPI resins. The improved flammability performance was likely due to the formation a higher quality char layer as a consequence of adding JF. The addition of CFF in these composites were generally beneficial for the same reasons mentioned for the resins.

This work also led to the development of neat SPI resins that were markedly different in color, mechanically, spectrally, and thermally from earlier iterations of SPI resins by other researchers. These changes likely originated from the improved thermodynamic environment (higher temperature, longer time) that the resins produced post COVID-19 were pre-cured in, as this was the only major difference. The DSC results point to this change in thermodynamic environment causing possible internal crosslinks or semi-crystallinity. Consequently, GA-free neat SPI resins and composites produced in this work tended to have superior or comparable values to 0/100 wGA resins. In the few instances 0/100 wGA outperformed the 0/100 resin, the introduction of CFF and JF diminished or outright eliminated the benefits attained by adding 10 wt% GA.

Ultimately, this is a very positive discovery, and future research with GA-free SPI could further improve its various properties. CFF restricting warping is an important observation as well, as the hydrophilicity of SPI – and its consequent warping – has been a major issue to tackle. The mechanical tests were performed at a higher humidity (65% RH) than the ASTM suggested 50% RH, meaning that the values obtained were conservative. This further supports the use of CFF, a waste, as a powerful green additive in the field of green resins and composites.

Willingly or unwillingly, the era of petroleum-based plastics is coming to an end. This research has shown that CFF, alongside SPI and JF, offer a sustainable path to replace these environmentally unfriendly materials and help create a greener future for all.

Chapter 6

FUTURE RESEARCH SUGGESTIONS

6.1 MATERIALS

6.1.1 Chicken Feather Fibers

The CFF used in this study were chopped prior to procurement, and thus did not retain the full mechanical benefits of using whole, unadulterated quills, which, as a reminder, is the strongest and stiffest part of the CF. The chopped CFF may not have maintained the minimum aspect ratio needed for proper stress transfer, and thus future work may benefit from either using whole feathers, or if this is too difficult, pulverizing the CFF until they become much smaller or granular in order to form more homogenous resins. Homogenized resins would be uniform and allow for better analysis as there would not be a worry for localized concentrations of CFF skewing results.

6.1.2 Jute

The JF used in this work was purchased from a common fabric store and while the composites created using it serve as good proof of concepts, it was found that the jute itself was weaker in tension than the SPI resin used in this study. Thus, either processing/treating the jute in order to improve its tensile properties or acquiring jute with higher tensile properties from a more specialized source, could benefit future composites.

6.2 METHODOLOGY

6.2.1 Plasticizer Content

D-Sorbitol (10%) with respect to SPI+CFF weight was used in this research. While 10% was enough to obtain satisfactory ductility in CFF/SPI resins and JF/(CFF/SPI) composites produced pre COVID-19, this amount contributed to why the CFF/SPI resins and JF/(CFF/SPI) composites produced post COVID-19 were so brittle. Typically, resins and composites based on SPI have used between 20-30% plasticizer with respect to protein weight for optimal mechanical properties.[10,11]

6.2.2 Glutaraldehyde Content

GA (10%) with respect to SPI+CFF weight was used in this work to create externally crosslinked resins. While GA-free resins were found to be superior, observing how much GA is necessary to match GA-free resins could be an interesting undertaking.

6.2.3 Composite Assembly

While care was taken to align the jute yarns as best as possible during hand-layup, improvements could be made to ensure the best possible alignment to increase mechanical properties.

6.3 COVID-19 RELATED ISSUES

6.3.1 Resins

As a result of strict lab time scheduling due to COVID-19 safety, the resin procedure had to be completely redone using different equipment and parameters. Consequently, the resins produced for mechanical, thermal, ATR-FTIR, and SEM characterization were stronger and less ductile than the jute yarns used for composites.

Producing a more ductile resin for use as a flexible matrix would have been ideal and moving forward should be implemented instead of the brittle one used in this research. As mentioned in Section 6.2.1, a straightforward solution would be to increase the plasticizer content past 10% with respect to protein weight.

6.3.2 Composites

If time permitted, the composite layers would have been arranged in a variety of stacking sequences based on fiber/yarn orientation and tested to determine the best layout following standard laminate theory. As it were, all composites were stacked with a 0° orientation in the interest of time.

6.3.3 Cone Calorimetry Characterization

While a full sample set was sent for cone calorimetry characterization, COVID-19 related lockdowns prevented these samples from being tested. This left the flammability characterization to come solely from the MCC results which could have potentially been affected by the fact that since only a few grams were tested for each sample, a representative volume may not have been truly followed in order to achieve the most accurate results. As mentioned earlier, the tested specimens could have been obtained from a localized CFF-rich or SPI-rich parts of the resin/composite, which may have affected the results.

6.4 ADDITIONAL STUDIES

6.4.1 Dynamic Mechanical Analysis (DMA) Characterization

DMA testing of the resins would add to the mechanical characterization of the resins and further reveal information about transition temperatures related to various molecular motions.

6.4.2 Moisture Absorbance and Swelling Characterization

Moisture absorbance testing would determine how these green resins and composites would fare in humid environments or when immersed in water. While the weight change was measured to determine the increase in mass post conditioning at 65% RH and 21 °C, these results do not address fully soaking the samples in water, a condition these composites may encounter during use.

6.4.3 Biodegradability Characterization

Because all components are biodegradable, it is assumed that these CFF/SPI resins and JF/(CFF/SPI) composites are fully biodegradable and compostable as earlier studies have confirmed this. However, testing the time required to fully biodegrade the CFF/SPI resins and JF/(CFF/SPI) composites would give concrete information to further validate the use for green resins and composites.

6.4.4 X-Ray Diffraction

X-ray diffraction would allow confirmation of the semi-crystallinity theorized to have been the root of the endothermic peaks found in the DSC studies.

APPENDIX

Appendix A: P-Value Tables

P-values from each t-test are compiled in the tables below. P-values less than 0.05 are presented in bold letters. Each CFF/SPI ratio was assigned a numerical value to facilitate comparisons. The numerical assignments are as follows below:

CFF/SPI Ratio	0/100	10/90	20/80	30/70	0/100 wGA	10/90 wGA	20/80 wGA	30/70 wGA
Assigned Number	1	2	3	4	5	6	7	8

A.1 MCC P-value Table for CFF/SPI Resins

pHRR	1-2	0.307	1-3	0.291	1-4	0.165	2-3	0.664	2-4	0.435	3-4	0.871
	5-6	0.237	5-7	**0.021**	5-8	0.122	6-7	0.459	6-8	0.556	7-8	0.982
	1-5	0.509	2-6	0.626	3-7	0.813	4-8	0.644				
TpHRR	1-2	0.916	1-3	0.924	1-4	0.976	2-3	0.855	2-4	0.916	3-4	0.896
	5-6	0.661	5-7	0.799	5-8	0.226	6-7	0.775	6-8	0.199	7-8	0.147
	1-5	0.481	2-6	0.735	3-7	0.542	4-8	0.306				
THR	1-2	0.447	1-3	0.494	1-4	0.911	2-3	0.349	2-4	0.382	3-4	0.422
	5-6	0.068	5-7	0.596	5-8	0.25	6-7	0.405	6-8	0.413	7-8	0.468
	1-5	0.725	2-6	0.057	3-7	0.306	4-8	0.543				

A.2 MCC P-value Table for JF/(CFF/SPI) Hybrid Composites

pHRR	1-2	0.234	1-3	0.175	1-4	0.183	2-3	0.131	2-4	0.368	3-4	0.142
	5-6	0.738	5-7	0.33	5-8	0.213	6-7	0.442	6-8	0.885	7-8	0.101
	1-5	0.113	2-6	0.496	3-7	0.415	4-8	0.487				
TpHRR	1-2	0.709	1-3	0.142	1-4	0.098	2-3	0.151	2-4	0.101	3-4	0.676
	5-6	0.378	5-7	0.988	5-8	0.952	6-7	0.243	6-8	0.381	7-8	0.955
	1-5	0.307	2-6	0.87	3-7	0.737	4-8	0.498				
THR	1-2	0.281	1-3	0.328	1-4	0.196	2-3	0.153	2-4	0.27	3-4	0.171
	5-6	0.448	5-7	**0.031**	5-8	0.628	6-7	0.316	6-8	0.433	7-8	**0.035**
	1-5	0.153	2-6	0.473	3-7	0.486	4-8	0.25				

A.3 Tensile P-value Table for JF Strips

Peak Tensile Stress	Warp-Weft	**0.004**
Tensile Strain at Peak Tensile Stress	Warp-Weft	0.3594
Young's Modulus	Warp-Weft	**0.026**

A.4 Tensile P-value Table for CFF/SPI Resins

Tensile Fracture Stress	1-2	**0**	1-3	**0**	1-4	**0**	2-3	0.073	2-4	**0.017**	3-4	0.316
	5-6	**0.099**	5-7	**0.024**	5-8	**0.015**	6-7	**0.008**	6-8	**0.001**	7-8	0.317
	1-5	**0.003**	2-6	**0.002**	3-7	**0**	4-8	**0**				
Tensile Fracture Strain	1-2	**0**	1-3	**0**	1-4	**0**	2-3	0.115	2-4	**0.006**	3-4	0.058
	5-6	0.051	5-7	**0.02**	5-8	**0.016**	6-7	**0.001**	6-8	**0**	7-8	0.375
	1-5	0.073	2-6	**0.032**	3-7	**0.004**	4-8	**0.022**				
Young's Modulus	1-2	**0.001**	1-3	**0**	1-4	**0**	2-3	0.433	2-4	**0.022**	3-4	0.078
	5-6	**0.003**	5-7	**0.001**	5-8	**0**	6-7	0.145	6-8	**0.003**	7-8	0.061
	1-5	0.379	2-6	0.435	3-7	0.813	4-8	0.753				

A.5 Tensile P-value Table for JF/(CFF/SPI) Hybrid Composites

Peak Tensile Stress	1-2	0.135	1-3	0.11	1-4	**0.01**	2-3	**0.002**	2-4	**0.001**	3-4	**0.111**
	5-6	**0**	5-7	**0.002**	5-8	**0**	6-7	**0**	6-8	**0.005**	7-8	**0**
	1-5	**0.002**	2-6	**0**	3-7	0.112	4-8	**0.027**				
Tensile Strain at Peak Tensile Stress	1-2	**0.002**	1-3	0.108	1-4	0.101	2-3	**0.01**	2-4	0.397	3-4	0.426
	5-6	0.22	5-7	**0.048**	5-8	0.054	6-7	0.518	6-8	0.559	7-8	0.933
	1-5	**0**	2-6	**0.039**	3-7	**0**	4-8	**0.039**				
Young's Modulus	1-2	0.951	1-3	0.667	1-4	0.953	2-3	0.518	2-4	0.882	3-4	0.639
	5-6	0.526	5-7	0.502	5-8	0.511	6-7	0.1	6-8	0.836	7-8	0.152
	1-5	0.256	2-6	**0.007**	3-7	0.254	4-8	**0.03**				

A.6 Flexural P-value Table for JF/(CFF/SPI) Hybrid Composites

Peak Flexural Stress	1-2	**0.012**	1-3	**0.04**	1-4	**0.027**	2-3	0.414	2-4	0.936	3-4	0.598
	5-6	0.196	5-7	0.262	5-8	0.166	6-7	0.81	6-8	0.719	7-8	0.966
	1-5	**0**	2-6	**0**	3-7	**0.018**	4-8	**0.019**				
Flexural Strain at Peak Flexural Stress	1-2	0.17	1-3	**0.005**	1-4	**0.042**	2-3	**0.036**	2-4	0.323	3-4	0.523
	5-6	0.268	5-7	0.06	5-8	**0**	6-7	0.248	6-8	**0.001**	7-8	0.085
	1-5	0.133	2-6	0.061	3-7	0.131	4-8	0.317				
Flexural Modulus	1-2	0.202	1-3	**0.038**	1-4	**0.025**	2-3	0.352	2-4	0.147	3-4	0.457
	5-6	**0.023**	5-7	**0.023**	5-8	**0**	6-7	0.138	6-8	**0.001**	7-8	0.333
	1-5	**0**	2-6	**0.001**	3-7	0.145	4-8	0.181				

A.7 TGA P-value Table for CFF/SPI Resins

Peak I	1-2	0.875	1-3	0.149	1-4	**0.074**	2-3	0.309	2-4	0.186	3-4	0.164
Temperature	5-6	0.106	5-7	0.258	5-8	0.345	6-7	0.105	6-8	**0.062**	7-8	0.113
	1-5	**0.039**	2-6	0.225	3-7	0.168	4-8	0.108				
Peak II	1-2	0.094	1-3	0.138	1-4	0.155	2-3	0.688	2-4	0.683	3-4	0.112
Temperature	5-6	0.117	5-7	**0.018**	5-8	0.092	6-7	0.347	6-8	0.645	7-8	0.595
	1-5	0.252	2-6	0.955	3-7	0.346	4-8	0.421				

A.8 TGA P-value Table for JF/(CFF/SPI) Hybrid Composites

Peak II	1-2	0.688	1-3	0.132	1-4	0.082	2-3	0.344	2-4	0.256	3-4	0.469
Temperature	5-6	0.481	5-7	0.316	5-8	0.192	6-7	0.523	6-8	0.147	7-8	0.8
	1-5	0.345	2-6	0.523	3-7	0.989	4-8	0.325				

A.9 DSC P-value Table for CFF/SPI Resins

Tm	1-2	0.32	1-3	0.14	1-4	0.346	2-3	0.498	2-4	0.966	3-4	0.515
	5-6	0.872	5-7	0.893	5-8	0.34	6-7	0.925	6-8	0.391	7-8	0.372
	1-5	0.514	2-6	0.553	3-7	0.77	4-8	0.241				
Enthalpy	1-2	0.359	1-3	0.634	1-4	0.416	2-3	0.229	2-4	0.42	3-4	0.299
Change	5-6	0.399	5-7	0.515	5-8	0.872	6-7	0.401	6-8	**0.006**	7-8	0.17
	1-5	0.888	2-6	0.681	3-7	0.401	4-8	0.108				

A.10 DSC P-value Table for JF/(CFF/SPI) Hybrid Composites

Tm	1-2	0.803	1-3	0.478	1-4	0.293	2-3	0.594	2-4	0.58	3-4	0.857
	5-6	0.769	5-7	0.77	5-8	0.253	6-7	0.663	6-8	0.445	7-8	0.437
	1-5	0.903	2-6	0.7	3-7	0.573	4-8	0.841				
Enthalpy	1-2	0.941	1-3	0.486	1-4	0.213	2-3	0.504	2-4	0.436	3-4	0.976
Change	5-6	0.789	5-7	0.4	5-8	0.104	6-7	0.546	6-8	0.69	7-8	0.119
	1-5	0.712	2-6	0.694	3-7	0.38	4-8	0.797				

BIBLIOGRAPHY

(1) Gurav, R. G.; Jadhav, J. P. A Novel Source of Biofertilizer from Feather Biomass for Banana Cultivation. *Environ Sci Pollut Res Int* **2013**, *20* (7), 4532–4539. https://doi.org/10.1007/s11356-012-1405-z.

(2) Blake, J. P. CAST Issue Paper 40 Task Force Members Authors Reviewers CAST Liaison https://www.semanticscholar.org/paper/CAST-Issue-Paper-40-Task-Force-Members-Authors-CAST-Blake/6fefbdb89277a38ad50a333bd00247ccecb019f4 (accessed 2020 -07 -07).

(3) Tesfaye, T.; Sithole, B.; Ramjugernath, D. Valorisation of Chicken Feathers: A Review on Recycling and Recovery Route—Current Status and Future Prospects. *Clean Techn Environ Policy* **2017**, *19* (10), 2363–2378. https://doi.org/10.1007/s10098-017-1443-9.

(4) Single-use plastics: New EU rules to reduce marine litter https://ec.europa.eu/commission/presscorner/detail/en/IP_18_3927 (accessed 2020 -07 -01).

(5) Reddy, N.; Yang, Y. Light-Weight Polypropylene Composites Reinforced with Whole Chicken Feathers. *Journal of Applied Polymer Science* **2010**, *116* (6), 3668–3675. https://doi.org/10.1002/app.31931.

(6) Szeteiová, K. AUTOMOTIVE MATERIALS PLASTICS IN AUTOMOTIVE MARKETS TODAY https://www.mtf.stuba.sk/buxus/docs/internetovy_casopis/2010/3/szeteiova.pdf.

(7) Chavan, V. Moldable ‘Green’ Composites Using Cross-Linked Soy Protein and Maleinized Boiled Linseed Oil (MBLO) and Micro-Fibrillated Cellulose (MFC), Cornell University, Ithaca, 2007.

(8) Netravali, A. N.; Huang, X.; Mizuta, K. Advanced ‘Green’ Composites. *Advanced Composite Materials* **2007**, *16* (4), 269–282.

(9) Ghosh Dastidar, T.; Netravali, A. N. A Soy Flour Based Thermoset Resin without the Use of Any External Crosslinker. *Green Chem.* **2013**, *15* (11), 3243–3251. https://doi.org/10.1039/c3gc40887f.

(10) Lodha, P.; Netravali, A. N. Thermal and Mechanical Properties of Environment-Friendly 'Green' Plastics from Stearic Acid Modified-Soy Protein Isolate. *Industrial Crops and Products* **2005**, *21* (1), 49–64. https://doi.org/10.1016/j.indcrop.2003.12.006.

(11) Lodha, P.; Netravali, A. N. Characterization of Phytagel® Modified Soy Protein Isolate Resin and Unidirectional Flax Yarn Reinforced "Green" Composites. *Polymer Composites* **2005**, *26* (5), 647–659. https://doi.org/10.1002/pc.20128.

(12) Huang, X.; Netravali, A. Biodegradable Green Composites Made Using Bamboo Micro/Nano-Fibrils and Chemically Modified Soy Protein Resin. *Composites Science and Technology* **2009**, *69* (7), 1009–1015. https://doi.org/10.1016/j.compscitech.2009.01.014.

(13) Huang, X.; Netravali, A. Characterization of Flax Fiber Reinforced Soy Protein Resin Based Green Composites Modified with Nano-Clay Particles. *Composites Science and Technology* **2007**, *67* (10), 2005–2014. https://doi.org/10.1016/j.compscitech.2007.01.007.

(14) Kim, J. T.; Netravali, A. N. Development of Aligned-Hemp Yarn-Reinforced Green Composites with Soy Protein Resin: Effect of PH on Mechanical and Interfacial Properties. *Composites Science and Technology* **2011**, *71* (4), 541–547. https://doi.org/10.1016/j.compscitech.2011.01.004.

(15) Development, O. of R. &. SUSTAINABLE PLASTICS: DESIGNING AND DEMONSTRATING RENEWABLE, BIODEGRADABLE PRODUCTS MADE OF SOY PROTEIN-BASED PLASTICS

https://cfpub.epa.gov/si/si_public_record_Report.cfm?Lab=NCER&dirEntryID=188277 (accessed 2020 -06 -29).

(16) Smith, A. K.; Circle, S. J. *SOYBEANS: CHEMISTRY AND TECHNOLOGY*; Smith, A. K., Circle, S. J., Eds.; AVI Publishing: Westport, United Kingdom, 1972; Vol. 1.

(17) Lusas, E.; Rhee, K. Chapter 8 - Soy Protein Processing and Utilization. In *Practical Handbook of Soybean Processing and Utilization*; Erickson, D., Ed.; AOCS Press: College Station, Texas, 1995; pp 117–160.

(18) Soy protein concentrate brochure https://ussec.org/resources/soy-protein-concentrate-brochure/ (accessed 2020 -06 -30).

(19) Islam, M. S.; Alauddin, M. World Production of Jute: A Comparative Analysis of Bangladesh. *International Journal of Management and Business Studies* **2012**, *2* (1), 014–022. https://doi.org/10.13140/2.1.1267.2964.

(20) Sanjay, M. R.; Arpitha, G. R.; Naik, L. L.; Gopalakrishna, K.; Yogesha, B. Applications of Natural Fibers and Its Composites: An Overview. *Natural Resources* **2016**, *7* (3), 108–114. https://doi.org/10.4236/nr.2016.73011.

(21) What are polymers? https://iupac.org/polymer-edu/what-are-polymers/ (accessed 2020 -07 -01).

(22) Brydson, J. A. *Plastics Materials*, 7th ed.; Gilbert, M., Ed.; Iliffe Books LTD: Oxford, United Kingdom, 1999.

(23) Peng, W.; Riedl, B. Thermosetting Resins. *J. Chem. Educ.* **1995**, *72* (7), 587. https://doi.org/10.1021/ed072p587.

(24) Pickering, S. J. Recycling Technologies for Thermoset Composite Materials—Current Status. *Composites Part A: Applied Science and Manufacturing* **2006**, *37* (8), 1206–1215. https://doi.org/10.1016/j.compositesa.2005.05.030.

(25) Feldman, D. Polymer History. *Designed Monomers and Polymers* **2008**, *11* (1), 1–15. https://doi.org/10.1163/156855508X292383.

(26) Freire, J.; Fernández, L.; Muiño, R. Role of the Spanish Scientific Community in the Initial Assessment and Management of the Environmental Damages Caused by the Prestige Oil Spill. *Marine Policy* **2006**, *30* (4), 308–314. https://doi.org/10.1016/j.marpol.2005.03.002.

(27) Bishop, R. C.; Boyle, K. J.; Carson, R. T.; Chapman, D.; Hanemann, W. M.; Kanninen, B.; Kopp, R. J.; Krosnick, J. A.; List, J.; Meade, N.; Paterson, R.; Presser, S.; Smith, V. K.; Tourangeau, R.; Welsh, M.; Wooldridge, J. M.; DeBell, M.; Donovan, C.; Konopka, M.; Scherer, N. Putting a Value on Injuries to Natural Assets: The BP Oil Spill. *Science* **2017**, *356* (6335), 253–254. https://doi.org/10.1126/science.aam8124.

(28) A, A.; Ologbonjaye, K.; Awosolu, O.; E, A. Public and Environmental Health Effects of Plastic Wastes Disposal: A Review. *Journal of Toxicology and Risk Assessment* **2019**, *5* (2), 1–13. https://doi.org/10.23937/2572-4061.1510021.

(29) Callister Jr., W.; Rethwisch, D. *Materials Science and Engineering: An Introduction*, 9th ed.; Sayre, D., Ed.; John Wiley and Sons, Inc.: Hoboken, New Jersey, 2014.

(30) Netravali, A. N.; Henstenburg, R. B.; Phoenix, S. L.; Schwartz, P. Interfacial Shear Strength Studies Using the Single-Filament-Composite Test. I: Experiments on Graphite Fibers in Epoxy. *Polymer Composites* **1989**, *10* (4), 226–241. https://doi.org/10.1002/pc.750100405.

(31) Kalita, D.; Netravali, A. N. Interfaces in Green Composites: A Critical Review. *Rev. Adhesion and Adhesives* **2015**, *3* (4), 386–443. https://doi.org/10.7569/RAA.2015.097311.

(32) Kulshreshtha, A. K.; Vasile, C. *Handbook of Polymer Blends and Composites*; Kulshreshtha, A. K., Vasile, C., Eds.; Rapra Technology Limited: Shawbury, United Kingdom, 2003; Vol. 1.

(33) A Brief History of Composites in the U.S. https://www.tms.org/pubs/journals/JOM/9602/Scala-9602.html (accessed 2020 -07 -01).

(34) Hilditch, T. B.; de Souza, T.; Hodgson, P. D. 2 - Properties and Automotive Applications of Advanced High-Strength Steels (AHSS). In *Welding and Joining of Advanced High Strength Steels (AHSS)*; Shome, M., Tumuluru, M., Eds.; Woodhead Publishing, 2015; pp 9–28. https://doi.org/10.1016/B978-0-85709-436-0.00002-3.

(35) Amieva, E. J.-C.; Velasco-Santos, C.; Martínez-Hernández, A.; Rivera-Armenta, J.; Mendoza-Martínez, A.; Castaño, V. Composites from Chicken Feathers Quill and Recycled Polypropylene. *Journal of Composite Materials* **2015**, *49* (3), 275–283. https://doi.org/10.1177/0021998313518359.

(36) Barone, J.; Schmidt, W.; Liebner, C. Compounding and Molding of Polyethylene Composites Reinforced with Keratin Feather Fiber. *Composites Science and Technology* **2005**, *65* (3–4), 683–692. https://doi.org/10.1016/j.compscitech.2004.09.030.

(37) Barone, J. R.; Schmidt, W. F. Polyethylene Reinforced with Keratin Fibers Obtained from Chicken Feathers. *Composites Science and Technology* **2005**, *65* (2), 173–181. https://doi.org/10.1016/j.compscitech.2004.06.011.

(38) Fraser, R. D. B.; Parry, D. A. D. The Molecular Structure of Reptilian Keratin. *International Journal of Biological Macromolecules* **1996**, *19* (3), 207–211. https://doi.org/10.1016/0141-8130(96)01129-4.

(39) Tesfaye, T.; Sithole, B.; Ramjugernath, D.; Chunilall, V. Valorisation of Chicken Feathers: Characterisation of Chemical Properties. *Waste Management* **2017**, *68*, 626–635. https://doi.org/10.1016/j.wasman.2017.06.050.

(40) Molecular biology of the cell / - فهرست آنلاین کتابخانه مرکزی دانشگاه علوم پزشکی تربت حیدریه http://dlib.thums.ac.ir/site/catalogue/7329 (accessed 2020 -07 -02).

(41) Tesfaye, T.; Sithole, B.; Ramjugernath, D.; Chunilall, V. Valorisation of Chicken Feathers: Characterisation of Physical Properties and Morphological Structure. *Journal of Cleaner Production* **2017**, *C* (149), 349–365. https://doi.org/10.1016/j.jclepro.2017.02.112.

(42) Bonser, R. H. C.; Purslow, P. P. The Young's Modulus of Feather Keratin. *Journal of Experimental Biology* **1995**, *198* (4), 1029–1033.

(43) Tesfaye, T.; Sithole, B.; Ramjugernath, D.; Mokhothu, T. Valorisation of Chicken Feathers: Characterisation of Thermal, Mechanical and Electrical Properties. *Sustainable Chemistry and Pharmacy* **2018**, *9*, 27–34. https://doi.org/10.1016/j.scp.2018.05.003.

(44) Krinski, T. L. Emerging Polymeric Materials Based on Soy Protein. In *Emerging Technologies for Materials and Chemicals from Biomass*; Rowell, R. M., Schultz, T. P., Narayan, R., Eds.; ACS Symposium Series; American Chemical Society: Washington, DC, 1992; Vol. 476, pp 299–312. https://doi.org/10.1021/bk-1992-0476.ch017.

(45) Erdman, J. W.; Badger, T. M.; Lampe, J. W.; Setchell, K. D. R.; Messina, M. Not All Soy Products Are Created Equal: Caution Needed in Interpretation of Research Results. *J Nutr* **2004**, *134* (5), 1229S-1233S. https://doi.org/10.1093/jn/134.5.1229S.

(46) Gianazza, E.; Eberini, I.; Arnoldi, A.; Wait, R.; Sirtori, C. R. A Proteomic Investigation of Isolated Soy Proteins with Variable Effects in Experimental and Clinical Studies. *J Nutr* **2003**, *133* (1), 9–14. https://doi.org/10.1093/jn/133.1.9.

(47) Gorissen, S. H. M.; Crombag, J. J. R.; Senden, J. M. G.; Waterval, W. A. H.; Bierau, J.; Verdijk, L. B.; van Loon, L. J. C. Protein Content and Amino Acid Composition of Commercially Available Plant-Based Protein Isolates. *Amino Acids* **2018**, *50* (12), 1685–1695. https://doi.org/10.1007/s00726-018-2640-5.

(48) Ishino, K.; Okamoto, S. Molecular Interaction in Alkali Denatured Soybean Proteins. *Cereal Chemistry* **1975**, *52* (1), 9–21.

(49) Yasir, S. B. M.; Sutton, K. H.; Newberry, M. P.; Andrews, N. R.; Gerrard, J. A. The Impact of Maillard Cross-Linking on Soy Proteins and Tofu Texture. *Food Chemistry* **2007**, *104* (4), 1502–1508. https://doi.org/10.1016/j.foodchem.2007.02.042.

(50) Chand, N.; Fahim, M. 1 - Natural Fibers and Their Composites. In *Tribology of Natural Fiber Polymer Composites (Second Edition)*; Chand, N., Fahim, M., Eds.; Woodhead Publishing Series in Composites Science and Engineering; Woodhead Publishing, 2021; pp 1–59. https://doi.org/10.1016/B978-0-12-818983-2.00001-3.

(51) Biswas, S.; Ahsan, Q.; Cenna, A.; Hasan, M.; Hassan, A. Physical and Mechanical Properties of Jute, Bamboo and Coir Natural Fiber. *Fibers Polym* **2013**, *14* (10), 1762–1767. https://doi.org/10.1007/s12221-013-1762-3.

(52) Chakravarty, A. C. Measurement of Density of Fibers of Jute by Density Gradient Column. *Journal of Polymer Science* **1961**, *54* (160), S52–S56. https://doi.org/10.1002/pol.1961.1205416040.

(53) Ray, D.; Sarkar, B. K.; Basak, R. K.; Rana, A. K. Study of the Thermal Behavior of Alkali-Treated Jute Fibers. *Journal of Applied Polymer Science* **2002**, *85* (12), 2594–2599. https://doi.org/10.1002/app.10934.

(54) Pandey, S. N.; Day, A.; Mathew, M. D. Thermal Analysis of Chemically Treated Jute Fibers. *Textile Research Journal* **1993**, *63* (3), 143–150. https://doi.org/10.1177/004051759306300303.

(55) Maity, S.; Singha, K.; Gon, D.; Paul, P.; Singha, M. A Review on Jute Nonwovens: Manufacturing, Properties and Applications. *International Journal of Textile Science* **2012**, *1*, 36–43. https://doi.org/10.5923/j.textile.20120105.02.

(56) Barone, J. R.; Schmidt, W. F.; Liebner, C. F. E. Thermally Processed Keratin Films. *J. Appl. Polym. Sci.* **2005**, *97* (4), 1644–1651. https://doi.org/10.1002/app.21901.

(57) Barone, J. R.; Schmidt, W. F.; Gregoire, N. T. Extrusion of Feather Keratin. *J. Appl. Polym. Sci.* **2006**, *100* (2), 1432–1442. https://doi.org/10.1002/app.23501.

(58) Tian, H.; Guo, G.; Fu, X.; Yao, Y.; Uuan, L.; Xiang, A. Fabrication, Properties and Applications of Soy-Protein-Based Materials: A Review. *International Journal of Biological Macromolecules* **2018**, *120*, 475–490. https://doi.org/10.1016/j.ijbiomac.2018.08.110.

(59) Mo, X.; Sun, X. Plasticization of Soy Protein Polymer by Polyol-Based Plasticizers. *J Amer Oil Chem Soc* **2002**, *79* (2), 197–202. https://doi.org/10.1007/s11746-002-0458-x.

(60) Migneault, I.; Dartiguenave, C.; Bertrand, M. J.; Waldron, K. C. Glutaraldehyde: Behavior in Aqueous Solution, Reaction with Proteins, and Application to Enzyme Crosslinking. *BioTechniques* **2004**, *37* (5), 790–802. https://doi.org/10.2144/04375RV01.

(61) Wang, Y.; Mo, X.; Sun, X. S.; Wang, D. Soy Protein Adhesion Enhanced by Glutaraldehyde Crosslink. *Journal of Applied Polymer Science* **2007**, *104* (1), 130–136. https://doi.org/10.1002/app.24675.

(62) Kiernan, J. A. Formaldehyde, Formalin, Paraformaldehyde And Glutaraldehyde: What They Are And What They Do. *Microscopy Today* **2000**, *8* (1), 8–13. https://doi.org/10.1017/S1551929500057060.

(63) Park, S. K.; Bae, D. H.; Rhee, K. C. Soy Protein Biopolymers Cross-Linked with Glutaraldehyde. *J Amer Oil Chem Soc* **2000**, *77* (8), 879–884. https://doi.org/10.1007/s11746-000-0140-3.

(64) Depalle, B.; Qin, Z.; Shefelbine, S. J.; Buehler, M. J. Influence of Cross-Link Structure, Density and Mechanical Properties in the Mesoscale Deformation Mechanisms of Collagen Fibrils. *J Mech Behav Biomed Mater* **2015**, *52*, 1–13. https://doi.org/10.1016/j.jmbbm.2014.07.008.

(65) Zheng, T.; Yu, X.; Pilla, S. Mechanical and Moisture Sensitivity of Fully Bio-Based Dialdehyde Carboxymethyl Cellulose Cross-Linked Soy Protein Isolate Films. *Carbohydrate Polymers* **2017**, *157*, 1333–1340. https://doi.org/10.1016/j.carbpol.2016.11.011.

(66) Lodha, P.; Netravali, A. N. Characterization of Stearic Acid Modified Soy Protein Isolate Resin and Ramie Fiber Reinforced 'Green' Composites. *Composites Science and Technology* **2005**, *65* (7), 1211–1225. https://doi.org/10.1016/j.compscitech.2004.12.036.

(67) Kumar, P.; Sandeep, K. P.; Alavi, S.; Truong, V. D.; Gorga, R. E. Preparation and Characterization of Bio-Nanocomposite Films Based on Soy Protein Isolate and Montmorillonite Using Melt Extrusion. *Journal of Food Engineering* **2010**, *100* (3), 480–489. https://doi.org/10.1016/j.jfoodeng.2010.04.035.

(68) Lodha, P.; Netravali, A. N. Effect of Soy Protein Isolate Resin Modifications on Their Biodegradation in a Compost Medium. *Polymer Degradation and Stability* **2005**, *87* (3), 465–477. https://doi.org/10.1016/j.polymdegradstab.2004.09.011.

(69) Reddy, N.; Jiang, J.; Yang, Y. Biodegradable Composites Containing Chicken Feathers as Matrix and Jute Fibers as Reinforcement. *J Polym Environ* **2014**, *22* (3), 310–317. https://doi.org/10.1007/s10924-014-0648-9.

(70) Huda, S.; Yang, Y. Feather Fiber Reinforced Light-Weight Composites with Good Acoustic Properties. *J Polym Environ* **2009**, *17* (2), 131–142. https://doi.org/10.1007/s10924-009-0130-2.

(71) Cheng, S.; Lau, K.; Liu, T.; Zhao, Y.; Lam, P.-M.; Yin, Y. Mechanical and Thermal Properties of Chicken Feather Fiber/PLA Green Composites. *Composites Part B: Engineering* **2009**, *40* (7), 650–654. https://doi.org/10.1016/j.compositesb.2009.04.011.

(72) Mohanty, A. K.; Misra, M.; Hinrichsen, G. Biofibres, Biodegradable Polymers and Biocomposites: An Overview. *Macromolecular Materials and Engineering* **2000**, *267–277* (1), 1–24. https://doi.org/10.1002/(SICI)1439-2054(20000301)276:1<1::AID-MAME1>3.0.CO;2-W.

(73) Lodha, P.; Netravali, A. N. Characterization of Interfacial and Mechanical Properties of "Green" Composites with Soy Protein Isolate and Ramie Fiber. *Journal of Materials Science* **2002**, *37* (17), 3657–3665. https://doi.org/10.1023/A:1016557124372.

(74) Babrauskas, V.; Peacock, R. D. Heat Release Rate: The Single Most Important Variable in Fire Hazard. *Fire Safety Journal* **1992**, *18* (3), 255–272. https://doi.org/10.1016/0379-7112(92)90019-9.

(75) Pearce, E. M.; Liepins, R. Flame Retardants. *Environmental Health Perspectives* **1975**, *11*, 59–69. https://doi.org/10.2307/3428325.

(76) Zhuge, J.; Chen, X.; Ks, A.; Manica, D. P. Microscale Combustion Calorimeter—Application and Limitation. *Fire and Materials* **2016**, *40* (8), 987–998. https://doi.org/10.1002/fam.2358.

(77) Osborne, T. B.; Leavenworth, C. S.; Brautlecht, C. A. THE DIFFERENT FORMS OF NITROGEN IN PROTEINS. *American Physiological Society* **1908**, *23* (3), 180–200.

(78) Wang, X.; Lu, C.; Chen, C. Effect of Chicken-Feather Protein-Based Flame Retardant on Flame Retarding Performance of Cotton Fabric. *Journal of Applied Polymer Science* **2014**, *131* (15). https://doi.org/10.1002/app.40584.

(79) Bartlett, A. I.; Hadden, R. M.; Bisby, L. A. A Review of Factors Affecting the Burning Behaviour of Wood for Application to Tall Timber Construction. *Fire Technol* **2019**, *55* (1), 1–49. https://doi.org/10.1007/s10694-018-0787-y.

(80) Shih, M.-C.; Hwang, T.-S.; Chou, H.-Y. Physicochemical and Functional Property Changes in Soy Protein Isolates Stored under High Relative Humidity and Temperature. *J Food Sci Technol* **2016**, *53* (1), 902–908. https://doi.org/10.1007/s13197-015-2057-z.

(81) Liu, B.-W.; Zhao, H.-B.; Chin, L.; Chen, L.; Wang, X.-L.; Wang, Y.-Z. Eco-Friendly Synergistic Cross-Linking Flame-Retardant Strategy with Smoke and Melt-Dripping Suppression for Condensation Polymers. *Composites Part B: Engineering* **2021**, *211*. https://doi.org/10.1016/j.compositesb.2021.108664.

(82) Basak, S.; Samanta, K. K. Thermal Behaviour and the Cone Calorimetric Analysis of the Jute Fabric Treated in Different PH Condition. *J Therm Anal Calorim* **2019**, *135* (6), 3095–3105. https://doi.org/10.1007/s10973-018-7522-2.

(83) Chan, M. Y.; Husseinsyah, S.; Sam, S. T. Chitosan/Corn Cob Biocomposite Films by Cross-Linking with Glutaraldehyde. *BioResources* **2013**, *8* (2), 2910–2923.

(84) Kawahara, J.; Ohmori, T.; Ohkubo, T.; Hattori, S.; Kawamura, M. The Structure of Glutaraldehyde in Aqueous Solution Determined by Ultraviolet Absorption and Light Scattering. *Analytical Biochemistry* **1992**, *201* (1), 94–98. https://doi.org/10.1016/0003-2697(92)90178-A.

(85) Ballesteros-Mártinez, L.; Pérez-Cervera, C.; Andrade-Pizarro, R. Effect of Glycerol and Sorbitol Concentrations on Mechanical, Optical, and Barrier Properties of Sweet Potato Starch Film | Elsevier Enhanced Reader. *NFS Journal* **2020**, *20*, 1–9. https://doi.org/10.1016/j.nfs.2020.06.002.

(86) Cho, S. Y.; Rhee, C. Sorption Characteristic of Soy Protein Films and Their Relation to Mechanical Properties. *LWT - Food Science and Technology* **2002**, *35* (2), 151–157. https://doi.org/10.1006/fstl.2001.0829.

(87) Sorbitol https://webbook.nist.gov/cgi/cbook.cgi?ID=C50704&Mask=80 (accessed 2021 -05 -15).

(88) Netravali, A. N.; Wallenberger, F. T.; Weston, N. E. Biodegradable 'Green' Composites Using Ramie Fibers and Soy Protein Polymer. In *'Natural Fibers, Plastics and Composites';* Kluwer Academic Publishers: Boston; pp 321–343.

(89) Sharma, S.; Gupta, A.; Saufi, S.; Chua, G. K.; Poddar, P.; Subramaniam, M.; Thuraisingam, J. Study of Different Treatment Methods on Chicken Feather Biomass.

International Islamic University Malaysia Engineering Journal **2017**, *18* (2), 47–55. https://doi.org/10.31436/iiumej.v18i2.806.

(90) Kann, Y.; Shurgalin, M.; Krishnaswamy, R. K. FTIR Spectroscopy for Analysis of Crystallinity of Poly(3-Hydroxybutyrate-Co-4 -Hydroxybutyrate) Polymers and Its Utilization in Evaluation of Aging, Orientation and Composition. *Polymer Testing* **2014**, *40*, 218–224. https://doi.org/10.1016/j.polymertesting.2014.09.009.

(91) Samanta, A. K.; Bhattacharyya, R.; Jose, S.; Basu, G.; Chowdhury, R. Fire Retardant Finish of Jute Fabric with Nano Zinc Oxide. *Cellulose* **2017**, *24* (2), 1143–1157. https://doi.org/10.1007/s10570-016-1171-z.

(92) Gautam, S. P.; Bundela, P. S.; Pandey, A. K.; Jamaluddin, J.; Awasthi, M. K.; Sarsaiya, S. A Review on Systematic Study of Cellulose. *JANS* **2010**, *2* (2), 330–343. https://doi.org/10.31018/jans.v2i2.143.

(93) Parrington, R. J. Fractography of Metals and Plastics. *Practical Failure Analysis* **2002**, *2* (5), 16–19. https://doi.org/10.1007/BF02715463.